The kinetics, mechanisms, and consequences of HTLV-1 plus-strand expression in naturally-infected T-cell clones

Saumya Ramanayake

A thesis submitted for the degree of Doctor of Philosophy

Department of Infectious Disease

Faculty of Medicine

Imperial College London

Declaration of originality

All experiments and data analysis presented in this thesis were performed by Saumya Ramanayake unless explicitly mentioned in the statement of collaborations.

Copyright declaration

Abstract

HTLV-1 replication requires the expression of plus-strand-encoded transcriptional transactivator protein Tax. However, Tax protein, a surrogate for HTLV-1 plus-strand expression is seldom detected in freshly isolated infected blood. The kinetics and consequences of plus-strand expression remain poorly understood. I used two fluorescent protein-based Tax reporter systems to study the dynamics and consequences of plus-strand expression and the changes to the host gene expression during plus-strand expression in naturally HTLV-1-infected, non-malignant T-cell clones.

Time-lapse live-cell imaging followed by single-cell analysis of two T-cell clones stably transduced with a short-lived enhanced green fluorescent protein Tax reporter system identified five patterns of Tax expression in both clones and the distribution of these patterns was different between the two clones. Mathematical modelling of the experimental data revealed that the mean duration of Tax expression differed between the two clones – 94 and 417 hours, respectively.

Host cell transcriptome analysis during successive stages of plus-strand strand expression using a fluorescent timer protein-based Tax reporter system in naturally-infected T-cell clones identified dysregulation in the expression of genes related to multiple cellular processes, including cell cycle, DNA damage response, and apoptosis at the initiation of the plus-strand transcriptional burst.

The plus-strand expression showed immediate but transient adverse effects, including reduced proliferation, increased apoptosis, upregulation of a DNA damage marker, and impaired cell cycle progression. In the longer term, the immediate negative consequences of Tax expression were offset by reduced apoptosis and increased proliferation as cells terminated plus-strand

expression. Plus-strand expression was also associated with cell-to-cell adhesion and reduced motility.

These findings show within and between clone variability in the patterns and duration of HTLV-1 plus-strand expression, changes to the host gene expression during successive stages of the plus-strand expression, and the balance between the beneficial and adverse effects on the host cell associated with the plus-strand expression.

Acknowledgements

Foremost, I would like to thank my supervisor, Professor Charles Bangham for providing me with the opportunity to pursue a PhD in his laboratory. The mentorship I received from him has turned me into a better scientist. I would also like to thank Professor Peter O'Hare for being my co-supervisor.

I would like to thank the members of the Bangham Laboratory for their support and helpful discussions. Dr Michi Miura, who was always there to help me when I first began working in the Bangham Laboratory, deserves my heartfelt gratitude. I also like to thank Helen for the helpful discussions regarding the analysis of RNA sequencing data.

I would also like to thank fellow PhD students Aris, Danai, Jonas, Charandeep, and Allison for sharing the joys and sorrows of the PhD journey and being great colleagues.

This multidisciplinary project would not have been possible without multiple collaborations. A special thank goes to Parisa for always agreeing to FACS sort my samples, even at short notice. I thank Dr Dale Moulding of University College London for helping me step into the world of bioimage analysis, a territory I was unfamiliar with at the start of my PhD. I thank Professor Abhyudai Singh for his help with the mathematical modelling and general discussions.

I thank my parents for constantly motivating me to be the best version of myself. Last, but not least, I would like to thank my wife, Meerani, for her continuous support, without which this work would have been impossible. A special thank goes to my daughter Nikini for being the most amazing daughter one could have.

Table of contents

List of figures

List of tables

List of abbreviations

53BP1	p53 binding protein 1
ADAR1	Adenosine deaminase acting on RNA 1
AhR	Aryl hydrocarbon receptor
AIDS	Acquired immunodeficiency syndrome
AO	Acridine orange
AP-1	Activator protein 1
APAF1	Apoptosis activating factor 1
APC	Antigen-presenting cell
As_2O_3	Arsenic trioxide
ATF	Activating transcription factor
ATL	Adult T-cell leukemia/lymphoma
ATM	Ataxia telangiectasia mutated
ATR	ATM and Rad3-related
AZT	Zidovudine
BAG1	Bcl-2-associated athanogene BAG1
BAX	Bcl-2-associated X BAX
BCL10	B-cell lymphoma/leukaemia 10 BCL10
BCL2	B-cell lymphoma 2
Bcl-2	B-cell lymphoma protein 2 Bcl-2
BCL2L1	B-cell lymphoma 2 like 1
BER	Base excision repair
BET	Bromodomain and extra-terminal domain
BLV	Bovine leukaemia virus BLV
BMI1	B lymphoma Mo-MLV insertion region 1 homolog BMI1
BTG2	B-cell translocation gene 2 BTG2
CA	Capsid
CAD	Caspase-activated DNase
cAMP	Cyclic adenosine monophosphate

CBP	CREB-binding protein
CCL22	C-C motif chemokine ligand 22
CCR4	C-C chemokine receptor type 4
CDC25	Cell division cycle 25
$CdCl_2$	Cadmium chloride
CDK	Cyclin-dependent kinase
ChIP	Chromatin immunoprecipitation
ChK	Checkpoint kinase
CKI	CDK inhibitors
CL3	Containment level 3
CMV	Cytomegalovirus
CNS	Central nervous system
CpG	Cytosine-guanine dinucleotide
CRE	cAMP-responsive element
CREB	cAMP response element-binding protein
CRM1	Chromosome region maintenance 1
CRMP2	Collapsing response mediator protein 2
CSF	Cerebrospinal fluid
Ct	Cycle threshold
CTCF	CCCTC-binding factor
CTL	Cytotoxic T lymphocyte
CYP1A1	Cytochrome P450 1A1
d2EGFP	Destabilised enhanced green fluorescent
DC	Dendritic cell
ddPCR	Digital droplet PCR
DDR	DNA damage response
DISC	Death-inducing signalling complex
DMSO	Dimethyl sulfoxide
DNA	Deoxyribonucleic acid
DNA pol II	DNA polymerase II

DNMTi	DNA methyltransferase inhibitor
DRE	Dioxin response element
ds	Double-stranded
DUB	Deubiquitinase
EBV	Epstein-Barr virus
ECM	Extracellular matrix
EdU	5-ethynyl-2'-deoxyuridine
EGFP	Enhanced green fluorescent protein
ER	Endoplasmic reticulum ER
FAAD	Fas-associated death domain
FACS	Fluorescence-activated cell sorting
FAS	Fas cell surface death receptor
FASLG	FAS ligand
FCS	Fetal calf serum
FDR	False discovery rate
FT	Fast timer protein
FV	Foamy virus
GADD45A	Growth arrest and DNA damage inducible alpha
GLM	Generalised linear model
GLUT-1	Glucose transporter 1
HAM/TSP	HTLV-1-associated myelopathy/tropical spastic paraparesis
HAT	Histone acetyltransferase
HBZ	HTLV-1 basic leucine-zipper
HCV	Hepatitis C virus
HDAC	Histone deacetylase
HDACi	Histone deacetylase inhibitor
HEK	Human embryonic kidney
HIV-1	Human immunodeficiency virus type 1
HMTi	Histone methyltransferase inhibitor
HR	Homologous recombination

HSP	Heat shock protein
HSPG	Heparin sulfate proteoglycan
HTLV-1	Human T-cell leukaemia virus type 1
ICAD	Inhibitor of caspase-activated DNase
ICAM-1	Intercellular cell adhesion molecule 1
IFN I	Type 1 interferons
IFN α	Interferon alpha
IFN γ	Interferon gamma
iKIR	Inhibitory killer-cell immunoglobulin-like receptor
IKK	IκB kinase
IL-2	Interleukin 2
ilastik	Interactive learning and segmentation toolkit
ILR2A	Interleukin-2 receptor alpha chain
IN	Integrase
iNKT	Invariant natural killer T-cell
IRF3	Interferon Regulatory Factor 3
ISG	Interferon-stimulated gene
KDM2B	Lysine demethylase 2B
LAMP-2A	Lysosome-associated membrane protein type 2A
LDH	Lactate dehydrogenase
LFA-1	Lymphocyte function-associated antigen 1
LFC	Log2 fold change
LMP1	Latent membrane protein 1
ln	Natural logarithm
LRA	Latency-reversing agent
LRT	Likelihood-ratio test
LTR	Long terminal repeat
MA	Matrix
MCL1	Myeloid cell leukaemia 1
MCP	MS2 coat protein

MDC1	Mediator of the DNA damage checkpoint protein 1
mRNA	Messenger ribonucleic acid
MFI	Median fluorescence intensity
MHC	Major histocompatibility complex
MMR	Mismatch repair
MODC	Mouse ornithine decarboxylase
MS	Multiple sclerosis
MSD	Mean square displacement
MuLV	Murine leukaemia virus
NAC	N-acetyl-L-cysteine
NAP 1	Nucleosome assembly protein 1
NC	Nucleocapsid
NER	Nucleotide excision repair
NES	Nuclear export signal
NF-κB	Nuclear factor kappa-light-chain-enhancer of activated B-cells
NHEJ	Non-homologous end joining
NK	Natural killer
NLS	Nuclear localisation signal
NRP-1	Neuropilin-1
NRTI	Nucleoside reverse transcriptase inhibitor
OCI	Oligoclonality index
ORF	Open reading frame
p38 MAPK	p38 mitogen-activated protein kinase
PBMC	Peripheral blood mononuclear cell
PCA	Principal component analysis
PCNA	Proliferating cell nuclear antigen
PCP	PP7 coat protein
pDC	Plasmacytoid dendritic cell
PDL	Poly-D-Lysine
PDMS	Polydimethylsiloxane

PE	Phycoerythrin
PHC2	Polyhomeotic homolog 2
PI	Propidium iodide
PI3K	Phosphoinositide-3-kinase
PIC	Preintegration complex
PIKK	Phosphoinositide 3-kinase-like kinase
PKB	Protein kinase B
PKC	Protein kinase C
PKR	Protein kinase R
PLCγ1	Phospholipase C gamma 1
PMA	Phorbol-12-myristate-13-acetate
PMAIP1	Phorbol-12-myristate-13-acetate-induced protein 1
PP2A	Phosphatase 2A
PR	Protease
PRC	Polycomb repressive complex
P-TEFb	Positive transcription elongation factor b
PTM	Post-translational modification
PVL	Proviral load
qPCR	Quantitative polymerase chain reaction
R	Repeated
Rb	Retinoblastoma
RING1	Ring finger protein 1
RNA	Ribonucleic acid
RNF4	Really interesting new gene finger protein 4
ROS	Reactive oxygen species
RSEM	RNA-seq by expectation maximization
RT	Reverse transcriptase
RxRE	Rex-response element
RYBP	RING1 and YY1 binding protein
SEM	Standard error of the mean

sHBZ	Spliced HBZ
SIR	Superinfection resistance
smFISH	Single-molecule RNA fluorescence in situ hybridisation
SOCS 1	Suppressor of cytokine signalling 1
Sp1	Specificity protein 1
SR1	StemRegenin1
SRE	Serum responsive element
SRF	Serum response factor
STAR	spliced transcripts alignment to a reference
STAT1	Signal transducers and activators of transcription factor 1
STLV	Simian T-cell leukaemia virus
SU	Surface subunit
SWI/SNF	Switch/sucrose non-fermentable
TAK 1	TGF-β activating kinase 1
TBHP	Tert-butyl hydroperoxide
TBK1	TANK Binding Kinase 1
TFBS	Transcription factor binding sites
TLR	Toll-like receptor
TM	Transmembrane
TNF	Tumour necrosis factor
TNFRSF	Tumour necrosis factor receptor superfamily
TP53	Tumour protein p53
TP63	Tumour protein p63
TxRE 1	Tax- responsive element 1
U3	Unique 3'
U5	Unique 5'
UIS	Unique integration site
usHBZ	Unspliced HBZ
USP20	Ubiquitin-specific peptidase 20
UTR	Untranslated region

vCRE	Viral CRE
VS	Virological synapse
VZV	Varicella-zoster virus
WHO	World Health Organisation
XPC	Xeroderma pigmentosum group C

Statement of collaboration

All experiments and data analysis were performed by the candidate (Saumya Ramanayake) except the following:

- Mathematical modelling described in section 2.7 to estimate the average duration of Tax expression was performed by Professor Abhyudai Singh of the University of Delaware.
- Mrs Parisa Amjadi at the Centre for Immunology and Vaccinology of Imperial College London performed FACS sorting described in section 2.3.7.
- The staff of Oxford Genomic Centre performed the preparation and sequencing of cDNA libraries from RNA samples described in section 2.6.1.
- The alignment and transcript quantification described in section 2.6.2 were performed by Miss Helen Kiik of Imperial College London.

Chapter 1 – Introduction

1.1 Human T-cell leukaemia virus type 1

The human T-cell leukaemia virus type 1 (HTLV-1) was isolated in 1979 as the first human retrovirus by Gallo and colleagues from a patient with cutaneous T-cell lymphoma (Poiesz et al., 1980). HTLV-1 is a member of the *Deltaretrovirus* genus that includes several other human and animal viruses, including HTLV-2, HTLV-3, HTLV-4, simian T-cell leukaemia virus (STLV) types 1-5, and bovine leukaemia virus (BLV) (Hajj et al., 2012). HTLV-1 causes a life-long infection by integrating its reverse-transcribed viral genome into the human host cell genome.

1.2 Epidemiology

It is estimated that between 5-20 million people are infected with HTLV-1 worldwide (Gessain and Cassar, 2012; de Thé and Kazanji, 1996). However, the actual number of infected individuals is likely higher than current estimates due to the lack of reliable epidemiological data covering the entire global population (Gessain and Cassar, 2012). HTLV-1 is not ubiquitously distributed: There are several endemic regions, including Southwestern Japan, sub-Saharan Africa, the Caribbean, South America, Australia, and Melanesia (Figure 1-1) (Gessain and Cassar, 2012; Proietti et al., 2005). There are an estimated 22500 HTLV-1 infected individuals in the UK, with most infected individuals representing either immigrants or their descendants from endemic regions, including the Caribbean and Africa (Tosswill et al., 2000).

There are seven subtypes of HTLV-1 based on the sequence variation of the isolates originating from patients of different endemic regions (Proietti et al., 2005): Subtype A, also known as the Cosmopolitan subtype, is the most prevalent and shows the greatest geographical distribution

(Proietti et al., 2005). Subtypes B, D and F are found in the Central African region, Subtype C in Australia and Melanesia and Subtype E in South and Central Africa (Slattery et al., 1999).

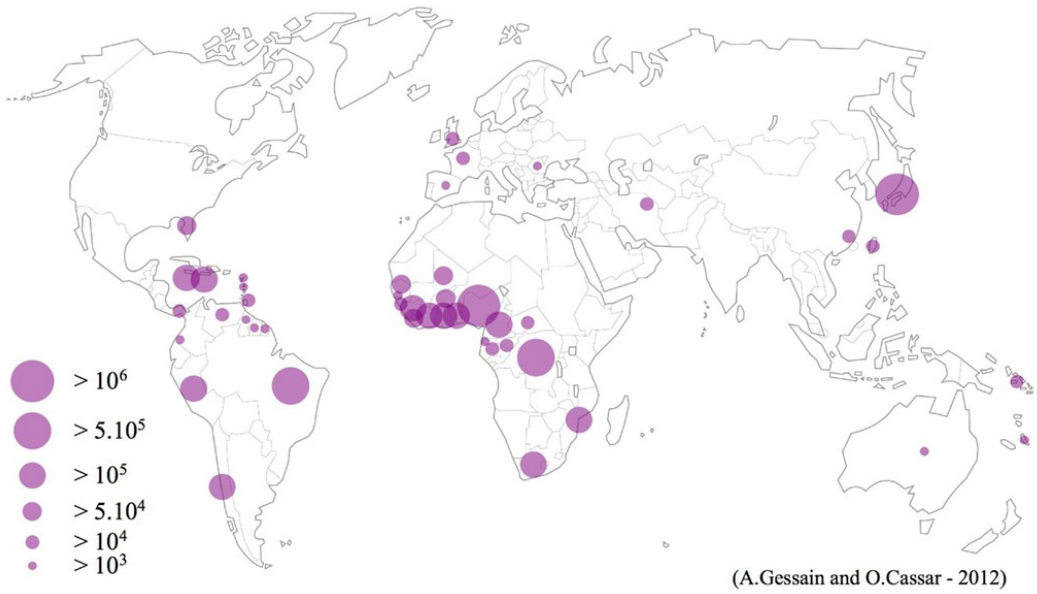

Figure 1-1. The distribution of the endemic regions of HTLV-1 infection.
Infection frequency was estimated based on studies in the endemic regions involving pregnant women, blood donors, and other adult groups.
Figure reproduced from (Gessain and Cassar, 2012) under the terms of the Creative Commons Attribution License.

1.3 Transmission and Diagnosis

The primary modes of HTLV-1 transmission include sexual intercourse, breastfeeding, and infected blood products. Vertical transmission from mother to child predominantly occurs through breastfeeding, and the risk of transmission increases with the duration of breastfeeding (Hino, 2011). Sexual transmission primarily occurs from male to female (Kajiyama et al., 1986). Infected blood transfusions are associated with a very high risk of HTLV-1 transmission, with one study reporting 63% of the recipients seroconverting (Okochi et al., 1984).

The initial diagnosis of HTLV-1 is typically performed by detecting HTLV-1-specific antibodies in the plasma using enzyme-linked immunoassays followed by a Western blot using HTLV-1 Gag- and Env-specific antibodies to confirm the positive cases (Thorstensson et al., 2002). Qualitative polymerase chain reaction is used to confirm inconclusive Western blot results (Kuramitsu et al., 2017). Quantitative polymerase chain reaction (qPCR) or digital droplet PCR (ddPCR) is used to quantify the number of integrated copies of the viral genome per one hundred circulating peripheral blood mononuclear cells (PBMCs) – proviral load (PVL) (Kuramitsu et al., 2017; Brunetto et al., 2014).

1.4 Molecular mechanisms of infection

HTLV-1 preferentially infects T lymphocytes with $CD4^+$ T-cells carrying 90%-99% of the proviral load (Richardson et al., 1990). The proviral load among $CD8^+$ cells is approximately 5% (Melamed et al., 2015). HTLV-1 is also detected in dendritic cells (DCs), monocytes, macrophages, and B-cells isolated from HTLV-1-infected individuals (Macatonia et al., 1992; Koyanagi et al., 1993; Journo and Mahieux, 2011).

Cell-free HTLV-1 viral particles are poorly infectious. According to one study, the efficiency of cell-to-cell transmission between co-cultured HTLV-1 transfected Jurkat T-cells and $CD4^+$ T-cells was ten thousandfold more than transmission by cell-free virions (Mazurov et al., 2010). In contrast, the cell-to-cell transmission of human immunodeficiency virus type 1 (HIV-1) was only two times as efficient as cell-free transmission (Mazurov et al., 2010). However, several studies have reported infection of primary DCs by cell-free virions (Jones et al., 2008; Jain et al., 2009). The scarcity of virions and viral products in freshly isolated infected blood and the lack of transmission through plasma transfusions from infected individuals suggest that

transmission by cell-free virions does not play a significant role *in vivo* (Satou et al., 2006; Okochi et al., 1984).

Cell-to-cell transmission of HTLV-1 requires the formation of either tight cell-to-cell contacts creating the virological synapse (VS) or cellular conduits (Gross and Thoma-Kress, 2016). To form the virological synapse (VS), an infected cell engages through its intercellular cell adhesion molecule 1 (ICAM-1) with its ligand, lymphocyte function-associated antigen 1 (LFA-1) on the target cell to induce polarisation of the microtubule network of the infected cell towards the cell-to-cell junction (Igakura et al., 2003; Barnard et al., 2005). The viral particles formed at the VS cross the synaptic cleft to contact the uninfected cell. Cell-to-cell transmission at the VS has also been shown to occur through "viral biofilms" (viral particles enclosed in an extracellular matrix – ECM) on the surface of the infected cell that readily get attached to the target cell upon contact (Pais-Correia et al., 2010). The formation of cellular conduits mediated by the viral accessory protein p8 is the other mode of cell-to-cell transmission of HTLV-1 (Van Prooyen et al., 2010).

Cellular receptors that mediate host cell entry of HTLV-1include glucose transporter 1 (GLUT -1) (Manel et al., 2003), heparin sulfate proteoglycans (HSPGs) (Jones et al., 2005) and neuropilin-1 (NRP-1) (Ghez et al., 2006). The initial step of cellular entry involves the engagement of the surface subunit (SU) of viral envelope glycoprotein with HSPG to form a complex that is stabilised by NRP-1. Subsequent interaction between SU and GLUT-1 facilitates membrane fusion and cellular entry (Jones et al., 2011).

1.5 Integration and clonality

Upon cellular entry, viral ribonucleic acid (RNA) is reverse transcribed by viral reverse transcriptase to double-stranded (ds) deoxyribonucleic acid (DNA), transported to the nucleus and integrated into the host cell genome. Integration is mediated through a catalytic reaction involving viral integrase and host protein phosphatase 2A (PP2A) (Maertens, 2016). In most cases, each infected cell has a single copy of the provirus (Cook et al., 2012). This observation is consistent with other retroviral infections, including HIV-1, Murine leukaemia virus (MuLV), Foamy virus (FV), and the phenomenon is termed superinfection resistance (SIR) (Nethe et al., 2005). Each cell with a unique integration site (UIS) of the provirus constitutes a clone with the position of proviral integration within the host genome providing a unique identifiable molecular signature of the infected cell and its progeny.

As with other retroviral infections, the genomic environment of the provirus plays a critical role in HTLV-1 replication and clonal proliferation. Integration is not random; similar to HIV-1, it is directed towards a common, non-palindromic region within the host genome (Kirk et al., 2016). In a landmark study, Schroder and colleagues discovered that HIV-1 integration had a strong bias towards transcriptionally active genes, particularly those activated by HIV-1 infection (Schröder et al., 2002). HTLV-1 also preferentially integrates into transcriptionally active areas in the host genome (Gillet et al., 2011). This common integration pattern between HIV-1 and HTLV-1 is likely due to the open chromatin conformation in transcriptionally active regions where DNA is readily accessible by the retrovirus' preintegration complex (PIC).

A study by Melamed and colleagues showed that HTLV-1 integration is favoured in regions within close proximity (less than one thousand kilobases) to certain transcription factor binding sites (TFBS), including signal transducers and activators of transcription factor 1 (STAT1), tumour protein p53 (TP53/p53), and histone deacetylase 6 (HDAC6) (Melamed et al., 2013).

The mechanism by which these specific transcription factor binding sites are targeted remains to be elucidated. PP2A or another unknown host factor may be involved in directing the PIC towards the target TFBSs.

Early estimates of clonal abundance in non-malignant HTLV-1 carriers reported that each individual carried around one hundred HTLV-1-infected clones (Wattel et al., 1995). A clone is defined as a population of cells that share an identical HTLV-1 proviral integration site. Integration site mapping using high throughput sequence analysis and population level frequency distribution analysis of clonal abundance have revealed that an individual with a non-malignant disease typically carries between 10^4 to 10^5 clones (Gillet et al., 2011; Laydon et al., 2014).

HTLV-1 persists in vivo by two main routes: infectious and mitotic spread. Infectious spread is predominant during the initial infectious stage, where thousands of clones are established through *de novo* infections. The proliferation of infected cells, termed "mitotic spread", is the primary mode of viral persistence during the chronic phase. The existence of long-lived, expanded, non-malignant clonal populations of T-cells and limited proviral sequence variation within and between individuals provide evidence for mitotic proliferation (Furukawa et al., 1992). Limited proviral sequence variation indicates the dominance of the high-fidelity host DNA polymerase II (DNA pol II) in genome replication during chronic infection, i.e., by mitosis. The lack of sequence variation observed with HTLV-1 contrasts with the productive infection of HIV-1, where sequence variation exists both within and between individuals, often producing defective proviruses as a consequence of the involvement of low-fidelity viral reverse transcriptase in the viral replication cycle (Hu and Hughes, 2012). There is new evidence that more than 50% of cells in the latent HIV-1 reservoir harbouring replication-competent proviruses are maintained through clonal expansion, implying the significance of mitotic spread in human retroviral infections (Liu et al., 2020).

Nevertheless, the presence of persistently active anti-HTLV-1 cytotoxic T lymphocytes (CTLs) during the chronic phase of infection provides evidence for ongoing proviral expression and infectious spread (Hanon et al., 2000; Parker et al., 1992). The relative contribution of infectious spread during the chronic phase of HTLV-1 infection was not known until recently. Using mathematical modelling of clonal abundance data from eleven non-malignant individuals, Laydon and colleagues estimated that on average of the ~$5x10^9$ newly infected cells generated each day during the chronic phase of infection, only ~175 cells were produced through *de novo* infection (Laydon et al., 2020).

There is evidence of *in vivo* HTLV-1 infection dynamics from organ recipients who seroconverted after receiving a transplant from an infected individual (Cook et al., 2016). In one such report from the UK, all three organ recipients from a single seropositive donor were PCR positive within 23 days of transplantation. In these immunosuppressed recipients, the maximum proviral load doubling time was 1.4 days, and the proviral load equilibrium was reached by 36 days of transplantation (Cook et al., 2016). The authors also reported higher than expected mitotic spread potentially due to the use of antiretroviral drugs upon recognition of donor seropositivity to minimise infectious spread. In a recent report by a Japanese group, a recipient of a liver transplant from an infected donor seroconverted within two weeks and the peak proviral load of 9.7% occurred by one month (Izaki et al., 2021). The frequency of the most common clones observed at the end of the first month had decreased by the end of the third month, with the emergence of new frequent clones which remained abundant by twelve months. The survival of donor-derived clones was also evident twelve months post-transplantation. The dynamic change in the clonal landscape during the early phase of HTLV-1 infection suggests the effect of forces, including host immune response and integration site that favour the selection of specific clones for long-term *in vivo* survival.

It has been shown that clones in which HTLV-1 is integrated into acrocentric chromosomes are favoured for *in vivo* selection, perhaps due to the positioning of acrocentric chromosomes near the transcriptionally repressive nucleolar periphery during interphase (Cook et al., 2014). There is novel evidence of preferential survival of clones in which proviral integration is near the nuclear lamina or nucleolar periphery (Melamed et al., 2022). Integration of the provirus near cytosine-guanine dinucleotide (CpG) islands, activating epigenetic marks, and in the same transcriptional orientation as the neighbouring host gene also favour *in vivo* clonal survival (Gillet et al., 2011).

Proviral load, the principal correlate of the development of HTLV-1-associated diseases, reaches a steady-state during the chronic phase of infection when a balance between viral replication and host immune response is established. Within-host variability of steady-state PVL is typically less than 5-fold. However, between-host variability can be up to several orders of magnitude (1000-fold) (Nagai et al., 1998). It was initially thought that oligoclonal expansion was a correlate of PVL. Quantification of clonal abundance using high throughput integration site analysis refuted this belief: PVL correlated with the total number of UISs, not with the oligoclonality index (OCI), a measure of the distribution of clonal frequency, with a value of one indicating a monoclonal population while zero represents a polyclonal population in which each clone is of equal abundance (Gillet et al., 2011).

1.6 HTLV-1-associated diseases

Most infected individuals remain disease-free lifetime carriers of HTLV-1. This contrasts with HIV-1, where almost all infected individuals without antiretroviral therapy develop acquired immunodeficiency syndrome (AIDS)-related diseases. There are two main HTLV-1-associated diseases: up to 5% of infected individuals develop an aggressive form of leukaemia or lymphoma of mature $CD4^+$ T-cells called adult T-cell leukemia/lymphoma (ATL). Another 1-4% develop a neuroinflammatory condition called HTLV-1-associated myelopathy/tropical spastic paraparesis (HAM/TSP).

1.6.1 Adult T-cell leukemia/lymphoma (ATL)

This unique form of leukaemia was first described in Japan (Uchiyama et al., 1977), and HTLV-1 was linked as its aetiological agent by Hinuma and colleagues in 1981 (Hinuma et al., 1981). The development of ATL is preceded by a long clinical latency period, often lasting several decades. The incidence of ATL is higher among males (6.6%) than females (2.1%) (Arisawa et al., 2000). ATL is an aggressive neoplasm of mature $CD4^+CD25^+$ T-cells with characteristic multilobed nuclei called the "flower cells" and frequently involves infiltration of organs, including liver, lungs, skin, and bone marrow. Patients often develop lymphadenopathy, hepatosplenomegaly, hypercalcemia, and elevated lactate dehydrogenase (LDH) levels (Nasr et al., 2017).

There are four clinical subtypes of ATL based on the clinical characteristics and prognosis: acute, chronic, lymphoma, and smouldering (Shimoyama, 1991). The acute and lymphoma subtypes are aggressive forms with a median survival time of eight and ten months, respectively, while chronic and smouldering subtypes show slower disease progression with a median survival period of thirty-one and fifty-five months, respectively (Katsuya et al., 2015).

The treatment options depend on the disease subtype. Muti-drug chemotherapy is ineffective against acute and lymphoma subtypes, with patients frequently developing either refractory disease or relapsing early (Nasr et al., 2017). Antiretroviral therapy with zidovudine (AZT) and interferon alpha (IFN α) has shown promise in smouldering and chronic ATL subtypes, with all patients surviving for at least five years (Bazarbachi et al., 2010). However, the overall five-year survival for acute and lymphoma subtypes was only 18% and 0%, respectively. Allogeneic hematopoietic stem cell transplantation is a therapeutic option. However, four-year overall survival post-transplantation was only 26% (Katsuya et al., 2015). Agents such as arsenic trioxide (As_2O_3), monoclonal antibodies against C-C chemokine receptor type 4 (CCR4) – mogamulizumab, and against CD25 – daclizumab are potential therapeutic options with their safety and efficacy being tested in clinical trials (Phillips et al., 2016).

1.6.2 HTLV-1-associated myelopathy/tropical spastic paraparesis (HAM/TSP)

The history of HAM/TSP dates back to the late nineteenth century: The chronic neuropathy known as tropical spastic paraparesis (TSP), first observed among Jamaican adults, was initially thought to be caused by malnutrition or toxins. (Montgomery et al., 1964). In separate studies, French (Gessain et al., 1985) and Japanese (Osame et al., 1986) groups established the link between HTLV-1 and HAM/TSP by detecting the antibodies against HTLV-1 in Caribbean patients with TSP and patients with myelopathy from South-Western Japan, respectively. HAM/TSP is a progressive neurological disorder caused by the immune response against infiltrating HTLV-1-infected cells and characterised by the chronic inflammation of the central nervous system (CNS).

The symptoms of HAM/TSP include progressive weakness in the lower limbs, lower back pain, constipation, bladder, and sexual dysfunction. The onset of symptoms follows a clinical latency period ranging from a few months to several decades, with a median onset time of 3.3 years after infection (Yamano and Sato, 2012). The incidence of HAM/TSP among women is two to three-fold higher than in men. As per World Health Organisation (WHO) guidelines, a definitive diagnosis of HAM/TSP requires the detection of antibodies against HTLV-1 in cerebrospinal fluid (CSF), as symptoms often overlap with other neurological disorders, including multiple sclerosis (MS) (Bangham et al., 2015). Although not typically a fatal disease, the life expectancy of HAM/TSP patients is lower than that of the general population matched by age. The deaths typically occur due to ATL, heart failure, and pneumonia (Nagasaka et al., 2020).

The curative therapeutic options are non-existent, and treatments mainly focus on relieving symptoms to improve the quality of life. Symptomatic treatments include using anti-inflammatory agents, especially corticosteroids to modulate the immune response or antivirals to reduce the proviral load, a marker of poor prognosis. A phase 1–2a clinical trial in Japan reported a reduction of proviral load and inflammation with minimal side effects among HAM/TSP patients treated with mogamulizumab, but the benefit was not sustained (Sato et al., 2018).

1.6.3 Other HTLV-1-associated diseases

Although less common, HTLV-1 infection is also associated with various inflammatory diseases involving organs other than the CNS, including uveitis, arthritis, polymyositis, and infective dermatitis (Bangham et al., 2015). Despite not causing direct immunosuppression, unlike HIV-1, infection with HTLV-1 predisposes to certain other opportunistic infectious

diseases such as strongyloidiasis (Montes et al., 2009) and tuberculosis (Verdonck et al., 2008). Opportunistic infections, including cytomegalovirus (CMV) pneumonitis, pulmonary aspergillosis, and disseminated infection of varicella-zoster virus (VZV), are typical among ATL patients due to their immunosuppressed state (Proietti et al., 2005).

In a meta-analysis covering epidemiological studies from five continents, Schierhout and colleagues showed that HTLV-1 infected individuals are at 57% more risk of premature death compared to HTLV-1 negative individuals, and this increased risk is independent of either ATL or HAM/TSP, the two most significant causes of mortality and morbidity among HTLV-1 patients (Schierhout et al., 2020). Although most HTLV-1-infected individuals remain disease-free from HTLV-1 for life, the minority developing HTLV-1-associated diseases has minimal therapeutic options, often palliative. Novel effective therapeutic interventions are critically needed to reduce the social and economic impact caused by HTLV-1-associated diseases.

1.7 HTLV-1 genome and viral proteins

HTLV-1 is a complex retrovirus that effectively uses its 9 kb RNA genome to encode multiple structural, enzymatic, regulatory, and accessory proteins through ribosomal frameshifting, alternative splicing, and bidirectional transcription. The HTLV-1 virion comprises two copies of single-stranded RNA genome that is reverse-transcribed and integrated into the host cell genome to form the provirus. HTLV-1 proviral genome contains the classic replication-competent exogenous retroviral structural and enzymatic genes *gag*, *pro*, *pol*, and *env* flanked by two identical long terminal repeats (LTRs) (Figure 1-2) (Boxus and Willems, 2009). The pX region between *env* and 3' LTR encodes the regulatory proteins Tax, HTLV-1 basic leucine zipper factor (HBZ), and Rex and the accessory proteins p12, p13, and p30.

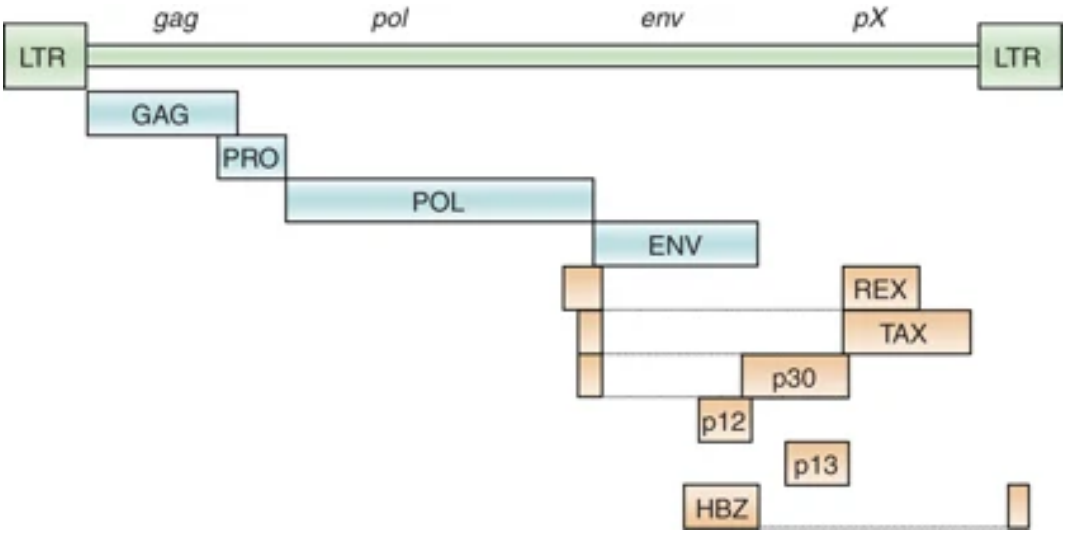

Figure 1-2. The genome of HTLV-1.
Two LTRs flank the 9 kb genome. In addition to *gag*, *pol*, and *env,* the *pX* region encodes several regulatory and accessory proteins.
Figure reproduced from (Boxus and Willems, 2009) under the terms of the Creative Commons Attribution License.

1.7.1 Long terminal repeats

The flanking 5' and 3' LTRs generated during the reverse transcription step act as promoters for viral gene expression from plus- and minus-strands, respectively. All viral proteins are expressed from the plus-strand, with the exception of HBZ, which is expressed from the minus-strand (Gaudray et al., 2002). The LTR comprises unique 3' (U3), repeated (R) and unique 5' (U5) regions. The U3 region contains three semi-conserved 21 base-pair repeats called the Tax-responsive element 1 (TxRE 1) that are crucial for Tax-mediated transactivation of viral transcription (Brady et al., 1987). The semi-conserved central domain (domain B) of each TRE 1 consists of eight nucleotides 5'-TGACG(T/A)(C/G)(T/A)-3', which is similar in sequence to the cyclic adenosine monophosphate (cAMP)-responsive element (CRE) 5'-TGACGTCA-3'

forming the viral CRE (vCRE) (Jeang et al., 1988). The 5' end of the central domain is flanked by a G-rich sequence (domain A), while a C-rich sequence (domain C) flanks the 3' end.

1.7.2 Structural proteins

1.7.2.1 Gag

Gag polyprotein (Gag, p55) is produced from the full-length messenger ribonucleic acid (mRNA). Gag is cleaved by the viral protease (PR) to form the structural proteins; matrix (MA, p19), capsid (CA, p24), and nucleocapsid (NC, p15) (Hattori et al., 1984). Matrix protein forms a shell in close proximity to the inner viral membrane and facilitates anchoring of Gag polyprotein to the plasma membrane (Lyngdoh et al., 2019). Nucleocapsid protein binds to the viral genomic RNA to create an NC-RNA complex that is surrounded by a spherical core formed by the capsid protein.

1.7.2.2 Pol

Gag-Pro and Gag-Pro-Pol polyproteins, produced through ribosomal frameshifting, undergo viral proteolytic cleavage to form Pro and Pol proteins, respectively (Nam et al., 1993). Pol polyprotein (p98) undergoes further viral proteolytic cleavage to form the reverse transcriptase (RT, p62) and integrase (IN, p49) enzymes. HTLV-1 reverse transcriptase catalyses the conversion of single-stranded viral RNA into double-stranded DNA that is subsequently integrated into the host cell DNA by the viral integrase.

1.7.2.3 Env

Envelope protein is produced from a singly spliced mRNA. As with other retroviruses, the precursor Env polyprotein (gp68) is cleaved by a cellular protease to form two subunits: surface glycoprotein (SU, gp46) and transmembrane protein (TM, gp21) (Delamarre et al., 1996). The envelope protein of HTLV-1 promotes infectivity through surface subunit-mediated receptor binding followed by membrane fusion facilitated by the transmembrane subunit (Manel et al., 2005).

1.7.3 pX

The pX region of HTLV-1 contains four open reading frames (ORFs) that encode several regulatory and accessory proteins. Rex, Tax, and HBZ are the important regulatory proteins and are the best characterised. The pX accessory proteins are expressed at low levels and their role in HTLV-1 infection and pathogenesis *in vivo* remains less well understood.

1.7.4 Regulatory proteins

1.7.4.1 Tax

Translated from a doubly spliced mRNA encoded by the ORF IV, the 40 kDa nuclear protein Tax is the most studied among the HTLV-1 regulatory proteins. Tax affects both proviral expression and multiple cellular signalling pathways by interacting with the viral promoter and cellular transcription factors (Boxus et al., 2008). The N-terminal region of the 353 amino acid residue HTLV-1 Tax contains a cAMP response element-binding protein (CREB)-binding domain necessary for viral promoter activation (Goren et al., 1995). The central region includes an NF-κB activation domain (Hirai et al., 1994) and two ZIP domains that are necessary for

protein dimerisation and DNA interaction (Basbous et al., 2003). The C-terminal region contains a CREB/ATF activation domain (Semmes and Jeang, 1995). Tax also contains a nuclear localisation signal (NLS) in its N-terminal region and a nuclear export signal (NES) in the central region (Shirinian et al., 2013).

The most important function of Tax protein is the transactivation of the HTLV-1 plus-strand transcription and is used as a surrogate for plus-strand expression (Billman et al., 2017). Tax does not bind DNA directly: its binding to the viral promoter depends on the interaction with CREB/activating transcription factor (ATF) family transcription factors (Giam and Xu, 1989). Among multiple CREB/ATF transcription factors recruited on the vCRE, CREB is the most important in Tax-mediated transactivation (Currer et al., 2012). CREB, upon its recruitment by Tax, forms a homodimer through its bZIP domain interactions on the vCRE (Zhao and Giam, 1992). Tax homodimer subsequently interacts with CREB homodimer to form the Tax-CREB-TxRE ternary complex (Tie et al., 1996). Tax dimer interacts with GC-rich sequences flanking the vCRE to stabilise the Tax-CREB-TxRE complex (Lundblad et al., 1998). The co-activators CREB-binding protein (CBP) and its homologue p300 are recruited to the Tax-CREB-TxRE ternary complex to form the Tax-CREB-TxRE-CBP/p300 quaternary complex (Kwok et al., 1996). Phosphorylation of CREB at serine 133 is essential for the recruitment of CBP/p300 and stabilising the quaternary complex to initiate transcription (Ramírez and Nyborg, 2007). Tax has been shown to induce phosphorylation of CREB (Kim et al., 2007).

The co-activator complex CBP/p300 is a histone acetyltransferase (HAT) and the initiation of Tax-mediated transcription from the HTLV-1 promotor is attributed to this HAT activity (Lu et al., 2002). Multiple lines of evidence show a positive correlation between the levels of bound CBP/p300 at the viral promoter and the acetylation of histones H3 and H4 of the nucleosomes at the viral promoter (Lu et al., 2002; Lemasson et al., 2002). A histone chaperone, nucleosome assembly protein 1 (NAP 1) promotes nucleosome eviction at the viral promoter by

disassembling acetylated histones (Sharma and Nyborg, 2008). Tax also interacts with RNA polymerase II and the chromatin remodelling complex switch/sucrose non-fermentable (SWI/SNF) to clear the nucleosomes at the viral promoter (Lemasson et al., 2006). Through its interaction with transcription factors and chromatin-modifying enzymes, Tax promotes an open chromatin state at the viral promoter to transactivate viral gene expression.

Tax activates both canonical (Chu et al., 1998) and noncanonical (Xiao et al., 2001) nuclear factor kappa-light-chain-enhancer of activated B-cells (NF-κB) pathways (Figure 1-3) (Currer et al., 2012). NF-κB regulates the expression of a range of genes affecting multiple cellular functions, including the immune response, cell proliferation, apoptosis, and response to stress. Mammalian NF-κB consists of five structurally related transcription factors, including NF-κB1 (p50 and its precursor p105), NF-κB2 (p52 and its precursor p100), RelA (p65), RelB, and c-Rel (Siebenlist et al., 1994). In the inactive form, NF-κB dimers are associated with the inhibitory κB (IκB) proteins in the cytoplasm. The IκB kinase (IKK) complex mediates the activation of canonical and noncanonical NF-kB dimers through phosphorylation, ubiquitination, and proteasomal targeting of IκB-α and p100, respectively (Liu et al., 2017). The subsequent nuclear translocation and binding to the κB enhancer of the target genes by p50/RelA and p50/c-Rel dimers - for canonical pathway or p52/RelB dimer - for noncanonical pathway mediate transactivation or repression (Liu et al., 2017).

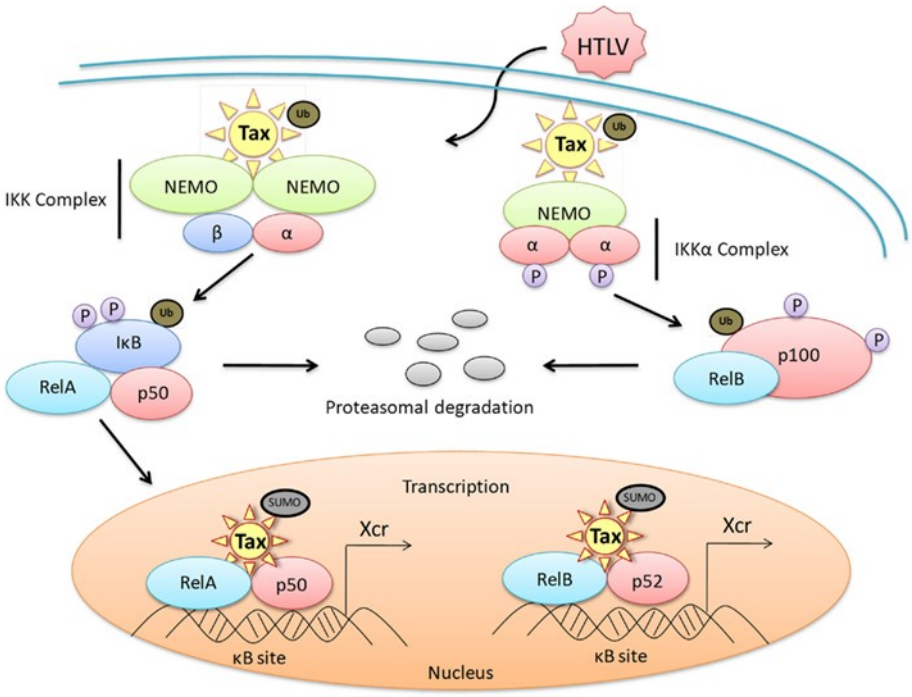

Figure 1-3. Tax-mediated activation of canonical and non-canonical NF-κB pathways. Ubiquitinated Tax interacts with NEMO, the regulatory subunit of IKK complex to promote phosphorylation, ubiquitination, and subsequent proteasomal degradation of IκB to release RelA-p50 dimer. Activated RelA-p50 translocates to the nucleus and binds the κB sites of the target genes to activate the canonical NF-κB pathway. Ubiquitinated Tax promotes the processing of p100 by IKK-α to form p52. RelB-p52 dimer shuttles to the nucleus to activate the non-canonical NF-κB pathway.
Figure reproduced from (Currer et al., 2012) under the terms of the Creative Commons Attribution License.

Tax interacts with both the regulatory (IKK-γ) (Jin et al., 1999) and catalytic (IKK-α and IKK-β) (Chu et al., 1998) subunits of the IKK complex to induce phosphorylation and proteasomal degradation of IκB-α and IκB-β to activate the canonical NF-κB pathway (Jin et al., 1999). Tax can also activate the canonical NF-κB pathway upstream of the IKK complex by activating and facilitating the physical interaction of TGF-β activating kinase 1 (TAK 1) and the IKK complex (Wu and Sun, 2007). Tax recruits IKK-α to the precursor protein p100/RelB dimer, leading to

the proteasomal processing of p100 to form the p52/RelB dimer, which subsequently translocates to the nucleus to activate the noncanonical NF-κB pathway (Xiao et al., 2001).

Tax functions as a cofactor for serum response factor (SRF) promoting its binding to the serum responsive elements (SREs) on target genes (Winter and Marriott, 2007). The co-activator complex CBP/p300 is recruited to the complex on SRE to activate Tax- and SRF-mediated transactivation (Shuh and Derse, 2000). Among the target genes of SRF are the activator protein 1 (AP-1) family of genes, which control various cellular functions, including proliferation, apoptosis, and transformation (Atsaves et al., 2019). It has been shown that Tax elevates the expression of several AP-1 genes, including *c-fos*, *fra 1*, *c-jun*, and *junD* (Hall and Fujii, 2005). AP-1 genes are also a target of the phosphoinositide-3-kinase/protein kinase B/Akt (PI3K-PKB/Akt) signalling pathway (Li et al., 2004). Tax directly binds to PI3K, thus activating it to promote the phosphorylation of Akt to activate the PI3K/Akt pathway (Peloponese and Jeang, 2006).

In addition to mediating the post-translational modifications (PTMs) on host cell proteins such as the IKK complex, Tax itself undergoes PTMs that determine its subcellular localisation and function. Ubiquitination of Tax medicated by an E2 ubiquitin-conjugating enzyme, Ubc13, is required for the binding of Tax to IKK γ to activate the canonical NF-κB pathway (Shembade et al., 2007). The ubiquitination of Tax by the E3 ubiquitin ligase, really interesting new gene (RING) finger protein 4 (RNF4), led to a change in Tax localisation pattern from nuclear to cytoplasmic, resulting in an increase in NF-κB activity and a reduction in LTR activity (Fryrear et al., 2012). The deubiquitinase, ubiquitin-specific peptidase 20 (USP20) inhibits Tax-mediated NF-kB activation by deubiquitinating Tax (Yasunaga et al., 2011). Acetylation of Tax by HAT, p300 is associated with increased NF-κB activation (Lodewick et al., 2009): Phosphorylation of Tax facilitates Tax-mediated activation of ATF/CREB and NF-κB pathways (Bex et al., 1999).

Tax expression upregulates the growth-promoting cytokine interleukin 2 (IL-2) (McGuire et al., 1993) and the alpha chain subunit of IL-2 receptor (IL-2Rα) (Ballard et al., 1988). One of the distinguishing characteristics of the cell transformation associated with HTLV-1 infection is the shift from an IL-2-dependent to an IL-2-independent proliferation status. HTLV-1 Tax has been shown to efficiently transform rat fibroblasts (Liu et al., 2001), mouse T-cells (Yoshita et al., 2012) and the development of leukaemia in transgenic mice (Grossman et al., 1995). However, *in vitro* transformation of primary human T-cells is rare (Bellon et al., 2010) and has only been achieved through transduction with Tax-expressing viral vectors (Grassmann et al., 2005). The observation that Tax expression is permanently silenced in half of ATL cases (Takeda et al., 2004) and the low frequency of expression among Tax-competent ATL cells (Mahgoub et al., 2018) suggest that Tax protein is only needed for the initial transformation, but not for the maintenance of the malignant clone, which may be achieved through the regulatory protein, HBZ.

In addition to activating viral transcription and multiple cellular signalling pathways discussed above, Tax protein through its interaction with multiple host cell proteins, exerts pleiotropic effects on the host cell, which are vital for viral persistence and pathogenesis. The effects of Tax protein on cellular processes, including cell cycle, proliferation, DNA damage response, and apoptosis are discussed in more detail in the subsequent chapters of this thesis.

1.7.4.2 HBZ

HBZ is the only HTLV-1 protein encoded on the minus-strand. HBZ was identified relatively late compared to the other HTLV-1 viral proteins – over two decades after the isolation of HTLV-1 (Gaudray et al., 2002). In addition to the N-terminal activation domain and the central domain, it contains a C-terminal leucine zipper motif, hence the name HTLV-1 Basic leucine-

zipper. There are two forms of *HBZ* mRNA transcripts: spliced *HBZ* (*sHBZ*), produced from several transcription start sites on U5 and R sections of the 3' LTR, and unspliced *HBZ* (*usHBZ*), transcribed from a single transcription start site in the pX region (Matsuoka and Green, 2009). Although the polypeptides translated from *sHBZ* and *usHBZ* are similar in size (206 and 209 amino acids, respectively), *sHBZ* is more abundant than *usHBZ* (Usui et al., 2008). There is also evidence that sHBZ protein is more stable than unspliced HBZ protein and that *sHBZ* mRNA, but not *usHBZ* mRNA, enhances cell proliferation (Yoshida et al., 2008). These observations suggest that sHBZ may be more important for the persistence and pathogenesis of HTLV-1.

HBZ mRNA (Billman et al., 2017) and protein (Hivin et al., 2005) are localised mainly within the nucleus through their poor polyadenylation (Ma et al., 2021) and nuclear localisation signals (Hivin et al., 2005), respectively. It has been previously shown that HBZ differentially affects the host cell at the protein and mRNA levels. According to one study, *HBZ* mRNA promoted proliferation while HBZ protein restricted Tax-induced transactivation of the 5' LTR (Satou et al., 2006). A study by Mitobe et al. reported that *HBZ* mRNA promoted the proliferation and survival of primary mouse T-cells, while HBZ protein induced proliferation and apoptosis (Mitobe et al., 2015). The diverse pathways induced by the different products of the *HBZ* gene may explain the observed differences in effects on the cell: *HBZ* mRNA upregulated genes associated with proliferation and survival, whereas HBZ protein altered the expression of genes affecting the immune function (Mitobe et al., 2015).

Many activities of HBZ protein directly antagonise those of Tax protein, suggesting the existence of a balance between the two opposing effects of Tax and HBZ in HTLV-1 persistence and pathogenesis. HBZ inhibits the Tax-activated canonical NF-κB pathway by downregulating the canonical NF-κB target genes, binding to p65 to reduce its DNA binding ability and enhancing the degradation of p65 through ubiquitination (Zhao et al., 2009). The

inhibition of the canonical NF-κB pathway by HBZ is indeed beneficial to the virus as it has been shown to mitigate the cellular senescence brought about by Tax-mediated NF-κB hyperactivation (Zhi et al., 2011). Through its bZIP domain, HBZ interacts with bZIP domain-containing AP-1 family transcription factors which are activated by Tax, including CREB/ATF, Jun, and Fos to suppress their activity (Matsumoto et al., 2005; Matsuoka and Mesnard, 2020). HBZ inhibits Tax-mediated transactivation at the 5' LTR by forming heterodimers with CREB protein 1 (CREB 1) (Lemasson et al., 2007) and protein 2 (CREB 2) (Gaudray et al., 2002), thus preventing the binding of CREB proteins to the vCRE. This control of proviral expression by HBZ may provide HTLV-1 with a survival advantage because the infected cell is less likely to be recognised by the host immune system.

There is evidence from patient PBMCs (Usui et al., 2008) and a rabbit model of HTLV-1 infection (Li et al., 2009) of a positive correlation between the *HBZ* mRNA levels and the PVL. According to a study by Saito and colleagues, there was a strong positive correlation between the *HBZ* mRNA levels and the disease severity among HAM/TSP patients (Saito et al., 2009). Tax expression is silenced in around half of ATL cases (Takeda et al., 2004), while *HBZ* mRNA is detected in all ATL patients (Satou et al., 2006). There are also several lines of evidence that suppression of *HBZ* expression results in diminished proliferative capacity of ATL cells (Satou et al., 2006; Nakagawa et al., 2018). These observations, combined with reduced PVL and HTLV-1-associated disease reported in individuals with an efficient CTL response against HBZ (Macnamara et al., 2010; Hilburn et al., 2011), provide strong evidence for the involvement of HBZ in HTLV-1 persistence and pathogenesis.

1.7.4.3 Rex

Rex is translated from a doubly spliced mRNA encoded by the ORF III. There are two isoforms: The full-length p27Rex and the truncated p21Rex produced from transcripts lacking exon 2 (Kiyokawa et al., 1985). The full-length Rex is localised in the nucleolus, while the truncated p21Rex, which lacks an NLS is cytoplasmic (Kiyokawa et al., 1985). The role of p21Rex in HTLV-1 infection remains unclear. From here onwards, the word "Rex" refers to p27Rex.

The initial phase of HTLV-1 proviral expression is characterised by the preferential production of doubly spliced *tax/rex* mRNA (Hidaka et al., 1988). Rex changes this expression pattern by stabilising the unspliced and partially spliced viral transcripts, which are otherwise prone to further splicing or degradation by the host cell RNA machinery. The stabilisation of unspliced or partially spliced transcripts is achieved by Rex binding and forming multimers on the Rex-response element (RxRE) at the 3' end of viral mRNA transcripts (Unge et al., 1991). The precise molecular mechanisms by which Rex limits further splicing remain to be elucidated. Rex interacts with the nuclear export protein, chromosome region maintenance 1 (CRM1) to mediate the preferential nuclear-to-cytoplasmic shuttling of the unspliced and singly spliced viral mRNAs (Hakata et al., 1998). Post-transcriptional regulation by Rex results in a biphasic pattern of HTLV-1 expression, which limits Tax-mediated transactivation (Rende et al., 2011).

1.7.5 Accessory proteins

1.7.5.1 p12

p12 is translated from a singly spliced mRNA encoded by the ORF I. p12 has been shown to suppress the in vitro CTL-mediated immune response against HTLV-1 through its interaction

with newly synthesised, free heavy chains of major histocompatibility complex (MHC) class I molecules, resulting in their proteasomal degradation (Johnson et al., 2001). There is also evidence for p12-mediated T-cell proliferation through its interaction with the β and γ chains of the IL-2 receptor to activate the downstream signalling pathways (Mulloy et al., 1996).

1.7.5.2 p8

Proteolytic cleavage of p12 to remove its endoplasmic reticulum (ER) retention motif forms the T-cell membrane resident viral accessory protein p8. It enhances HTLV-1 infectivity through induction clustering of LFA-1 molecules on the infected cell surface and increasing the frequency and length of cellular conduits (Van Prooyen et al., 2010).

1.7.5.3 p30

ORF II encodes p30 from a doubly spliced mRNA. At lower concentrations, it has been shown that p30 activates the HTLV-1 LTR, while at high concentrations, it represses HTLV-1 LTR-driven reporter activity (Zhang et al., 2000). p30 also acts as a negative regulator of HTLV-1 expression at the post-transcriptional level by binding and inhibiting the nuclear export of the doubly-spliced *tax/rex* mRNA (Nicot et al., 2004).

1.7.5.4 p13

p13, produced from a single-spliced mRNA encoded by the ORF II, primarily localises within mitochondria. Ectopic p13 expression has been shown to induce mitochondrial swelling by increasing their membrane permeability to increase the inward flow of potassium ions (K^+) and augment the production of reactive oxygen species (ROS) (Silic-Benussi et al., 2009). These

p13-mediated changes in mitochondria may have significant consequences on cellular processes controlled by mitochondria, including metabolism, apoptosis, and intracellular signalling.

1.8 Immune response to HTLV-1

HTLV-1 is an obligatory intracellular pathogen that causes a lifelong persistent infection. It encounters a robust cellular immune response *in vivo* that determines the clonal diversity and abundance, and hence the PVL set point, the principal predictor of HTLV-1-associated diseases.

1.8.1 Innate immune response

The cells of the adaptive immune system, primarily $CD4^+$ T-cells are the main target of HTLV-1 infection *in vivo*. Several cell types of the innate immune system, including DCs, natural killer (NK) cells, monocytes, and macrophages are susceptible to HTLV-1 infection either *in vivo* or *in vitro* or both (Journo and Mahieux, 2011).

Dendritic cells, specifically plasmacytoid DCs (pDCs) are the principal producers of Type 1 interferons (IFN I). IFN I are one of the first cytokines produced in response to a viral infection and play a critical role in controlling the infection by inducing the expression of interferon-stimulated genes (ISGs) (Schoggins et al., 2011). Several groups have independently demonstrated an IFN I-mediated antiviral response against HTLV-1 *in vitro*: Co-culture with cell-free HTLV-1 induced IFN α production in primary human pDCs (Colisson et al., 2010). In a recent study, Assil and colleagues showed that HTLV-1 viral biofilms induced a more robust IFN I response in pDCs compared to cell-free virions (Assil et al., 2019). The degree of

IFN I production by pDCs was dependent on the composition of the ECM around the viral biofilm and negatively correlated with the level of β-galactoside glycosylation. Cachat et al. showed that IFN α inhibited *de novo* infections in primary lymphocytes by activating the ISG, protein kinase R (PKR) resulting in decreased expression of viral proteins (Cachat et al., 2013). In a subsequent study, the same research group showed that PKR was not activated by IFN α in the presence of exogenous adenosine deaminase acting on RNA 1 (ADAR1), another ISG that is elevated in naturally HTLV-1-infected primary $CD4^+$ T-cells, thus abolishing the inhibitory effect of IFN α on HTLV-1 infection (Cachat et al., 2014). Based on these *in vitro* studies, it seems the equilibrium between inhibitory and activating ISGs determines the course of the initial stages of HTLV-1 infection.

The role of IFN I in HTLV-1 infection and pathogenesis *in vivo* is less clear. The use of IFN I for treating HTLV-1-associated diseases has yielded promising results. According to a meta-analysis, using IFN α in combination with nucleoside reverse transcriptase inhibitor (NRTI) AZT as first-line antiretroviral therapy resulted in higher five-year overall survival in chronic, smouldering, and acute ATL patients compared to patients who received first-line chemotherapy (Bazarbachi et al., 2010). However, the patients with lymphoma ATL who received antiretroviral therapy with IFN α and AZT had a lower five-year overall survival than those who received first-line chemotherapy. The favourable outcome observed in most ATL subtypes in response to combined IFN α and AZT treatment was attributed to the activation of the p53 pathway resulting in apoptosis of ATL patient-derived cell lines (Kinpara et al., 2013). A study in Japan involving twenty-five HAM/TSP patients showed that IFN α treatment reduced PVL and improved clinical symptoms, particularly in patients with mild symptoms and short disease duration (Saito et al., 2004).

According to one study, the number of circulating pDCs was lower in ATL patients and their PBMCs produced significantly less IFN α *ex vivo* than PBMCs from asymptomatic carriers

(Hishizawa et al., 2004). These observations suggest that an impaired IFN I response contributes to the development of ATL. On the other hand, microarray analysis of *ex vivo* PBMCs revealed overexpression of ISGs in HAM/TSP patients compared to asymptomatic carriers (Tattermusch et al., 2012). The intensity of ISG overexpression correlated with disease severity among HAM/TSP patients, and the treatment of *ex vivo* $CD8^+$ T-cell-depleted PBMCs with exogenous IFN did not affect the expression of the viral transcriptional transactivator protein, Tax (Tattermusch et al., 2012). These findings suggest that an elevated IFN response contributes to the HAM/TSP pathogenesis without significant antiviral activity.

HTLV-1 has evolved to counterbalance the effects of IFN I through multiple mechanisms. HTLV-1 Tax protein suppresses IFN 1 signalling and production through upregulation and stabilisation of suppressor of cytokine signalling 1 (SOCS 1) and inhibition of TANK Binding Kinase 1 (TBK1), the enzyme responsible for activation of Interferon Regulatory Factor 3 (IRF3), a transcription factor which activates IFN promoters (Charoenthongtrakul et al., 2011; Yuen et al., 2016).

The frequency of innate immune cells, including NK, and invariant natural killer T-cells (iNKTs) is lower in ATL and HAM/TSP patients (Azakami et al., 2009). NK cells from HTLV-1-infected individuals showed spontaneous expansion *ex vivo*, which weakly correlated with the PVL (Norris et al., 2010). There is also evidence of e*x vivo* expansion of iNKT-cells and subsequent reduction in PVL in PBMCs from asymptomatic carriers but not ATL or HAM/TSP patients (Azakami et al., 2009). However, the contribution of NK and iNKT-cells to controlling HTLV-1 infection *in vivo* is unknown.

1.8.2 Adaptive immune response

There is a robust host humoral immune response against HTLV-1 infection. Antibodies against the core structural protein Gag are the first to appear, followed by antibodies against the envelope glycoprotein (Manns et al., 1991). Antibodies against the regulatory proteins Tax and HBZ are also detected and vary according to the disease status: Anti-Tax antibodies were detected in 96% of HAM/TSP patients, 42% of ATL patients, and 59% of asymptomatic carriers (Lal et al., 1994). Anti-HBZ antibodies were detected in 10% of asymptomatic carriers, 17% of ATL patients, and 11% of HAM/TSP patients (Shiohama et al., 2016). The low frequency of anti-HBZ antibodies might be due to the low level of HBZ protein expression and its low immunogenicity. Due to the cell-intrinsic nature of HTLV-1, the impact of the humoral immune response in controlling HTLV-1 infection is minimal.

Chronically activated circulating HTLV-1 antigen-specific CTLs are a hallmark of HTLV-1 infection (Jacobson et al., 1990; Parker et al., 1992). Anti-HTLV-1 $CD8^+$ T-cells exert a robust immune response against HTLV-1 antigens, particularly Tax protein (Goon et al., 2004a). There is compelling evidence from multiple studies that CTL response against HTLV-1 reduces PVL and risk of HAM/TSP: Jeffery and colleagues showed that carrying either of HLA class 1 genes *HLA-A*02* or *HLA-Cw*08* was associated with a lower PVL and a reduced risk of inflammatory disease among HTLV-1-infected individuals from a population with endemic HTLV-1 infection in Southern Japan (Jeffery et al., 1999). Using gene expression analysis, Vine et al. showed high expression levels of genes associated with cell-mediated cytotoxicity in circulating $CD8^+$ T-cells from infected individuals with low PVL (Vine et al., 2004). Furthermore, it has been shown using *ex vivo* lysis assays that autologous CTLs eliminate naturally-infected Tax-expressing cells in a dose-dependent manner (Hanon et al., 2000; Asquith et al., 2005). In a recent study, Boelen et al. showed that the interaction of the inhibitory isoform of the killer-cell immunoglobulin-like receptor (iKIR) on $CD8^+$ T-cells with their HLA

class 1 ligand enhanced the CTL responses against chronic viral infections, including HTLV-1, HIV-1, and hepatitis C virus (HCV) (Boelen et al., 2018).

However, it has also been reported that HTLV-1 PVL and functional anti-HTLV-1 CTLs showed a positive correlation in HAM/TSP patients (Kubota et al., 2000), suggesting the increase of CTL numbers is simply a consequence of the increase in PVL and potentially contributes to the pathogenesis. Kattan and colleagues showed that the lytic efficacy of HTLV-1-specific $CD8^+$ T-cells cells negatively correlated with both PVL and proviral expression (Kattan et al., 2009). On the other hand, the avidity of the CTLs positively correlated with lytic efficacy. It is now accepted that the principal determinant of the efficacy of the CTL-mediated immune response is not the frequency but the "quality" of HTLV-1-specific CTLs, which depends on the avidity of the CTL for its cognate antigen (Bangham, 2009).

In principle, one would expect the CTL response against the highly expressed and immunodominant Tax protein would determine the PVL and risk of HTLV-1-associated diseases. The work of MacNamara et al. proved this is not the case (Macnamara et al., 2010). Using epitope prediction methods to measure the peptide binding affinities, they found that the strength of HBZ peptide binding of HLA Class 1 alleles from asymptomatic carriers was significantly higher than that of HAM/TSP patients. The frequency of HBZ peptide-binding HLA class 1 alleles also strongly inversely correlated with the PVL in both asymptomatic carriers and HAM/TSP patients. *Ex vivo* analysis of infected blood samples showed that HBZ-specific CTL responses were more frequent among asymptomatic carriers with low PVL (Hilburn et al., 2011), providing further evidence to suggest the protective role of anti-HBZ CTL response against HTLV-1.

$CD4^+$ T-cells are the primary target of HTLV-1, carrying more than 90% of the PVL (Richardson et al., 1990). The anti-HTLV-1 $CD4^+$ immune response is primarily directed

towards the envelope glycoprotein (Goon et al., 2004b). Although the frequency of the responding T-cells is lower, smaller responses against the structural proteins, Gag and Pol and the regulatory proteins Tax and Rex do occur. Although the $CD4^+$ T-cell response is required for an efficient CTL and antibody response, there is little evidence to suggest that the HTLV-1-specific $CD4^+$ T-cell response itself provides effective protection against HTLV-1-associated diseases. However, several lines of evidence suggest that the $CD4^+$ T-cell response against HTLV-1 contributes to HAM/TSP pathogenesis: First, the frequency of infiltrating $CD4^+$ cells in the inflammatory lesions in the CNS of HAM/TSP patients correlated positively with the PVL in the lesions (Kubota et al., 1994). Second, HAM/TSP patients had a 25-fold higher frequency of interferon gamma (IFN γ)-secreting anti-HTLV-1 $CD4^+$ T-cells than asymptomatic carriers with comparable PVLs (Goon et al., 2004b).

HTLV-1-infected cells, including malignant cells express several immune markers that are characteristic of regulatory T-cells, such as CD4, FoxP3, CD25, and CCR4. HTLV-1 Tax protein induces the infected cells to produce C-C motif chemokine ligand 22 (CCL22), a chemokine that binds CCR4 (Hieshima et al., 2008). Tax-mediated CCL22 production sustains the high frequency of circulating $CD4^+FoxP3^+$ T-cells – which include regulatory T-cells observed in HTLV-1 infection (Toulza et al., 2010). Using an *ex vivo* lysis assay, Toulza and colleagues showed a strong inverse correlation between the abundance of $CD4^+FoxP3^+$ T-cells and the clearance of HTLV-1 infected cells by the CTLs, suggesting that regulatory T-cells may dampen the CTL-mediated immune response to HTLV-1 (Toulza et al., 2008).

1.9 The regulation of HTLV-1 proviral latency and expression

The regulation of HTLV-1 proviral gene expression is critical for its persistence and pathogenesis. The proviral expression is essential for *de novo* infection both within and between hosts, but comes at a cost due to the exposure to the host's immune system. Therefore, the virus must balance between proviral expression and latency through the concerted expression of its viral proteins.

HTLV-1 virions and plus-strand transcripts are rarely detected in freshly isolated infected blood (Satou et al., 2006; Demontis et al., 2015). The lack of detectable viral transcripts and the existence of long-lived non-malignant T-cell clones have led to the belief that the provirus is transcriptionally silent *in vivo*. However, two key questions contradict this view: First, what confers the long-term survival advantage to the infected cells over uninfected cells? In other words, what drives the clonal expansion of the infected cells? Second, how does a chronically activated CTL response against HTLV-1 antigens exist if the provirus is latent *in vivo*? Persistent CTL activation requires the presentation of newly processed viral peptides on MHC class l molecules on the surface of the infected cells, implying the frequent synthesis of viral antigens, particularly the immunodominant Tax. Indeed, there is recent evidence from the single-cell analysis of *ex vivo* PBMCs (Miura et al., 2019), naturally-infected T-cell clones (Billman et al., 2017), and ATL cell lines (Mahgoub et al., 2018) that both the plus- and minus-strands of HTLV-1 are expressed in intermittent bursts.

The precise mechanisms by which the proviral expression from plus- and minus-strands of HTLV-1 are initiated *in vivo* remain largely unexplored. There is evidence of biphasic HTLV-1 proviral gene expression through transcriptional analysis of *ex vivo* patient PBMCs (Rende et al., 2011). During the initial phase of HTLV-1 proviral expression, doubly spliced *tax/rex* mRNA is produced by the host cell splicing machinery (Hidaka et al., 1988). Tax is

preferentially translated over Rex due to its robust Kozak sequence (Rosenblatt et al., 1988). Tax, in turn mediates a positive feedback loop (discussed in detail in section 1.7.4.1) that increases plus-strand transcription, producing more doubly spliced viral transcripts. During the second phase, the progressive accumulation of Rex mediates the nuclear export of unspliced and singly spliced viral transcripts (Hakata et al., 1998) to promote the translation of viral structural proteins to initiate viral replication. Several negative regulatory mechanisms limit proviral expression: HBZ competes with Tax to bind CREB (Lemasson et al., 2007) and CBP/p300 (Clerc et al., 2008) to limit Tax mediated transactivation. The binding of p13 to Tax suppresses the interaction of Tax with co-activators CBP/p300 (Andresen et al., 2011). The nuclear retention of *tax/rex* mRNA by p30 results in decreased Tax and Rex proteins levels leading to diminished proviral expression and replication, promoting the entry to proviral latency (Nicot et al., 2004).

Ex vivo culture of HTLV-1-infected PBMCs leads to spontaneous proviral plus-strand reactivation (Hanon et al., 2000) in a p38 mitogen-activated protein kinase (p38 MAPK) dependent manner (Kulkarni et al., 2018). Hypoxia, a stimulus known to activate p38 MAPK, augmented HTLV-1 reactivation in PBMCs, whereas small-molecule inhibition of glycolysis and mitochondrial electron transport chain suppressed proviral reactivation (Kulkarni et al., 2017). $CD4^+$ T-cells, the primary reservoir of HTLV-1, spend most of their time in the lymphatic system, an environment that is more hypoxic than the peripheral circulation (Tsai et al., 2004). Although the HTLV-1 provirus is latent in the peripheral circulation, tissue compartments with low oxygen tension may be more conducive to active proviral expression. Consistent with this idea, there is evidence from a Japanese macaque model of enhanced *tax* mRNA expression in the bone marrow, a tissue that is known to be hypoxic (Furuta et al., 2017).

The genomic environment of the host cell into which HTLV-1 is integrated affects the proviral expression. Spontaneous proviral expression is associated with the integration of the provirus within a host gene (Melamed et al., 2013). Integration in the same transcriptional orientation as a neighbouring host gene in close proximity (1 kb) is associated with proviral silencing, possibly through transcriptional interference (Melamed et al., 2013).

The epigenetic landscape of the provirus, particularly its promotor regions, affects proviral expression. The HTLV-1 5' LTR shows variable degrees of methylation, and its hypermethylation is associated with proviral silencing, while the 3' LTR is rarely methylated (Taniguchi et al., 2005). The reason for the differential DNA methylation patterns between 5' and 3' LTRs of HTLV-1 was not known until recently: Within the pX region of HTLV-1 genome is a binding site for the architectural protein CCCTC-binding factor (CTCF) (Satou et al., 2016). In addition to functioning as a transcription factor regulating gene expression, CTCF functions as an insulator limiting the propagation of epigenetic marks (Ong and Corces, 2014). Indeed, it has recently been shown that mutation of the CTCF binding site augmented the DNA methylation downstream of the CTCF binding site extending up to the 3' LTR (Cheng et al., 2021).

Histone acetylation is vital for HTLV-1 plus-strand transactivation, as evidenced by the recruitment of HATs CBP and p300 to the viral promoter by Tax and pCREB to meditate nucleosome eviction, as explained in more detail in section 1.7.4.1. HTLV-1 reactivation and Tax expression are associated with the enrichment of multiple activatory histone modifications, including H3K4me3, H3K36me3, H3K9Ac, and H3K27Ac at the viral promoter (Kulkarni et al., 2017; Miura et al., 2018). Proviral latency is associated with the presence of H2AK119ub1 at the viral promoter, potentially forming an epigenetic barrier to proviral reactivation (Kulkarni et al., 2018). Since epigenetic modifications are frequently both the cause and the consequence of host gene expression, it remains unclear which epigenetic modifications are

responsible for proviral reactivation, and which are merely an effect of the surrounding created during the reactivation.

There is significant variation in the expression levels of the plus-strand at the single-cell level (Billman et al., 2017; Miura et al., 2019). The plus-strand bursts are rare and often intense, while the bursts of *HBZ* are more frequent and lower in intensity. Different promoter architectures that control the expression of the plus- and minus-strands may explain these differences. HTLV-1 plus-strand is expressed from a promoter with a TATA-box sequence. *HBZ,* on the other hand is transcribed from a TATA-less promoter, and transcriptional factor specificity protein 1 (Sp1) is crucial for its promoter activity (Yoshida et al., 2008). The TATA-box is a promoter element with a short stretch of TA nucleotides. Promoters containing the TATA-box are typically associated with variable gene expression levels, while TATA-less promoters typically drive more constant gene expression (Landry et al., 2007). Until recently, it was believed that HBZ is constitutively expressed in all HTLV-1 infected cells. There is recent evidence from the single-cell analysis of naturally HTLV-1-infected T-cell clones (Billman et al., 2017) and *ex vivo* PBMCS from HTLV-1-infected individuals (Miura et al., 2019) that *HBZ* is expressed only in a subset (20% to 50%) of infected cells at any given time.

1.10 Aims

Only a handful of studies to date have characterised the dynamics of HTLV-1 expression at the single-cell resolution (Billman et al., 2017; Mahgoub et al., 2018; Miura et al., 2019). While these studies provided valuable insights into HTLV-1 proviral expression, each study had its own limitations – discussed in section 3.2.3. Several studies, including (Kataoka et al., 2015; Mahgoub et al., 2018; Melamed et al., 2018; Vandermeulen et al., 2021) have reported host gene expression during HTLV-1 expression. However, none of these studies investigated the changes in the host gene expression during the successive phases of an HTLV-1 plus-strand burst. The impact of HTLV-1 expression, specifically Tax, on the host cell has been studied extensively. However, most of these studies, which have sometimes yielded conflicting observations, have been performed using recombinant plasmid-based systems in cell types that are not generally associated with HTLV-1 infection or HTLV-1-infected transformed cell lines that express Tax continuously at high levels, in contrast to naturally-infected T-cells.

Using naturally HTLV-1-infected non-malignant $CD4^+$ T-cell clones as the model system, I aimed to answer three main questions during this project:

1. What are the dynamics and the extent of heterogeneity of plus-strand (Tax) expression at the single-cell level?
2. How does the host cell transcription change during successive stages of an HTLV-1 plus-strand burst?
3. What are the immediate and longer-term consequences of plus-strand (Tax) expression on the host cell?

Chapter 2 – Materials and methods

2.1 Cell culture

HTLV-1-infected T-cell clones, the type 2 defective T-cell clone, and the uninfected T-cell clone used in this thesis were isolated by Lucy Cook and colleagues by limiting dilution of $CD4^+CD25^+$ T-cells from HAM/TSP patients (Cook et al., 2012). All cultures were propagated in a 37ºC, 5% CO_2 incubator. The details of T-cell clones and cell lines used in this thesis are given in Table 1.

2.1.1 HTLV-1 infected and uninfected T-cell clones

Each T-cell clone is a population of cells that share a unique HTLV-1 proviral integration site. All T-cell clones were cultured in RMPI-1640 (Sigma-Aldrich) supplemented with 20% fetal calf serum (FCS), 50 IU/ml penicillin, 50 µg/ml streptomycin, 2 mM L-glutamine (all from Thermo Fisher Scientific), and 100 IU/ml human IL-2 (Miltenyi Biotec). Ten micromolar of an integrase inhibitor, raltegravir (Selleck Chemicals) were added to HTLV-1-infected T-cell clones to prevent secondary infections. The cultures were re-supplemented with IL-2 and raltegravir twice a week.

2.1.2 Cell-lines

All cell lines were cultured in RMPI-1640 supplemented with 10% FCS, 50 IU/ml penicillin, 50 µg/ml streptomycin, and 2 mM L-glutamine.

Table 1. Details of T-cell clones and cell lines used in this thesis.

T-cell clone/cell line	Patient Code	Proviral integration site – GRCh38	Remarks
TBX4B	TBX	Chr 22: 43, 927, 318	T-cell clone with a single provirus
TBW 11.50	TBW	Chr 19: 27, 791, 679	T-cell clone with a single provirus
TBJ 3.60	TBJ	Chr 4: 69, 701, 567	T-cell clone with a single provirus
TCX 8.13	TCX	Chr 16: 53, 567, 147	T-cell clone with a single type 2 defective provirus incapable of expressing the plus-strand
TBW 13.50	TBW	Not applicable	Uninfected T-cell clone
FT TBX4B	TBX	Chr 22: 43, 927, 318	TBX4B stably transduced with pLJM1-LTR-FT
FT TBJ 3.60	TBJ	Chr 4: 69, 701, 567	TBJ 3.60 stably transduced with pLJM1-LTR-FT
d2EGFP TBX4B	TBX	Chr 22: 43, 927, 318	TBX4B stably transduced with pLJM1-LTR-d2EGFP
d2EGFP TBW 11.50	TBW	Chr 19: 27, 791, 679	TBW 11.50 stably transduced with pLJM1-LTR-d2EGFP
d2EGFP TBW 13.50	TBW	Not applicable	TBW 13.50 stably transduced with pLJM1-LTR-d2EGFP
d2EGFP MT2	Not applicable	Not available	HTLV-1-infected transformed cell line stably transduced with pLJM1-LTR-d2EGFP
d2EGFP ED	Not applicable	Not available	HTLV-1-infected ATL cell line with a mutation in the *tax* gene stably transduced with pLJM1-LTR-d2EGFP

2.1.3 Automated cell counting

Automated fluorescence cell counting was performed using LUNA-FL automated cell counter (Logos Biosystems) using acridine orange (AO)/propidium iodide (PI) dye combination (Logos Biosystems). Eighteen microliters of cell suspension were mixed with 2 µl dye combination, and 10 µl of the cell-dye mixture was loaded into a counting slide. The viable cells that fluoresce green were distinguished from the dead ones that fluoresce red.

2.2 Production of HTLV-1-infected T-cell clones and cell lines expressing Tax reporter systems

I generated HTLV-1-infected T-cell clones and cell lines expressing the d2EGFP or fast timer protein Tax reporter system prior to officially registering for the PhD. Molecular cloning and lentiviral transduction used to create these Tax reporter T-cell clones and cell lines are described here for the completeness.

2.2.1 Molecular cloning

The d2EGFP Tax reporter system (pLJM1-LTR-d2EGFP) was created by digesting pLJM1-EGFP (Addgene 19319) with Ndel and EcoRl to generate the vector backbone. A PCR using a forward primer (5'-GCCACCATGGTGAGCAAGG-3') and a reverse primer (5'-TCGAGGTCGAGAATTCCTACACATTGATCCTAGCAGAAGC-3') with 15 bp overlap with the vector backbone were used to amplify the *destabilised enhanced green fluorescent (d2EGFP)* gene from pcDNA3.3_d2eGFP plasmid (Addgene 26821). A fragment containing nine copies of TRE type 1 and type 3 and a truncated 5' LTR was amplified from SMPU-18x21-EGFP plasmid (Zhang et al., 2006) by PCR using forward (5'-

AAATGGACTATCATATGCGGGTTTATTACAGGGACAGCG-3') and reverse (5'-GCTCACCATGGTGGCATCTCGCCAAGCTTGGATCTGT-3') primers with 15 bp overlap with the vector backbone and d2EGFP PCR product, respectively. Two PCR products were inserted into the digested vector backbone using In-Fusion HD Cloning Kit (Takara Bio). The sequence of the inserts within the lentiviral transfer plasmid was verified using sanger sequencing (GATC Biotech).

The fast timer protein Tax reporter system (pLJM1-LTR-FT) was created by digesting pLJM1-EGFP (Addgene 19319) with Ndel and EcoRl to generate the vector backbone. A PCR using a forward primer (5'-ATGGTGAGCAAGGGCGAG-3') and a reverse primer (5'-TCGAGGTCGAGAATTCTTACTTGTACAGCTCGTCCATGC-3') with 15 bp overlap with the vector backbone were used to amplify the *fast timer protein (FT)* gene from the pFast-FT-N1 plasmid (Addgene 31910). A fragment containing five tandem repeats of TRE type 2 and a truncated 5' LTR was amplified from WT-Luc plasmid (Fujisawa et al., 1989) by PCR using forward (5'-AAATGGACTATCATATGGGGAGGTACCGAGCTCTTACGC-3') and reverse (5'-GCCCTTGCTCACCATGGTGGCGGGCCAAGCCGGCAGTCA-3') primers with 15 bp overlap with the vector backbone and FT PCR product, respectively. In-Fusion HD Cloning Kit was used to insert the two PCR fragments into the digested vector backbone. Sanger sequencing was used to confirm the sequence of the inserts in the transfer vector.

2.2.2 Lentiviral production

Nineteen million human embryonic kidney (HEK) 293T cells were seeded per 150 mm tissue culture-treated dish (Corning) on the day before transfection to reach 95% confluency on the day of transfection. HEK 293T cells were co-transfected with either pLJM1-LTR-d2EGFP or pLJM1-LTR-FT, psPAX2 (Addgene 12260), and pCMV-VSV-G (Addgene 8454) using

Lipofectamine 3000 (Invitrogen) following manufacturer's protocol. Viral supernatants harvested 24- and 52-hours post-transfection were centrifuged at 2000 rpm for 10 minutes and filtered through a 0.45 μm filter (Sartorius). Viral supernatants were concentrated 150-fold through ultracentrifugation at 25000 rpm for 2 hours at 4ºC.

2.2.3 Transduction

One hundred thousand cells were spinoculated with 100 μl of concentrated lentiviral supernatant in the presence of 8 μg/ml polybrene and 10 mM HEPES (both from Sigma-Aldrich) at 800 g, 32ºC for 2 hours. Upon washing, transduced T-cell clones were cultured in complete medium supplemented with IL-2 and cell lines were cultured in complete medium without IL-2. Transduced cultures were supplemented with 2 μg/ml puromycin dihydrochloride (Thermo Fisher Scientific) twice weekly for 14 days starting on day 3 post-transduction to eliminate non-transduced cells. Puromycin was maintained at 1 μg/ml twice weekly to prevent the emergence of cells that do not have a functional antibiotic resistance transgene. d2EGFP or fast timer protein-expressing T-cell clones were subjected to fluorescence-activated cell sorting (FACS) to isolate cell populations expressing the reporter protein.

2.3 Flow cytometry

All flow cytometry and FACS sorting incubation and washing steps were performed at room temperature unless otherwise specified. All samples were acquired on a BD LSRFortessa flow cytometer (BD Biosciences) unless otherwise stated. Flow cytometry data were analysed using the FlowJo software (BD Biosciences).

2.3.1 Intranuclear protein staining

The cells were stained with the LIVE/DEAD Fixable Near-IR (Thermo Fisher Scientific) viability dye – referred to as viability dye here after unless a different viability dye was used, diluted at 1 μg/ml in phosphate-buffered saline (PBS) for 5 minutes after a single wash with PBS. After a single wash in FACS buffer (PBS + 5% FCS), the cells were fixed with fixation/permeabilisation buffer of eBioscience FOXP3/Transcription Factor Staining Buffer Set (Thermo Fisher Scientific) for 30 minutes. They were then washed once with the permeabilisation buffer of the FOXP3/Transcription Factor Staining Buffer Set and stained with 1 μg/ml anti-Tax monoclonal antibody conjugated to Alexa Fluor 647 (clone LT-4) diluted in permeabilisation buffer for 30 minutes. Either 2.5 μg/ml anti-Ki-67-Phycoerythrin (PE – BioLegend) or 1 μg/ml anti-γ-H2AX-PE (clone 2F3, BioLegend) antibodies were also added along with anti-Tax antibody in proliferation or DNA damage assays, respectively. IgG3 κ-AF-647 (clone MG3-35, BioLegend) was used as the isotype control for the anti-Tax antibody, while IgG1 κ-PE (clone MOPC-21, BioLegend) served as the isotype control for anti-Ki-67 and anti-γ-H2AX antibodies. The cells were washed twice in permeabilisation buffer and resuspended in FACS buffer.

2.3.2 Fluorescent protein detection

The cells were stained with the viability dye diluted at 1 μg/ml in PBS for 5 minutes after a single wash with PBS. They were then washed once with FACS buffer and fixed with 4% formaldehyde (Thermo Fisher Scientific) for 30 minutes. The cells were washed twice and resuspended in FACS buffer.

For simultaneous detection of fast timer and Tax proteins, the cells were fixed with 4% formaldehyde for 15 minutes following a wash with PBS and staining with the viability dye.

They were then washed with FACS buffer and permeabilised with 0.1% Triton X-100 (Thermo Fisher Scientific) for 15 minutes. After a single wash in FACS buffer, the cells were stained with 1 µg/ml anti-Tax monoclonal antibody diluted in FACS buffer for 30 minutes. They were subsequently washed twice and resuspended in FACS buffer.

2.3.3 Cell surface protein staining

The cells were washed once in PBS and incubated with the viability dye diluted at 1 µg/ml in PBS for 5 minutes. They were then washed once with FACS buffer before staining with either 1 µg/ml anti-ICAM-1-PE (clone HA-58, BioLegend) or 1 µg/ml anti-CCR4-PE (clone L291H4, BioLegend) diluted in FACS buffer for 30 minutes. IgG1 κ-PE (clone MOPC-21, BioLegend) was as the isotype control for anti-ICAM and anti-CCR4 antibodies. The cells were washed twice in FACS buffer, fixed with 4% formaldehyde for 30 minutes, washed twice and resuspended in FACS buffer.

2.3.4 Analysis of apoptotic cells

The recombinant protein, annexin V which binds to the externalised phosphatidylserine in apoptotic cells in a calcium-dependent manner (van Engeland et al., 1998) was used to detect the apoptotic cells. The cells were washed once with annexin V binding buffer (BioLegend), following a single wash with PBS. The cells were co-stained with 0.5 µg/ml annexin V-PE (BioLegend) and 1 µg/ml viability dye diluted in annexin V binding buffer for 15 minutes. They were then washed once with annexin V binding buffer supplemented with 5% FCS and fixed with 4% formaldehyde diluted 1:1 with annexin V binding buffer for 30 minutes. The cells were washed twice and resuspended in annexin V binding buffer containing 5% FCS.

2.3.5 Quantification of reactive oxygen species

CellRox Deep Red probe (Thermo Fisher Scientific) that fluoresces after ROS-mediated oxidation was used to detect ROS. One hundred thousand d2EGFP TBX4B and d2EGFP TBW 11.50 cells resuspended in complete medium were seeded into FACS tubes. The positive control included one hundred micromolar of tert-butyl hydroperoxide (TBHP), an inducer of ROS (Zhao et al., 2017), while 250 µm of a ROS scavenger, N-acetyl-L-cysteine (NAC) (Halasi et al., 2013) was used as the negative control. The cells were cultured for one hour. Five hundred nanomolar of CellRox Deep Red probe was added to each sample and incubated for further 45 minutes. The cells were washed once and resuspended in phenol red-free RPMI-1640 (Thermo Fisher Scientific) supplemented with 2% FCS. One micromolar SYTOX blue viability dye (Thermo Fisher Scientific) was added to the cells and incubated for 15 minutes. The cells were immediately acquired on a BD FACSAria lll cell sorter (BD Biosciences) housed under containment level 3 (CL3) conditions. The incubations were performed in a humidified incubator at 37°C, with 5% CO_2 and the washing was carried out at room temperature.

2.3.6 Analysis of cell cycle progression

A previously published assay (Mahgoub et al., 2018) that utilises the components of the Click-iT plus EdU AF-647 flow cytometry assay kit (Thermo Fisher Scientific) was used to determine the cell cycle progression among Tax-expressing and non-Tax-expressing cells. In this pulse-chase assay, 5-ethynyl-2'-deoxyuridine (EdU), a thymidine analogue is incorporated into the newly synthesised DNA of the proliferating cells during the pulse. The cells that have taken up EdU can be "chased" to determine the kinetics of cell cycle progression. Five hundred thousand d2EGFP TBX4B and d2EGFP TBW 11.50 cells cultured in a 48-well plate (Corning) were

pulsed with 10 µM EdU for 1.5 hours. The cells were washed three times in complete medium to remove any unincorporated EdU. Half of the cells were cultured in complete medium for a further 6.5 hours, which was the chase period. The cells harvested after the EdU pulse were treated to the point of fixation and stained together with the cells collected at the end of the EdU chase. The cells collected at the end of EdU pulse and chase were washed once in PBS and stained with the viability dye diluted at 1 µg/ml in PBS for 5 minutes. They were then washed once in FACS buffer and fixed with 4% formaldehyde for 30 minutes. The samples were permeabilised with 0.1% Triton X-100 for 15 minutes after two washes with FACS buffer. The cells were then washed twice and resuspended in 100 µl of FACS buffer before staining EdU with 500 µl of Click-iT plus reaction mix consisting of 438 µl PBS, 10 µl copper protectant, 2.5 µl AF-647 picolyl azide, 50 µl reaction buffer additive for 30 minutes. The samples were washed twice in FACS buffer and stained with 1 µg/ml FxCycle Violet DNA dye (Thermo Fisher Scientific) diluted in FACS buffer. The samples were acquired after 30 minutes of staining. EdU pulse and chase were performed in a humidified, 37ºC, 5% CO_2 incubator. Dean-Jett-Fox algorithm in FlowJo was used to determine the cell cycle stage of EdU^+ cells. The fraction of EdU^+ cells that had progressed to the G1 phase of the next cell cycle was determined using the gating strategy described by Weber et al. and depicted in Figure 5-1G (Weber et al., 2014).

2.3.7 FACS sorting

Mrs Parisa Amjadi performed FACS sorting of cells under CL3 conditions on a BD FACSAria lll cell sorter (BD Biosciences) housed in a custom tissue culture hood to maintain the sterility of the samples. All washes and incubations performed on cells before sorting were carried out at room temperature.

For sorting of viable, d2EGFP (d2EGFP$^+$ and d2EGFP$^-$) and fast timer protein (Blue$^-$Red$^-$, Blue$^+$Red$^-$, Blue$^+$Red$^+$ and Blue$^-$Red$^+$) populations, the cells were washed once with PBS and stained with 1 µg/ml viability dye diluted in PBS for 5 minutes. The cells were washed once and resuspended in RPMI-1640 without phenol red supplemented with 2% FCS before sorting the desired cell subsets.

For FACS sorting of viable apoptotic and non-apoptotic cells, the cells were washed once with PBS followed by a single wash with annexin V binding buffer. They were then co-stained with 0.5 µg/ml annexin V-PE and 1 µg/ml viability dye diluted in annexin V binding buffer for 15 minutes. Finally, the cells were washed and resuspended in annexin V binding buffer supplemented with 2% FCS before sorting.

2.3.8 Detection of Tax and d2EGFP expression in JPX-9 cells

Five hundred thousand d2EGFP JPX-9 cells were treated with either 10 µm cadmium chloride ($CdCl_2$ – Sigma-Aldrich) or water, the vehicle control for 24 hours in duplicate. Each sample was split in half and subjected to flow cytometry analysis after staining for either Tax or d2EGFP, as described in section 2.3.1 or 2.3.2, respectively.

2.3.9 Quantification of d2EGFP half-life

One hundred thousand cells from d2EGFP TBW 11.50 were treated with either 10 µg/ml protein synthesis inhibitor cycloheximide (Schneider-Poetsch et al., 2010) or the vehicle control, dimethyl sulfoxide (DMSO) (both from Sigma-Aldrich) in duplicate. The cells harvested at 0-, 3-, and 6-hours post-treatment were analysed by flow cytometry to detect d2EGFP expression as described in section 2.3.2. FlowJo software was used to determine the

median fluorescence intensity (MFI) of viable d2EGFP$^+$ cells. Linear regression analysis of the natural logarithm (ln) of d2EGFP MFI against time was performed using GraphPad Prism (GraphPad Software). Half-life ($T_{1/2}$) was calculated using the formula:

$$T_{1/2} = \frac{\ln(2)}{\alpha}$$

Here, α is the slope of the fitted line that indicates the protein degradation rate (Eden et al., 2011).

2.3.10 Toxicity quantification of latency-reversing agents

One hundred thousand d2EGFP TBX4B and d2EGFP TBW 11.50 cells were treated with either 10 nM bryostatin-1 (APExBIO) or 300 nM prostratin (Abcam) for 20 hours. Phorbol-12-myristate-13-acetate (PMA) at 50 ng/ml and ionomycin at 1 μm (both from Abcam) were used as the positive control, while DMSO was the vehicle control. The cells were analysed by flow cytometry to determine the proportion of early (annexin V$^+$ viability dye$^-$) and late (annexin V$^+$ viability dye$^+$) apoptotic cells after staining, as described in section 2.3.4.

2.4 Live-cell imaging

Incucyte S3 imaging system (Sartorius) housed in a humidified incubator maintained at 37ºC, 5% CO_2 was used for live-cell imaging. The acquisition time for green and red fluorescence images was 300 ms and 400 ms, respectively. Green fluorescence was used to detect HTLV-1 plus-strand (Tax)-expressing cells, while red fluorescence was used to identify the non-viable cells.

2.4.1 Single-cell analysis of Tax expression patterns

Five thousand d2EGFP TBX4B and d2EGFP TBW 11.50 cells resuspended in complete growth medium were seeded into a 96-well flat bottom tissue culture plate (Corning) pre-coated with 1 mg/ml Poly-D-Lysine (PDL – Sigma-Aldrich). Phase-contrast and green fluorescence time-lapse live-cell images were captured every 20 minutes for 30 hours using the 20x objective.

Unless otherwise specified, image analysis and quantification were done using ImageJ (Schneider et al., 2012). The initial image processing was done using a bespoke ImageJ macro that utilised the rolling ball algorithm to remove background noise from green fluorescence images and the Correct 3D drift plugin (Parslow et al., 2014) to correct the XY drift in the consecutive images. The phase-contrast image stack was exported and "trained" using the pixel classification workflow in the interactive learning and segmentation toolkit (ilastik) (Berg et al., 2019), which relies on pixel properties, including intensity and texture to identify the cells from the background. Using a second custom ImageJ macro, the segmented stack was imported, converted to a binary stack, and merged with the phase-contrast and green fluorescence stacks to create a three-channel hyper stack. The TrackMate plugin (Tinevez et al., 2017) was used to identify and track the individual cells in the binary channel whose mean green fluorescence intensity rose above the background during the observation period to identify different patterns of Tax expression.

2.4.2 Quantification of HTLV-1 plus-strand expression by latency reversing-agents

Twenty thousand cells from d2EGFP TBX4B and d2EGFP TBW 11.50 were seeded into a 96-well flat bottom plate pre-coated with 1 mg/ml PDL. The cells were treated with either single or dual latency-reversing agents (LRAs) at the following concentrations for 20 hours: 50 ng/ml PMA, 1 μM ionomycin, 10 nM bryostatin-1, 300 nM prostratin, 500 nM disulfiram (APExBIO), 1 μM JQ1 (APExBIO), 30 nM panobinostat (APExBIO), 40 nM romidepsin (APExBIO), and 5 μM valproate (APExBIO). The concentrations of LRAs were based on Laird et al. (Laird et al., 2015), except valproate, which was based on Mahgoub et al. (Mahgoub et al., 2018). The combination of PMA and ionomycin was the positive control, and DMSO was the vehicle control. The final percentage of DMSO was less than or equal to 0.25% (v/v) for single or dual LRA treatment conditions. Dead cells were labelled using 100 nM YOYO-3 Iodide dye (Thermo Fisher Scientific).

Nine phase-contrast, green, and red fluorescence images were captured for each treatment condition every 4 hours using the 20x objective. The images were analysed using the "Non-adherent Cell-by-Cell" image analysis module of Incucyte software using the parameters outlined in Table 2. The percentage of viable d2EGFP$^+$ cells for each treatment condition at 20 hours post-treatment was calculated and normalised to the DMSO treatment.

Table 2. Analysis parameters used to quantify the frequency of viable d2EGFP$^+$ cells in sections 2.4.2, 2.4.3, and 2.4.4.

Channel	Target cell type	Method of background fluorescence subtraction	Segmentation parameters
Phase	All	Not applicable	Sensitivity (threshold = 9, texture = 10, edge = 10), particle area = 30 – ∞ μm^2
Green	d2EGFP$^+$	Top-Hat with 50 μm radius	Not applicable
Red	Non-viable	Top-Hat with 50 μm radius	Not applicable

2.4.3 Quantification of spontaneous and maximal reactivation of latent HTLV-1

Fifteen thousand FACS-sorted d2EGFP$^-$ cells from d2EGFP TBX4B and d2EGFP TBW 11.50 were seeded into a 96-well flat bottom plate pre-coated with 1 mg/ml PDL. Bryostatin-1 and prostratin, the most potent single LRAs, were used at 10 nM and 300 nM, respectively. The combination of 50 ng/ml PMA and 1 μM ionomycin was used as the control for maximal reactivation. DMSO served as the vehicle control, while media alone was used to evaluate spontaneous proviral reactivation. One hundred nanomolar of YOYO-3 Iodide dye were used to identify dead cells. Nine phase-contrast, green, and red fluorescence images were captured for each treatment condition every 4 hours for 20 hours using the 20x objective. The images were processed using Incucyte software's "Non-adherent Cell-by-Cell" image analysis module with the settings listed in Table 2 to quantify the percentage of viable d2EGFP$^+$ cells under each treatment condition.

2.4.4 Quantifying the effect of AhR signalling on HTLV-1 plus-strand expression

FACS-sorted d2EGFP$^+$ and d2EGFP$^-$ cells from d2EGFP TBW 11.50 were seeded into a 96-well flat bottom plate pre-coated with 1 mg/ml PDL. AhR ligands ITE (APExBIO) and FICZ (a kind gift from Professor Brigitta Stockinger of Crick Institute) were added at 10 µM and 5 nM, respectively. The treatments also included AhR antagonists StemRegenin 1 (SR1 – APExBIO) at 1 µM and CH223191 (APExBIO) at 10 µM and an inhibitor of CYP1A1 enzymatic activity, Khellinoflavanone 4l (IIIM-517 – a kind gift from Dr Sandip Bharate of Indian Institute of Integrative Medicine) at 50 nM. YOYO-3 Iodide dye at 100 nM was used to distinguish dead cells. Nine phase-contrast, green, and red fluorescence images were captured for each treatment condition every 6 hours using the 20x objective. "Non-adherent Cell-by-Cell" image analysis module of Incucyte software was used to analyse images using the parameters outlined in Table 2 to calculate the percentage of viable d2EGFP$^+$ cells under each treatment condition over time.

2.4.5 Analysis of cell-to-cell adhesion

Five thousand flow cytometry sorted d2EGFP$^+$ and d2EGFP$^-$ cells from d2EGFP TBX4B and d2EGFP TBW 11.50 and viable cells from TCX 8.13 and TBW 13.50 were cultured in a 96-well flat bottom plate. For the experiments involving the inhibition of ICAM-1/LFA-1 engagement or CCR4 expression, five thousand FACS-sorted d2EGFP$^+$ cells from d2EGFP TBW 11.50 were pre-treated with the inhibitors or controls for one hour at the following concentrations: 100 nM A286982 (Cayman Chemical), 50 ng/ml A205804 (Cayman Chemical), 200 µM c.LABL (a kind gift from Professor Teruna Siahaan of the University of Kansas), 200 µM RD-LBEC (a kind gift from Professor Teruna Siahaan of the University of

Kansas), 40 µg/ml α-ICAM-1 antibody (clone LB-2 – BD Biosciences), 40 µg/ml isotype control antibody for α-ICAM-1 antibody (clone 27-35 – BD Biosciences), 100 nM CCL22 (PeproTech) and 1 µM C021 dihydrochloride (APExBIO). DMSO was used as the vehicle control for A286982, A205804 and C021. d2EGFP$^-$ cells from d2EGFP TBW 11.50 was used as the negative control for cell-to-cell adhesion. One hundred nanomolar YOYO-3 Iodide was used to identify dead cells. Whole-well phase-contrast, green, and red fluorescence images were captured every 4 hours for 12 hours using the 4x objective.

The initial image processing was done using a custom-written ImageJ macro that used the rolling ball algorithm to remove background noise from green and red fluorescence images and corrected the XY drift using the Correct 3D drift plugin. Phase-contrast, green and red fluorescence image stacks were exported to ilastik and segmented using the pixel classification workflow. The segmented image stacks were imported and converted to binary image stacks using bespoke ImageJ macros that subsequently processed the images to calculate the mean object area of d2EGFP$^+$ and d2EGFP$^-$ cells. The regions occupied by non-viable and d2EGFP$^-$ cells were subtracted from d2EGFP$^+$ binary stacks to compute the mean object area of d2EGFP$^+$ cells. The mean object area of d2EGFP$^-$ cells was calculated by removing the areas occupied by d2EGFP$^+$ and non-viable cells from d2EGFP$^-$ binary image stacks.

2.4.6 Single-cell analysis of T-cell motility

FACS-sorted d2EGFP$^+$ and d2EGFP$^-$ cells from d2EGFP TBX4B and d2EGFP TBW 11.50 were mixed 1:1 and cultured at 10000 cells per well in a 48-well plate (Corning). The bottom of the wells was pre-laid with a polydimethylsiloxane (PDMS) grid containing an array of 500 µm x 500 µm microwells (microsurfaces) to prevent the cells from moving out of the field of view during imaging. One hundred nanomolar YOYO-3 Iodide was added to the wells to detect

dead cells. Phase-contrast, green, and red fluorescence images were captured every 3- or 4-minutes for one hour using the 10x objective.

Images were processed using a custom-written ImageJ macro that used the rolling ball algorithm to remove background noise from the fluorescence images and corrected the XY drift of the sequential images using the Correct 3D drift plugin. Pixel classification workflow in ilastik was used to segment the phase-contrast image stack. Segmented phase-contrast image stack was imported, converted to a binary stack and merged with phase-contrast, green, and red image stacks to create a 4-channel hyper stack using a bespoke ImageJ macro. The TrackMate plugin in ImageJ was used to detect and track cells. Only the single, viable cells tracked for the entire duration of imaging were included in the quantification. The mean speed and directionality values were obtained from the TrackMate data. Position data obtained from the TrackMate were used in the Chemotaxis and Migration Tool (ibidi) to generate the trajectory plots in Figure 5-4A. A published MATLAB (MathWorks) script (Tinevez and Herbert, 2020) was used to calculate the mean square displacement (MSD) of the single cells. The same script was used to perform straight-line fitting of log (MSD) vs log (time) data to obtain the motility patterns described in Figure 5-4E. The events where the goodness of fit – R^2 was below 0.8 were excluded from the analysis. Subdiffusive movement is when the upper bound of the 95% confidence interval of the gradient is below 1; diffusive movement is when the upper and lower bounds of the 95% confidence interval of the gradient are above and below 1, respectively; and superdiffusive movement is when the lower bound of the 95% confidence interval of the gradient is above 1 (Tinevez and Herbert, 2020).

2.5 Real-time quantitative reverse transcription PCR

RNeasy Plus Mini Kit (Qiagen) was used to extract RNA following the manufacturer's recommendations. RNA was converted to cDNA using the transcriptor first strand cDNA synthesis kit (Roche) with random hexamer primers. No reverse transcriptase control was included to ensure the absence of genomic DNA in the RNA samples. PCR amplification was performed on a ViiA 7 real-time PCR machine (Thermo Fisher Scientific) with a master mix containing template cDNA, gene-specific primers and Fast SYBR Green master mix (Thermo Fisher Scientific). LinRegPCR-Ct method (Cikos et al., 2007) was used for target RNA quantification. The target mRNA quantity (R0) was calculated with the equation

$$R0 = \text{threshold}/E^{Ct}$$

where the threshold and the mean PCR efficiency (E) data were derived from the LinReg PCR software and the cycle threshold (Ct) values were obtained from the QuantStudio software (Thermo Fisher Scientific). The gene-specific values were normalised to their corresponding 18S rRNA values, which served as the internal PCR control. The gene-specific primers are listed in Table 3.

Table 3. Gene-specific primers used in sections 2.5.1, 2.5.2, and 2.5.3.

Target gene	Orientation	Sequence	Reference
tax	Forward	5'-CCGGCGCTGCTCTCATCCCGGT-3'	(Satou et al., 2016)
	Reverse	5'-GGCCGAACATAGTCCCCCAGAG-3'	
sHBZ	Forward	5'-GGACGCAGTTCAGGAGGCAC-3'	
	Reverse	5'-CCTCCAAGGATAATAGCCCG-3'	
18S rRNA	Forward	5'-GTAACCCGTTGAACCCCATT-3'	
	Reverse	5'-CCATCCAATCGGTAGTAGCG-3'	
d2EGFP	Forward	5'-AAGCTGACCCTGAAGTTCATCTGC-3'	(Martinat et al., 2006)
	Reverse	5'-CACCTTGATGCCGTTCTTCTGCTT-3'	
CCL22	Forward	5'-AGGACAGAGCATGGCTCGCCTACAGA-3'	(Hieshima et al., 2008)
	Reverse	5'-TAATGGCAGGGAGGTAGGGCTCCTGA-3'	
CYP1A1	Forward	5'-CACCATCCCCCACAGCAC-3'	(Lin et al., 2003)
	Reverse	5'-ACAAAGACACAACGCCCCTT-3'	
CYP1B1	Forward	5'-GCTGCAGTGGCTGCTCCT-3'	
	Reverse	5'-CCCACGACCTGATCCAATTCT-3'	

2.5.1 Quantification of *tax*, *sHBZ*, *d2EGFP*, and *CCL22* expression

Unsorted, FACS-sorted d2EGFP^{+} and d2EGFP^{-} cells from d2EGFP TBX4B and d2EGFP TBW 11.50 were subjected to real-time quantitative reverse transcription PCR (real-time qRT-PCR) as described in section 2.5. The data were normalised against the "Unsorted" sample.

2.5.2 Quantification of HTLV-1 transcription in response to LRAs

One hundred thousand cells from clones TBX4B, TBW 11.50, and TBJ 3.60 were treated with 10 nM bryostain-1 or 300 nM prostratin for 20 hours. PMA at 50 ng/ml and ionomycin at 1 µM served as the positive control, while DMSO was the vehicle control. The samples were analysed by real-time qRT-PCR as detailed in section 2.5.

2.5.3 Measuring the effect of AhR signalling on plus- and minus-strands transcription

One hundred thousand cells from TBX4B and TBW 11.50 were treated with AhR ligands – ITE at 10 μM, FICZ at 5 nM or AhR antagonists – SR1 at 1 μM, CH223191 at 10 μM or an inhibitor of CYP1A1 enzymatic activity at 50 nM for 24 hours. DMSO was used as the vehicle control. The samples were analysed by real-time qRT-PCR as described in section 2.5.

2.6 RNA sequencing

2.6.1 Sample preparation and sequencing

Duplicate parallel cultures of each timer protein expressing T-cell clone – FT TBX4B and FT TBJ 3.60 were FACS-sorted as described in section 2.3.7. RNA was extracted from the FACS-sorted subpopulations using RNeasy Plus Micro Kit (Qiagen). RNA concentration and integrity were quantified using RNA 6000 pico kit (Agilent) using a 2100 Bioanalyser (Agilent). All samples had an RNA integrity value greater than 8.80.

The staff of Oxford Genomic Centre performed the preparation and sequencing of cDNA libraries. The RNA samples were used to construct polyA-enriched cDNA libraries using NEBNext Ultra ll Directional RNA Library Prep Kit for Illumina (New England BioLabs). One hundred fifty base pair paired-end fragments were sequenced using HiSeq 4000 System (Illumina).

2.6.2 Alignment and quantification

Alignment and transcript quantification were performed by Miss Helen Kiik of Imperial College London. The quality of the sequence data for each sample was assessed using FASTQC (version 0.11.8) and MultiQC (version 1.8) pre and post adaptor trimming using Trim Galore (version 0.6.4). A custom reference genome was created by merging the human genome (GRCh38) with the sequences of the fast timer protein and HTLV-1 genome (AB513134). A bespoke gene transfer format file containing features of the human genome, coordinates of the HTLV-1 genome, and timer protein was also created. The sequencing reads were aligned to the custom reference genome and output as transcript coordinates using the spliced transcripts alignment to a reference (STAR) aligner (version 2.7.3a) (Dobin et al., 2013). Transcript quantification was performed using RNA-seq by expectation maximization (RSEM) (version 1.3.1) (Li and Dewey, 2011).

2.6.3 Differential expression analysis

Differential expression analysis was performed on RSEM transcript counts using DESeq2 package (version 1.32.0) (Love et al., 2014) in R (version 4.1.2). Differential expression analysis in DESeq2 involves modelling individual transcript counts from each sample using a generalised linear model (GLM), with the negative binomial distribution serving as the underlying probability distribution (Love et al., 2014). Each clone was analysed separately. Genes with a total transcript count of less than two across all samples were excluded from the analysis. The Wald test was performed for pairwise comparison between $Blue^{+}Red^{-}$ and $Blue^{-}Red^{+}$ populations. To determine the significantly differentially expressed genes, a false discovery rate (FDR)-adjusted p-value threshold of less than 0.05 and an absolute log2 fold change (LFC) threshold of greater than 0.58 corresponding to a fold change of at least 1.5 were

used. The likelihood ratio test (LRT) results with an FDR-adjusted p-value of less than 0.05 cut-off were used to determine the significantly differentially expressed genes across all four stages of plus-strand expression (timer protein populations).

2.7 Mathematical modelling

Mathematical modelling to estimate the mean duration of Tax expression was performed by Professor Abhyudai Singh at the University of Delaware. The estimation assumed that the period of plus-strand expression is exponentially distributed with a mean of $1/k_{off}$, where k_{off} is the rate of switching to the "off" state – off rate. The probability of a Tax-expressing cell not switching off Tax after time T (30 in this case) is $e^{-k_{off}T}$.

In clone d2EGFP TBX4B, of 72 cells that were Tax positive at the start of imaging (continuous, silencing and fluctuating patterns), 67 remained Tax positive for the entire 30-hour imaging, while the remaining five cells had either fluctuating or silencing Tax expression. This gave the probability of being Tax positive for the entire 30-hour period to be

$$e^{-k_{off}T} \approx \frac{67}{72} = 0.93$$

$$k_{off} = -\ln(67/72)/\,30 = 0.002399$$

Solving the equation yields a mean Tax duration ($1/k_{off}$) of 416.8 hours. The lower and upper 95% confidence interval values for Tax burst duration were 218.7 and 2782 hours, respectively.

For clone d2EGFP TBW 11.50, of 77 cells that were Tax positive at the start of imaging (continuous, silencing, and fluctuating patterns), 56 remained Tax positive for the entire 30-hour imaging, while the remaining 21 cells showed either fluctuating or silencing Tax expression. This yielded the probability of being Tax positive for the whole 30-hour period to be

$$e^{-k_{off}T} \approx \frac{56}{77} = 0.73$$

$$k_{off} = -\ln(56/77)/30 = 0.010615$$

Solving the equation yields a mean Tax duration ($1/k_{off}$) of 94.2 hours. The lower and upper 95% confidence interval values for Tax burst duration were 64.4 and 157.7 hours, respectively.

2.8 Statistical analysis

GraphPad Prism (GraphPad Software) and R were used for statistical analysis and creating graphs unless otherwise specified. The statistical tests performed are specified in the figure legends. The statistical significance was indicated in the following manner: $P \geq 0.05$ ns – not significant, *$P < 0.05$, **$P < 0.01$, ***$P < 0.001$, and ****$P < 0.0001$.

Chapter 3

3.1 Chapter Summary

This chapter includes the work of analysing the dynamics of Tax expression in naturally HTLV-1-infected, non-malignant $CD4^+$ T-cell clones at the single-cell resolution. A Tax reporter system comprising a chimeric HTLV-1 promoter and a short-lived version of an enhanced green fluorescent protein – d2EGFP was stably transduced into two naturally-infected, non-malignant T-cell clones. Tax-mediated d2EGFP expression in the reporter system was validated using transformed cell lines capable and incapable of expressing Tax. FACS sorting and subsequent staining with an anti-Tax antibody and real-time qRT-PCR analysis further validated the Tax-driven nature of d2EGFP expression in naturally-infected T-cell clones. I then developed a pipeline to identify and track the fluorescence trajectories of individual cells from live-cell images for up to 30 hours. Single-cell analysis of live-cell imaging data showed five patterns of Tax expression in both T-cell clones. Most Tax-expressing cells did so throughout the entire 30 hours of imaging. Mathematical modelling of the experimental data revealed that the two T-cell clones expressed Tax for an average of 94 and 417 hours, respectively. I then tested the efficacy and toxicity of LRAs in reactivating latent HTLV-1 in naturally-infected T-cell clones. The protein kinase C (PKC) agonists, bryostatin-1 and prostratin were the most potent single agents that induced HTLV-1 plus-strand expression. Finally, I compared the spontaneous reactivation of HTLV-1 plus-strand in two T-cell clones and showed clone-specific differences in the frequency of spontaneous proviral reactivation. This work is the first to quantify HTLV-1 proviral expression dynamics at the single-cell resolution in naturally-infected, non-malignant T-cell clones.

Publication based on the data presented in this chapter:

Ramanayake S, Moulding DA, Tanaka Y, Singh A, Bangham CRM. Dynamics and consequences of the HTLV-1 proviral plus-strand burst. PLoS Pathog. 2022;18: e1010774.

3.2 Introduction

HTLV-1 proviral expression is crucial for *in vivo* persistence and pathogenesis and the provirus is entirely dependent on host cell transcriptional machinery for its expression. Although HTLV-1 proviral expression has been studied extensively, only a handful of studies have quantified HTLV-1 proviral expression at the single-cell resolution. These studies had their limitations – refer to section 3.2.3. Therefore, studying the dynamic pattern of proviral expression at the single-cell level is crucial for a comprehensive understanding of the proviral behaviour in individual cells.

3.2.1 Gene expression

There are two modes of gene expression (Lenstra et al., 2016). First is the constitutive expression, where the likelihood of transcription initiation remains constant with time. The number of transcripts between cells follows a Poisson distribution with constitutive transcription. The second mode is the episodic expression that results in high variability in transcript counts between cells that deviates from a Poisson distribution to follow a negative binomial with a much wider distribution (Raj et al., 2006). It is now evident that most mammalian genes are produced through the episodic mode of gene expression, characterised by periods of promoter inactivity that follow the periods of promoter activity (Ross et al., 1994; Dar et al., 2012).

Gene expression is inherently stochastic, requiring multiple biochemical reactions that involve several biomolecules (Raj and van Oudenaarden, 2008). Due to the low copy number of the target genes in each cell, the randomness of the biological processes involving protein production does not simply average out, resulting in significant variation in protein expression even among isoclonal populations of cells.

3.2.2 Fluorescent-based methods used to study gene expression dynamics

Owing to the heterogeneity of gene expression, single-cell analysis is imperative to get a comprehensive picture that would otherwise be masked in cell population level studies. Although techniques such as flow cytometry, single-cell qPCR, and RNA sequencing allow studying gene expression at the single-cell resolution, their "static" and "non-spatial" nature hinder sequential measurements and obtaining spatial data of gene expression, respectively. Microscopy-based techniques on the other hand provide spatial information and depending on the application used, allow dynamic measurements on the same cell. Several image-based techniques have been used to study gene expression dynamics in mammalian cells.

The most widely used current imaging technique to study gene expression at the single-cell level is single-molecule RNA fluorescence *in situ* hybridisation (smFISH). smFISH relies on using one to several fluorescent-labelled probes that hybridise to their target mRNA to simultaneously detect mRNA transcripts from single to several genes in fixed single cells (Raj et al., 2008). Transcript quantification with smFISH allows determining the size (number of mRNA transcripts produced per burst) of transcriptional bursts. The main disadvantage of smFISH is that it requires the fixation of cells: Therefore, the acquisition of temporal gene expression data is impossible. However, it is possible to estimate the transcriptional burst parameters and infer the dynamics of transcriptional bursts by fitting transcript distributions predicted through mathematical modelling to the transcript distribution obtained from smFISH (Nicolas et al., 2017).

The use of RNA-binding proteins such as MS2 coat protein (MCP) (Bertrand et al., 1998) and PP7 coat protein (PCP) (Chao et al., 2008), which are bacteriophage coat proteins that interact with a specific RNA stem-loop structure allows the visualisation of transcription dynamics at the single RNA molecule resolution in individual living cells. In the two-plasmid system, the

first plasmid contains the gene of interest and its downstream is a sequence that encodes an array (typically 24) of RNA stem-loops. The second plasmid encodes the coat protein fused to a fluorescent protein. Upon expression following transfection or electroporation, the fluorescent protein-tagged coat protein binds to the target RNA with stem-loops, thus allowing the visualisation of target gene expression in live cells. One disadvantage of this method is the lack of ability for multiplexing since fluorescent protein-tagged coat protein cannot distinguish different target RNAs with identical stem-loops.

Visualisation of the expression of destabilised reporter proteins is another common technique used to study gene expression dynamics. Here, a destabilised version of a reporter protein gene such as GFP or luciferase placed under the control of the promoter of the gene of interest is stably transduced into the genome of the target cells. The kinetics of the promoter activity is inferred by observing the expression pattern of the reporter protein in living cells.

3.2.3 Previous studies of HTLV-1 expression

HTLV-1 expression has been extensively studied. These studies have been primarily performed using animal models of HTLV-1 infection (Arnold et al., 2006; Li et al., 2009) or HTLV-1-infected transformed cell lines (Kimata and Ratner, 1991; Cheng et al., 2021) that typically do not have the same expression pattern as naturally-infected cells. Rende et al. observed a bi-phasic expression pattern of HTLV-1 mRNA in *ex vivo* PBMCs, where other viral transcripts followed early-expressed *tax/rex* transcripts (Rende et al., 2011). Crucially, the studies mentioned above and a majority of others quantified the gene expression at the cell population level, which masks cell-to-cell variations in gene expression that can only be quantified using single-cell studies.

Only a handful have quantified the HTLV-1 expression pattern at the single-cell resolution: Billman et al. used smFISH to show the cell-to-cell variation in the expression of both HTLV-1 plus- and minus-strands in naturally HTLV-1-infected T-cell clones (Billman et al., 2017). Miura and colleagues performed time-course smFISH on *ex vivo* cultured HTLV-1-infected PBMCs and observed strong heterogeneity in plus-strand reactivation (Miura et al., 2019). Owing to the "static" nature of smFISH, temporal measurements of individual cells were not possible in both these studies. In a recent study, a Japanese group reported transient expression of Tax protein in the ATL cell line, MT1 using live-cell imaging of a short-lived GFP reporter system (Mahgoub et al., 2018). While this study is the only one to quantify the dynamics of HTLV-1 proviral expression at the single-cell resolution to this date, it was performed on a transformed cell line harbouring multiple copies of HTLV-1 provirus (Miyoshi et al., 1980). Naturally-infected T-cells typically harbour a single copy of the provirus (Cook et al., 2012). Furthermore, the expression pattern of Tax in ATL cell lines is distinct from that of non-transformed cells: Tax expression is often very low or suppressed in ATL cell lines (Takeda et al., 2004).

3.2.4 The effect of latency-reversing agents on HTLV-1 reactivation

The chronic phase of HTLV-1 infection is characterised by the presence of latently infected $CD4^+$ T-cells (Hanon et al., 2000). Like in HIV-1 infection, the latent reservoir of $CD4^+$ T-cells remains one of the primary obstacles to HTLV-1 eradication. "Shock and kill" is one of the strategies used in an attempt to reduce or eliminate HIV-1 reservoirs. In this two-step process, either single or multiple LRAs are used to reactivate HIV-1 gene expression (the "shock" step), and the reactivated cells are subsequently cleared either due to viral cytopathic effects or host immune-mediated elimination (the "kill" step). LRAs can be broadly categorised into two

classes (Rodari et al., 2021): The first category is the epigenetic LRAs that include histone deacetylase inhibitors (HDACi), histone methyltransferase inhibitors (HMTi) and DNA methyltransferase inhibitors (DNMTi). The agents that activate host transcription factors constitute the second class of LRAs. Some of the second class of LRAs include PKC agonists, toll-like receptor (TLR) agonists and the inhibitors of bromodomain and extra-terminal domain (BET) protein family.

There are multiple lines of evidence of LRA-mediated HTLV-1 Tax expression: HDACis panobinostat and vorinostat induced Tax protein expression in MT1-GFP cells (Mahgoub et al., 2018). Treatment with valproate reduced PVL in HAM/TSP patients (Lezin et al., 2007) and increased Tax expression in *ex vivo* PBMCs of asymptomatic individuals and HAM/TSP patients (Belrose et al., 2011). In a recent study, Schnell et al. showed increased levels of *tax* transcripts in chronically HTLV-1-infected cell lines and PBMCs of HTLV-1-infected individuals cultured *ex vivo* (Schnell et al., 2022).

3.2.5 Fluorescence reporter system used to study HTLV-1 Tax expression

HTLV-1 Tax protein is inherently non-fluorescent and predominantly nuclear localised (Semmes and Jeang, 1996). The detection of Tax protein requires cell fixation followed by permeabilisation of the nuclear membrane for the fluorescent labelled anti-Tax antibody to bind to the epitope of the intranuclear Tax protein. This approach kills the cells, making certain assays, including those that require the subsequent culture of Tax-expressing cells or live-cell imaging of Tax-expressing cells impossible. To circumvent this issue, fluorescence- or luminescence-based Tax reporter systems have been developed (Wang et al., 2002; Zhang et al., 2006; Alais et al., 2017).

I modified a previously described enhanced green fluorescent protein (EGFP)-based Tax reporter system (Zhang et al., 2006) containing a chimeric HTLV-1 promoter with nine copies of TRE type 1 and type 3 and a truncated HTLV-1 LTR. The relatively long half-life of EGFP of ~15 hours (Danhier et al., 2015) makes it unsuitable for studying the transient changes of gene expression. I generated a Tax reporter system capable of detecting transient gene expression changes by placing a destabilised version of the EGFP under the control of the chimeric HTLV-1 promoter. This destabilised version of EGFP has been created by linking the mouse ornithine decarboxylase (MODC) degradation domain with the carboxyl terminus of EGFP, resulting in a 2-hour half-life (Li et al., 1998).

3.3 Results

3.3.1 Tax dependent d2EGFP expression in inducible Tax-expressing JPX-9 cell line

I took multiple approaches to validate the Tax dependent d2EGFP expression in both cell lines and naturally HTLV-1-infected T-cell clones: I stably expressed the d2EGFP Tax reporter system (Figure 3-1A) in the JPX-9 cell line through lentiviral transduction. JPX-9 is a Jurkat-derived cell line that is stably transfected with a plasmid containing an inducible *tax* gene under the control of a murine metallothionein promoter (Nagata et al., 1989). Tax expression in JPX-9 cells depends on the metallothionine promoter's activation by cadmium or zinc (Napolitano et al., 1991).

To demonstrate Tax-driven d2EGFP expression, I treated d2EGFP JPX-9 cells for twenty-four hours with either $CdCl_2$ to induce Tax expression through the metallothionine promoter activation or water, which served as the negative control. The cells were subsequently analysed by flow cytometry to detect Tax or d2EGFP expression. There was minimal Tax and d2EGFP protein expression in the absence of metallothionein promoter activation by water (Figure 3-1B). Cadmium chloride treatment induced equivalent levels of both Tax and d2EGFP proteins.

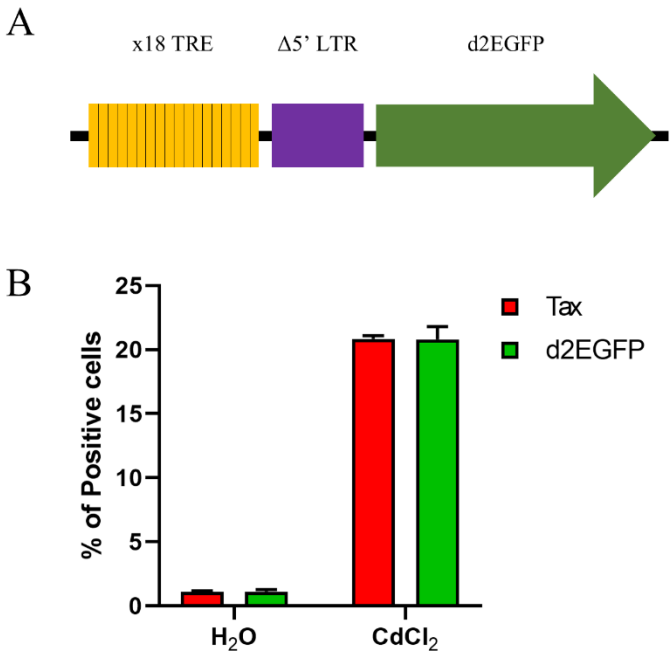

Figure 3-1. Validation of the d2EGFP-based Tax reporter system in JPX-9 cell line.
(A) Schematic of the Tax reporter construct containing 18 copies of TREs and a truncated HTLV-1 LTR upstream of the *d2EGFP* gene. (B) JPX-9 cells stably transduced with the d2EGFP Tax reporter system were treated with either water (the negative control) or $CdCl_2$ for 24 hours before flow cytometric acquisition. The bar plot represents the mean and standard error of the mean (SEM) from technical duplicates of a single experiment.

3.3.2 d2EGFP expression is associated with Tax expression and is independent of HTLV-1 infection

I generated multiple cell lines and T-cell clones stably expressing the d2EGFP-based Tax reporter system (Section 2.1.2 – Table 1). Live-cell images confirmed d2EGFP expression only among the cell lines and T-cell clones that are capable of expressing Tax protein. A minority of cells of two HTLV-1-infected T-cell clones, TBX4B and TBW 11.50 expressed d2EGFP, consistent with a previous study from our group (Billman et al., 2017). On the other hand, virtually all MT2 cells, an HTLV-1-infected transformed cell line that constitutively expresses Tax (Miyoshi et al., 1981) were $d2EGFP^{+}$. The uninfected T-cell clone TBW 13.50 did not

express d2EGFP. No d2EGFP expression was observed among ED cells, an ATL cell line with a mutation in the *tax* gene, therefore incapable of expressing Tax (Maeda et al., 1985).

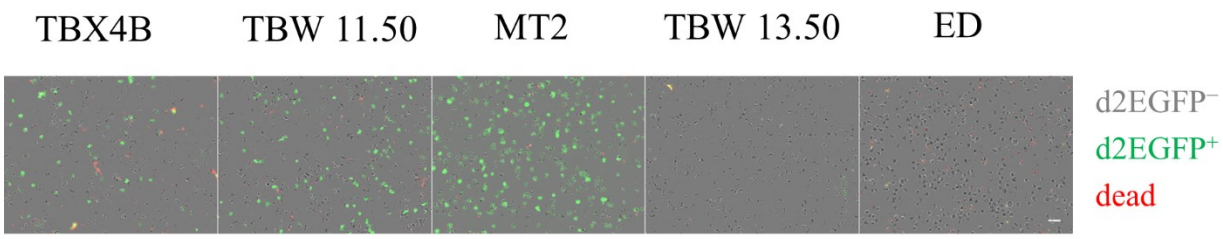

Figure 3-2. d2EGFP expression in T-cell clones and cell lines.
T-cell clones and cell lines stably transduced with the d2EGFP-based Tax reporter system were subjected to live-cell imaging in phase-contrast (d2EGFP$^-$ cells), green (d2EGFP$^+$ cells), and red (YOYO-3 Iodide – dead cells) channels using the Incucyte S3 live-cell imaging system. The scale bar is 50 µm.

3.3.3 The association between Tax and d2EGFP expression at protein and transcript levels in naturally HTLV-1-infected T-cell clones

I then investigated the relationship between Tax and d2EGFP expression in the naturally HTLV-1-infected T-cell clones at the protein and transcript levels. I FACS sorted d2EGFP positive and negative cells and subsequently stained these with an anti-Tax antibody. Flow cytometry analysis showed a strong association between d2EGFP and Tax expression in both naturally HTLV-1-infected T-cell clones (Figure 3-3A and 3-3B). Real-time qRT-PCR was performed on the FACS-sorted d2EGFP positive and negative populations to quantify *tax* and *d2EGFP* transcript levels to investigate the association between Tax and d2EGFP expression at the transcript level. Substantially elevated levels of both *tax* and *d2EGFP* transcripts were seen in the d2EGFP$^+$ population of both clones compared to the unsorted population (Figure 3-3C). Both clones had minimal *tax* and *d2EGFP* transcripts in the FACS-sorted d2EGFP$^-$ cells. Since I have shown that these clones express d2EGFP through a Tax-dependent mechanism, I will interchange the terms "Tax" and "d2EGFP" throughout the remainder of the thesis.

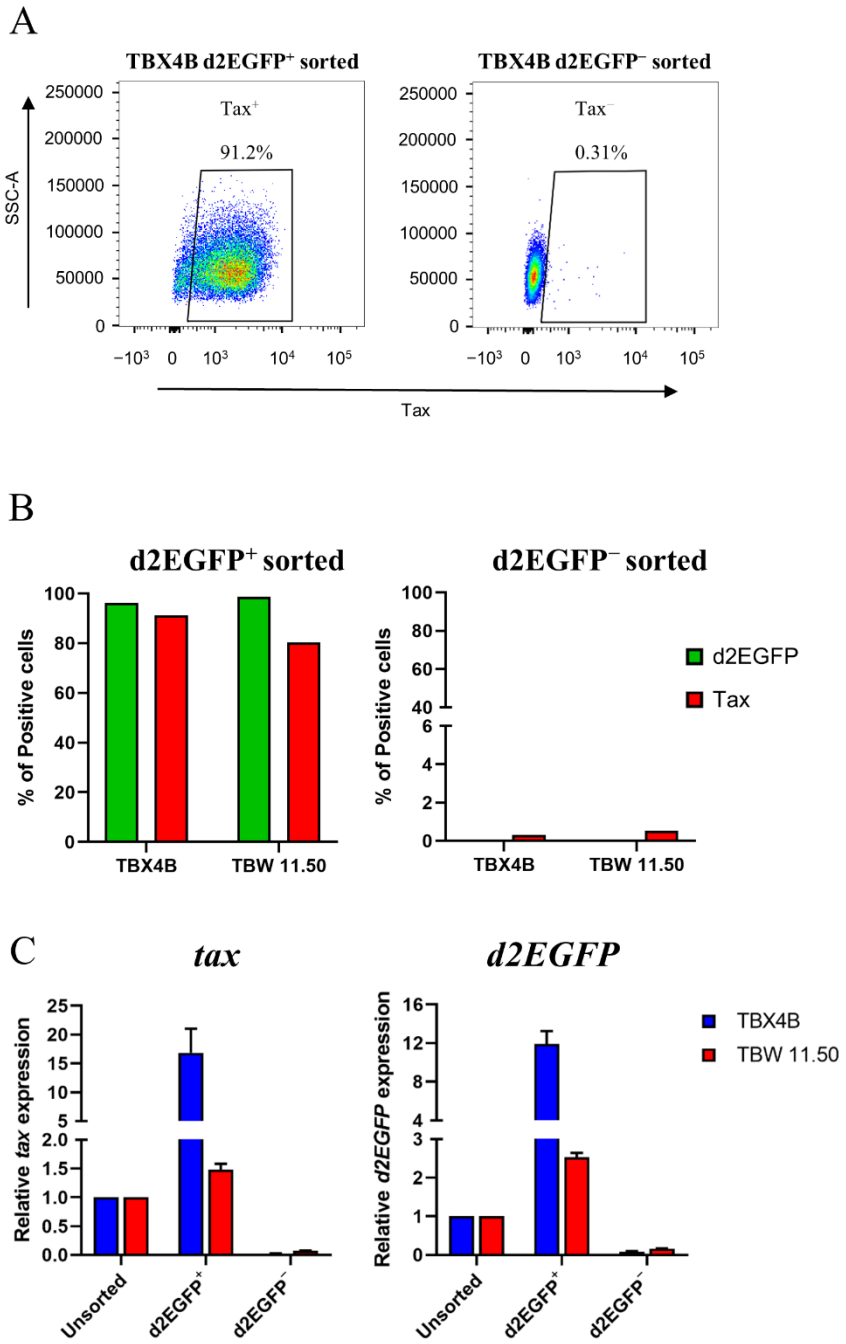
A
TBX4B d2EGFP+ sorted
TBX4B d2EGFP− sorted
Tax+
91.2%
Tax−
0.31%
SSC-A
Tax
B
d2EGFP+ sorted
d2EGFP− sorted
% of Positive cells
d2EGFP
Tax
TBX4B
TBW 11.50
C
tax
d2EGFP
Relative tax expression
Relative d2EGFP expression
TBX4B
TBW 11.50
Unsorted
d2EGFP+
d2EGFP−

Figure 3-3. The association between Tax and d2EGFP expression in naturally HTLV-1-infected T-cell clones.
(A) Representative flow cytometry plots demonstrating Tax protein expression among FACS-sorted d2EGFP positive and negative populations of clone d2EGFP TBX4B. (B) The expression of d2EGFP and Tax proteins in d2EGFP positive and negative populations of clones d2EGFP TBX4B and d2EGFP TBW 11.50. The data are from a single FACS sort experiment. (C) The levels of *tax* and *d2EGFP* transcripts in d2EGFP positive and negative populations relative to the unsorted population in clones d2EGFP TBX4B and d2EGFP TBW 11.50. The data shown are the mean and SEM from real-time qRT-PCR technical duplicates from a single FACS sort experiment.

3.3.4 Quantification of d2EGFP protein half-life

It is imperative to use a short-lived fluorescent reporter protein to study the transient changes in gene expression dynamics that would otherwise be lost with a stable reporter protein. I used a cycloheximide chase assay to quantify the degradation kinetics of the destabilised EGFP in a naturally HTLV-1-infected T-cell clone. One hundred thousand d2EGFP TBW 11.50 cells were treated with either protein synthesis inhibitor cycloheximide or DMSO, the vehicle control in duplicates. The cells were harvested and fixed at 0-, 3- and 6-hours post-treatment and subsequently analysed by flow cytometry to calculate the half-life of d2EGFP as described in section 2.3.9. The half-life of d2EGFP was 3.39 hours (95% confidence interval 2.81-4.29 hours) (Figure 3-4).

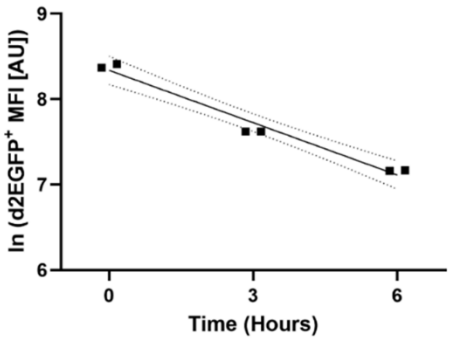

Figure 3-4. The half-life of d2EGFP protein.
The cells were treated with either protein synthesis inhibitor, cycloheximide or DMSO, the vehicle control and harvested at 0-, 3- and 6-hours post-treatment. Harvested cells were fixed immediately and subsequently acquired on a flow cytometer. The MFI of d2EGFP$^+$ cells was computed and graphed over time after conversion to the natural logarithm. The data shown are technical duplicates from a single experiment using the clone d2EGFP TBW 11.50. The solid line shows the least-squares regression line and the dashed lines depict the 95% confidence interval. The protein half-life was determined as described in section 2.3.9.

3.3.5 Single-cell analysis reveals multiple patterns of Tax expression

Multiple studies in our lab using smFISH provide evidence that plus- and minus-strands of HTLV-1 are expressed as sporadic transcriptional bursts in *ex vivo* PBMCs (Miura et al., 2019) and naturally HTLV-1-infected T-cell clones (Billman et al., 2017). Since smFISH analysis loses valuable temporal information due to the requirement of cell fixation prior to the hybridisation and subsequent imaging, I wished to extend our previous studies by performing temporal analysis of HTLV-1 plus-strand expression – reported by the expression of d2EGFP transactivated by Tax protein at the single-cell resolution. Five thousand d2EGFP TBX4B and d2EGFP TBW 11.50 cells were seeded into a PDL-coated 96 well plate. Phase contrast and green fluorescence images were captured at 20-minute frequency for 30 hours. Live-cell imaging followed by the analysis of d2EGFP fluorescence trajectories of individual cells revealed five different patterns of Tax expression during the 30-hour observation period

(Figure 3-5A). The five patterns are designated as follows: continuous, reactivating, silencing, fluctuating, and transient (Figure 3-5B). The most frequent pattern of Tax expression observed in both clones was the continuous pattern, with 65% of Tax-expressing d2EGFP TBX4B cells and 46% of Tax-expressing cells of d2EGFP TBW 11.50 exhibiting this pattern (Figure 3-5A and 3-5C).

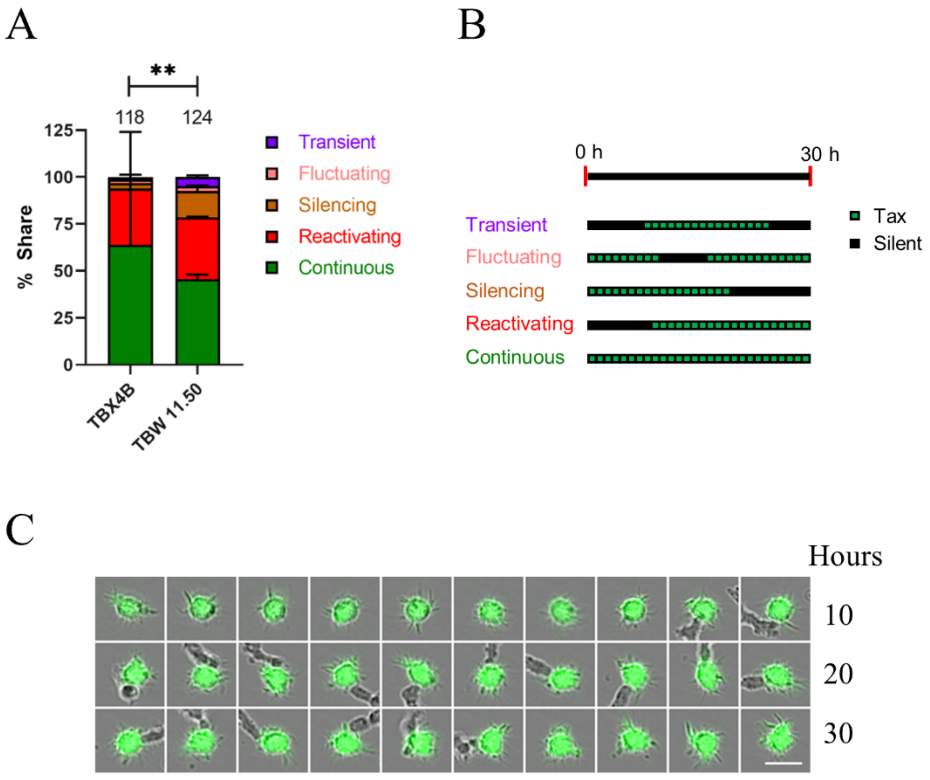

Figure 3-5. Live cell imaging followed by single-cell analysis reveals multiple patterns of Tax expression in naturally HTLV-1-infected T-cell clones.
(A) Time-lapse live-cell imaging was performed on clones d2EGFP TBX4B and d2EGFP TBW 11.50 at a 20-minute frequency for 30 hours. Single d2EGFP$^+$ cells were identified and tracked to determine the trajectory of d2EGFP fluorescence over time from which the pattern of Tax expression was established. The mean and SEM of the data from two independent experiments are shown. The numbers at the top of the bars show the total number of individual cells analysed from each clone. (B) Five patterns of Tax expression determined from single-cell analysis of live-cell imaging data: Continuous – d2EGFP-expressing throughout the observation period; reactivating – starting d2EGFP expression during the imaging period; silencing – terminating d2EGFP expression during the observation period; fluctuating – when a d2EGFP-expressing cell became d2EGFP-negative and subsequently re-expressed d2EGFP; and transient – short-lived period of d2EGFP positivity during the observation period. (C) A montage of hourly time-lapse images of a single cell from clone d2EGFP TBX4B showing the continuous pattern of Tax expression during 30-hour imaging. The scale bar is 20 μm. A chi-squared test was used to analyse the data in panel A. **$P < 0.01$.

3.3.6 Mathematical modelling predicts different duration of Tax expression between naturally-infected T-cell clones

Our live-cell imaging data showed that the predominant pattern of Tax expression was the continuous pattern in both clones during the 30-hour observation period. However, longer-term imaging and subsequent single-cell tracking proved difficult owing to cell detachment from the Poly-D-Lysine-coated well surface and formation of cell clumps. We therefore estimated the average duration of Tax expression in individual clones using the experimental data in a random telegraph model. This model, described in section 2.7, was developed by Professor Abhyudai Singh of the University of Delaware in the USA. The average duration of Tax expression in d2EGFP TBX4B was 416.8 hours (95% confidence interval, 218.7–2782.0 hours), while for d2EGFP TBW 11.50, it was 94.2 hours (95% confidence interval, 64.4–157.7 hours).

3.3.7 Latency-reversing agents induced Tax expression with minimal toxicity

It has been suggested that HIV-1 and HTLV-1 may use similar mechanisms to maintain latent reservoirs (Mahgoub et al., 2018). I investigated the effect of LRAs belonging to multiple classes: PKC agonists – bryostatin-1 and prostratin; HDACis – panobinostat, romidepsin, and valproate; Akt signalling pathway activator – disulfiram; BET inhibitor – JQ1 on HTLV-1 plus-strand expression at the protein and transcript levels in naturally HTLV-1-infected T-cell clones.

To investigate the effect of LRAs on HTLV-1 Tax protein expression, I treated twenty thousand cells from d2EGFP TBX4B and d2EGFP TBW 11.50 with either single or dual LRA combinations and captured live-cell images. The combination of PKC agonist, PMA and calcium ionophore, ionomycin served as the positive control, while DMSO was used as the vehicle control. I quantified the fold increase in d2EGFP expression relative to DMSO after 20 hours of treatment. Of all the single LRA treatments, PKC activators bryostatin-1 and prostratin induced the highest proviral expression, 2.6- and 2.3-fold relative to DMSO, respectively (Fig 3-6A). The bromodomain inhibitor, JQ1 was the only other single LRA that induced significant levels of Tax expression – 1.3-fold. Using either bryostatin-1 or prostratin in combination with another class of LRA did not result in significant proviral expression than using them alone (Fig 3-6A).

I then evaluated the effect of bryostatin-1 and prostratin – the most potent inducers of HTLV-1 Tax protein on the transcription of HTLV-1 plus- and minus-strands. One hundred thousand cells from three naturally HTLV-1-infected T-cell clones (TBX4B, TBW 11.50, and TBJ 3.60) were treated with either bryostatin-1 or prostratin for 20 hours before quantifying *tax* and *sHBZ* mRNA levels. DMSO and PMA/ionomycin were used as the vehicle and positive controls,

respectively. Both bryostatin-1 and prostratin induced significantly higher levels of HTLV-1 plus-strand expression without affecting the minus-strand expression (Figure 3-6B).

One major limitation of using LRAs is their toxicity (Zhao et al., 2019). I tested the toxicity of the most effective LRAs, bryostatin-1 and prostratin. One hundred thousand d2EGFP TBX4B and d2EGFP TBW 11.50 cells were treated for 20 hours with either bryostatin-1 or prostratin, along with positive and vehicle controls, PMA/ionomycin and DMSO, respectively. The cells were subsequently analysed by flow cytometry after staining with a viability dye and apoptosis indicator protein, annexin V. The treatment with either bryostatin-1 or prostratin did not induce a significantly high proportion of early (annexin V^+ viability dye^-) or late (annexin V^+ viability dye^+) apoptotic cells compared to the DMSO control, suggesting minimal toxicity associated with these LRAs (Figure 3-6C).

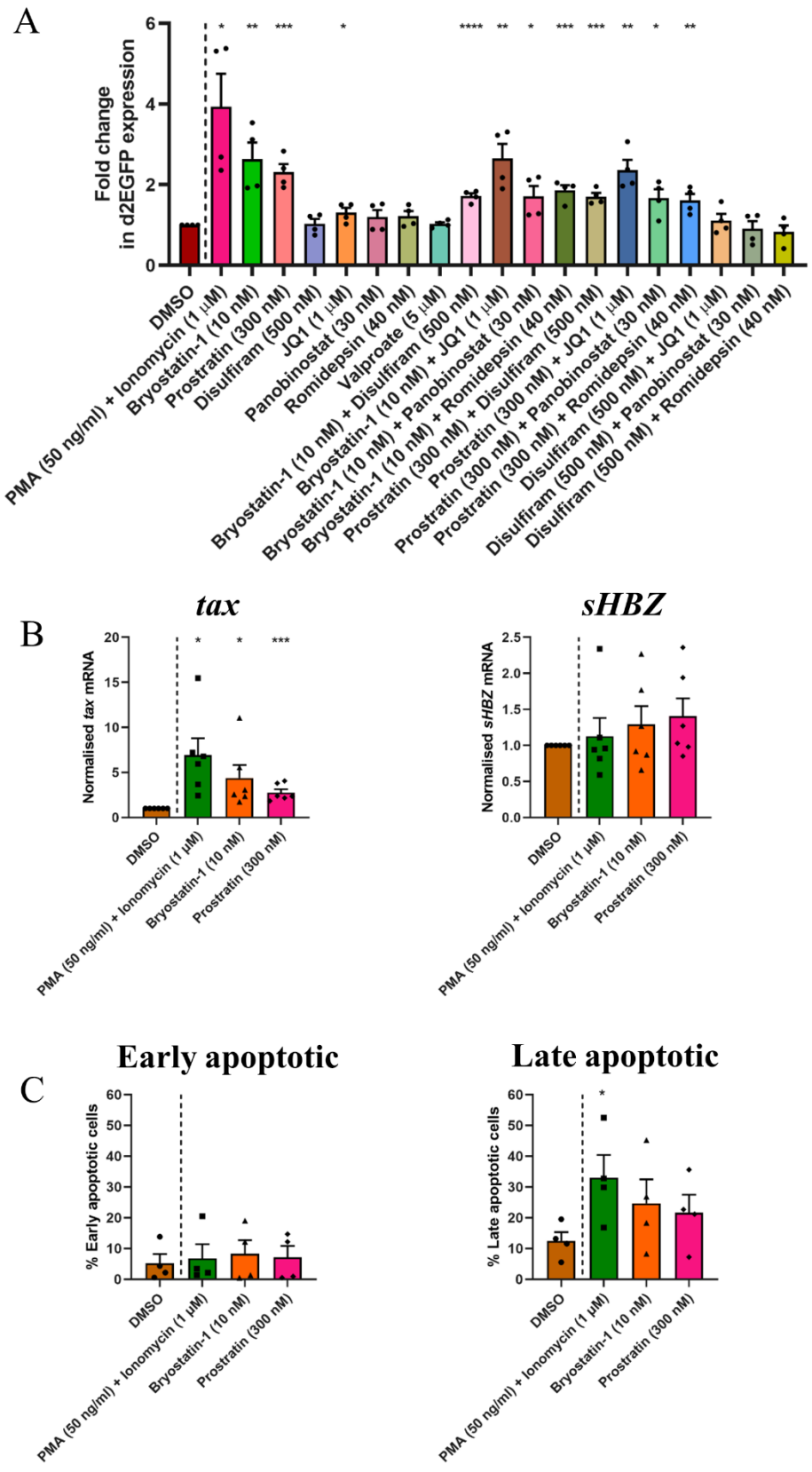
A
Fold change in d2EGFP expression
DMSO
PMA (50 ng/ml) + Ionomycin (1 μM)
Bryostatin-1 (10 nM)
Prostratin (300 nM)
Disulfiram (500 nM)
JQ1 (1 μM)
Panobinostat (30 nM)
Romidepsin (40 nM)
Valproate (5 μM)
Disulfiram (500 nM) + JQ1 (1 μM)
Bryostatin-1 (10 nM) + Disulfiram (500 nM)
Bryostatin-1 (10 nM) + Panobinostat (30 nM)
Bryostatin-1 (10 nM) + Romidepsin (40 nM)
Prostratin (300 nM) + Disulfiram (500 nM)
Prostratin (300 nM) + JQ1 (1 μM)
Prostratin (300 nM) + Panobinostat (30 nM)
Prostratin (300 nM) + Romidepsin (40 nM)
Disulfiram (500 nM) + JQ1 (1 μM)
Disulfiram (500 nM) + Panobinostat (30 nM)
Disulfiram (500 nM) + Romidepsin (40 nM)
B
tax
sHBZ
Normalised tax mRNA
Normalised sHBZ mRNA
C
Early apoptotic
Late apoptotic
% Early apoptotic cells
% Late apoptotic cells

Figure 3-6. Bryostatin-1 and prostratin induced HTLV-1 plus-strand expression with minimal toxicity.
(A) Tax protein induction by different LRAs. d2EGFP TBX4B and d2EGFP TBW 11.50 cells were treated with LRAs at the indicated concentrations for 20 hours. DMSO and PMA/ionomycin were used as the vehicle and positive controls, respectively. The dead cells were labelled with YOYO-3 iodide. Time-lapse live-cell images in phase-contrast, green and red channels were captured at 4-hour frequency for 20 hours. The percentage of d2EGFP-expressing cells among viable cells at 20 hours post-treatment was calculated and normalised against the DMSO treatment. (B) The effect of the most potent LRAs on HTLV-1 plus- and minus-strands transcription. Clones TBX4B, TBW 11.50 and TBJ 3.60 were treated at the concentrations indicated with either bryostatin-1 or prostratin along with PMA/ionomycin – the positive control and DMSO – the vehicle control for 20 hours. RNA extracted from treatment conditions was analysed by real-time qRT-PCR using primers specific for *tax* (HTLV-1 plus-strand) or *sHBZ* (HTLV-1 minus-strand). (C) Toxicity of bryostatin-1 and prostratin on naturally HTLV-1-infected T-cell clones. Cells from d2EGFP TBX4B and d2EGFP TBW 11.50 were treated with either bryostatin-1 or prostratin for 20 hours and subsequently analysed by flow cytometry to determine the percentage of early and late apoptotic cells. PMA/Ionomycin and DMSO were used as the positive and vehicle controls, respectively. Mean and SEM from two independent experiments are shown in each panel. Statistical analysis was performed using unpaired two-tailed t-tests comparing DMSO treatment against the other treatment conditions. $^{*}P < 0.05$, $^{**}P < 0.01$, $^{***}P < 0.001$, $^{****}P < 0.0001$.

3.3.8 Clone-specific differences in spontaneous plus-strand reactivation

To study clone-specific variations in spontaneous proviral plus-strand expression, I cultured fifteen thousand flow-sorted d2EGFP negative cells from clones d2EGFP TBX4B and d2EGFP TBW 11.50 and performed live-cell imaging on them for 20 hours. The combination of PMA and ionomycin served as the positive control for maximal reactivation, while the most potent single LRAs, bryostatin-1 and prostratin were also included along with DMSO, the vehicle control. Media alone served as the condition for spontaneous proviral reactivation. The mean percentage of cells that underwent spontaneous reactivation at the end of the 20-hour imaging period was markedly different between the two clones, 6.7% for d2EGFP TBX4B and 25.3% for d2EGFP TBW 11.50 (Figure 3-7A and 3-7B). The mean percentage of reactivated cells treated with PMA and ionomycin, the positive control for maximal reactivation followed a similar trend to that of the "spontaneously reactivated" population, with only 18.5% of latent

d2EGFP TBX4B cells expressing Tax at the end of the 20-hour treatment compared to 85.4% of latent d2EGFP TBW 11.50 cells (Figure 3-7A and 3-7B). These results suggest clone-specific differences in the reactivation of latent HTLV-1.

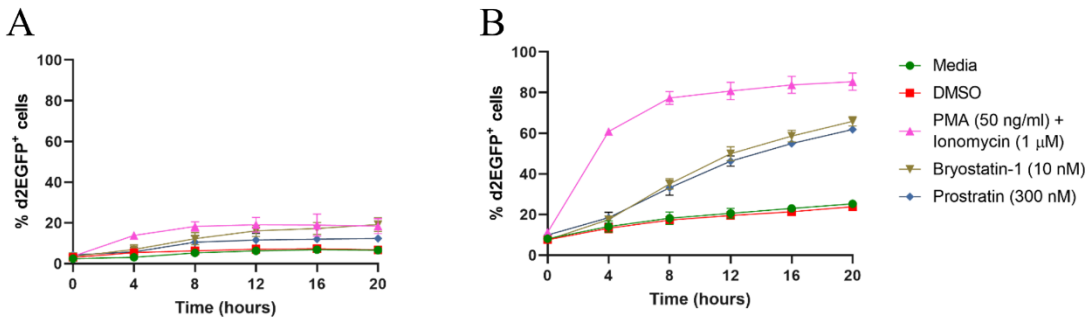

Figure 3-7. The frequency of cells undergoing spontaneous plus-strand reactivation differed between the clones.
The proportion of non-Tax-expressing cells of (A) d2EGFP TBX4B and (B) d2EGFP TBW 11.50 that started expressing Tax. FACS-sorted non-Tax-expressing cells of clones d2EGFP TBX4B and d2EGFP TBW 11.50 were cultured with PMA and ionomycin, the positive control for maximal reactivation. Cells cultured in media alone were used to determine the percentage of cells undergoing spontaneous HTLV-1 reactivation, while DMSO served as the vehicle control. PKC activators bryostatin-1 and prostratin, the most potent LRAs were also included. The dead cells were labelled with YOYO-3 iodide. Twenty hours of time-lapse live-cell images were collected in phase-contrast, green, and red channels at 4-hour frequency. The percentage of viable d2EGFP^{+} cells was calculated at each time point. The data shown are the mean and SEM from two independent experiments.

3.4 Discussion

The chronic phase of HTLV-1 infection is characterised by the lack of detectable virions, proteins and transcripts in the peripheral blood of infected individuals, suggestive of minimal proviral expression *in vivo* (Satou et al., 2006; Demontis et al., 2015). Another indicator of limited proviral expression *in vivo* is the minimal sequence variation of HTLV-1 within infected people over time (Gessain et al., 1992), implying that the virus spreads within the host primarily through the clonal expansion instead of *de novo* infection that requires proviral expression and subsequent reverse transcription by the error-prone viral reverse transcriptase. A conundrum to the apparent lack of proviral expression *in vivo* is the presence of a persistently activated CTL response against HTLV-1 antigens (Jacobson et al., 1990; Parker et al., 1992), suggesting that either proviral expression is predominantly confined to areas outside peripheral circulation or occurs sporadically in the peripheral circulation or both. Indeed, now there is evidence of both these hypotheses: Furuta and colleagues observed higher levels *tax* transcripts in the bone marrow than in the peripheral blood of Japanese macaques infected with STLV-1 (Furuta et al., 2017). Our group recently used smFISH to show that both plus- and minus-strands of HTLV-1 in *ex vivo* PBMCs (Miura et al., 2019) and naturally HTLV-1-infected T-cell clones (Billman et al., 2017) are expressed in transcriptional bursts with only a minority of the cells expressing the plus-strand at any given time. However, the dynamic pattern of HTLV-1 Tax expression and its cell-to-cell heterogeneity remained unexplored in naturally HTLV-1-infected, non-malignant T-cell clones.

To explore the dynamics of HTLV-1 Tax expression, I used live-cell imaging, which circumvented the limitation of lack of temporal measurement of gene expression of the same cell associated with smFISH. Our study used a single-cell analysis approach, since cell population-based analysis often obscure cell-to-cell variation. The fluorescent reporter protein (d2EGFP) expression in our chimeric HTLV-1 Tax reporter system was dependent on Tax

expression (Figures 3-1, 3-2, 3-3A-C). The short-lived nature of the fluorescent reporter protein that is critical to study gene expression dynamics was confirmed using a cycloheximide chase assay described in section 2.3.9 (Figure 3-4). Live-cell imaging followed by single-cell tracking and d2EGFP fluorescence analysis revealed five distinct patterns of Tax expression during the 30-hour observation period (Figures 3-5A and 3-5B). Most Tax-expressing cells showed continued expression during the 30-hour analysis period (Figures 3-5A and 3-5C). Our observation contrasts a recent study that remains the only one to quantify the dynamics of HTLV-1 Tax expression at the single-cell resolution to date (Mahgoub et al., 2018). In that study, Mahgoub and colleagues reported that Tax is transiently expressed in most Tax-expressing MT1 cells with a mean duration of 19 hours. These differences in Tax expression dynamics do not come as a surprise, given the substantial differences between non-malignant T-cell clones and the MT1 leukemic cell line. MT1 cells were derived from a malignant T-cell of a Japanese ATL patient over four decades ago (Miyoshi et al., 1980) and are documented to harbour an average of 7.1 HTLV-1 proviral copies per cell (Saito et al., 2009). Naturally HTLV-1-infected, non-malignant T-cell clones typically harbour only a single copy of the HTLV-1 proviral genome (Cook et al., 2012). Also, the Tax expression profile between malignant and non-malignant clones is different: While non-malignant infected clones typically retain the ability to express Tax, expression of Tax is permanently silenced in approximately 60% of ATL patients (Matsuoka and Jeang, 2007) through multiple mechanisms, including DNA methylation of the HTLV-1 provirus (Taniguchi et al., 2005), deletion of the 5' LTR (Tamiya et al., 1996), and mutation of the *tax* gene (Furukawa et al., 2001).

Similar to (Mahgoub et al., 2018), I observed multiple patterns of Tax expression in the two clones (Figures 3-5A and 3-5B). Notably, a minority of Tax-expressing cells from both clones displayed short-lived (transient) and repeated (fluctuating) episodes of Tax expression. One

key determinant of HTLV-1 proviral expression is its integration site (Melamed et al., 2013). Each T-cell clone I studied harbours a single HTLV-1 proviral copy at a unique position in the genome that is identical across the population and cultured under identical conditions. Different patterns of Tax expression in clonal populations cultured under identical conditions suggest the differences in intracellular factors such as the availability of transcription factors and the epigenetic modifications at the viral promoter of the individual cells that are known to regulate retroviral expression (Lu et al., 2002; Pearson et al., 2008).

PKC-induced HIV-1 reactivation through IκB-α phosphorylation leading to the activation of NF-κB signalling is well documented (Kinter et al., 1990; Pätzold et al., 1993). Multiple lines of evidence demonstrate that the PKC agonists bryostatin-1 and prostratin effectively reactivate latent HIV-1 (Williams et al., 2004; Rullas et al., 2004; Laird et al., 2015; Díaz et al., 2015). Consistent with the observations in HIV-1, bryostatin-1 and prostratin were the most potent inducers of HTLV-1 plus-strand expression (Figures 3-6A and 3-6B), without causing significant toxicity (Figure 3-6C) in our naturally HTLV-1-infected, non-malignant T-cell clones, suggesting shared molecular mechanisms of HIV-1 and HTLV-1 latency. Consistent with a recent study (Schnell et al., 2022), HDACis did not induce significant reactivation of latent HTLV-1 at the protein level (Figure 3-6A). There is evidence that combining LRAs of different classes leads to enhanced reactivation of latent HIV-1 (Laird et al., 2015; Darcis et al., 2015). However, I did not observe enhanced reactivation of HTLV-1 when either bryostatin-1 or prostratin was used in combination with other classes of LRAs (Figure 3-6A). The poor efficacy of reactivation at the protein level of other classes of LRAs could be due to the existence of post-transcriptional blocks as reported in HIV-1 (Mohammadi et al., 2014). However, the efficacy of other classes of LRAs, including HDACis in triggering plus-strand transcription in naturally HTLV-1-infected T-cell clones needs to be investigated to verify if the inefficiency of reactivation is at the transcriptional or post-transcriptional level.

I observed clone-specific differences in the frequency of spontaneous reactivation of HTLV-1 plus-strand (Figures 3-7A and 3-7B). This phenomenon has also been observed in latently HIV-1-infected clones (Pearson et al., 2008). It is likely that variable reactivation thresholds exist because of the varying amounts of silencing associated with each unique integration site giving rise to the observed clone-specific variations of reactivation. Even the maximal T-cell activation with PMA and ionomycin induced HTLV-1 expression only in a minority of cells from the clone d2EGFP TBX4B (Figure 3-7A). It is now evident that multiple molecular mechanisms regulate retroviral latency (Mbonye and Karn, 2017; Kulkarni and Bangham, 2018). Multiple mechanisms may account for the latency in clonal cells as a consequence of prolonged *in vitro* culture, resulting in the heterogeneity of reactivation observed in clonal cells.

Chapter 4

4.1 Chapter Summary

This chapter describes the validation of a novel fluorescent timer protein-based reporter system that separates HTLV-1 plus-strand (Tax) expression into four distinct phases: silent, early, mid, and late. Bulk RNA sequencing analysis of FACS-sorted naturally HTLV-1-infected, non-malignant T-cells at different stages of plus-strand expression revealed dysregulated expression of genes associated with multiple cellular processes at the initiation of plus-strand expression. The genes related to cell cycle regulation were dysregulated during plus-strand expression in a clone-dependent way. DNA damage repair and non-canonical PRC1 genes were upregulated at the start of plus-strand expression. Apoptosis-related genes were deregulated during plus-strand expression, with the upregulation of some pro-apoptotic genes outlasting the plus-strand burst. AhR signalling enhanced and sustained HTLV-1 proviral expression, but the inhibition of AhR signalling was insufficient to block the reactivation of plus-strand expression. This study is the first to report the dysregulation of host gene transcription during distinct stages of HTLV-1 proviral plus-strand expression.

Publication based on the data presented in this chapter:

Kiik H*, Ramanayake S*, Miura M, Tanaka Y, Melamed A, Bangham CRM. Time-course of host cell transcription during the HTLV-1 transcriptional burst. PloS Pathog. 2022;18: e1010387.

*Co-first authors

4.2 Introduction

The expression of Tax protein is crucial for the persistence and pathogenesis of HTLV-1. Tax protein interacts with a wide array of host factors to modulate multiple signalling pathways that ultimately has a plethora of effects on the host cell, including altered gene expression (Boxus et al., 2008; Currer et al., 2012). However, it is unknown if the effects of Tax protein – a surrogate for HTLV-1 plus-strand expression on host gene expression are immediate, delayed, or secondary. To address this issue, I used a novel fluorescent timer protein-based Tax reporter system to separate HTLV-1 plus-strand bursts into four stages to study host gene expression during each stage of plus-strand expression.

4.2.1 Fluorescent timer proteins

Since the isolation of GFP from *Aequorea victoria* in the 1960s (Shimomura et al., 1962), its biological, chemical, and fluorescent properties have been improved (Cubitt et al., 1995). These improved variants of GFP and other fluorescent proteins have been used to study many biological processes, including promoter activity, protein localisation, and protein dynamics through photobleaching (Zimmer, 2002).

Fluorescent proteins are excellent tools for investigating spatial aspects of biological processes. However, fluorescent proteins are not ideal for studying temporal aspects of cellular mechanisms due to their single emission wavelength. To overcome this issue, fluorescent timer proteins that change their emission wavelength over time have been developed. Terskikh et al. developed the first such protein by randomly mutating the drFP583 (DsRed) fluorescent protein to generate a fluorescent protein that shifted its fluorescence emission wavelength from green to red over time (Terskikh et al., 2000). *C.elegans* embryos that harboured the fluorescent timer protein under the control of the *C.elegans* heat shock protein (*hsp 16-41*) promoter produced

no fluorescence under ambient conditions. Heat shock resulted in green and red fluorescence expression by 2- and 5-hours post-heat shock, respectively (Terskikh et al., 2000).

DsRed fluorescent timer protein created by Terskikh and colleagues is a tetramer which limits its use in certain instances such as fusing to a target protein which could potentially lead to the formation of intracellular clumps (Verkhusha and Lukyanov, 2004). To address this issue, Subach and colleagues mutated the mCherry fluorescent protein, a monomeric form of DsRed to create three monomeric fluorescent timer proteins with varying maturation times (Subach et al., 2009). These fluorescent timer proteins spontaneously and irreversibly change colour from blue to red over time and are termed "fast", "medium", or "slow" based on the maturation kinetics of blue chromophores of the purified proteins at 37ºC. The fast timer protein reaches the maximum blue intensity in 15 minutes, the medium timer protein in 1.2 hours, and the slow timer protein in 9.8 hours (Subach et al., 2009). The authors demonstrated the application of fluorescent timers by generating a fusion protein of medium fluorescent timer protein and lysosome-associated membrane protein type 2A (LAMP-2A) to elucidate the intracellular trafficking pathway of LAMP 2A. These fluorescent timer proteins have been successfully used in other domains of biomedical research, including studying the insulin sensitivity of hepatocytes (McKimpson and Accili, 2019) and monitoring *Foxp3* expression dynamics *in vivo* during the immune response (Bending et al., 2018).

4.2.2 Previous studies of host transcription during HTLV-1 infection

Early investigations of transcription were limited to low-throughput techniques like qPCR and northern blot. The invention of DNA microarrays that rely on the hybridisation of fluorescent-tagged cDNA to a fixed set of probes from a known cDNA library allowed high-throughput transcriptome analysis (Trevino et al., 2007). Despite their low cost, microarrays have several

drawbacks, including high background noise due to cross-hybridisation, requirement of prior knowledge about sequences investigated, and the inability to measure the weakly and very strongly expressed genes reliably – low dynamic range (Shendure, 2008). The field of transcriptomics has grown exponentially with the advent of next-generation sequencing. RNA sequencing (RNA-seq) that relies on next-generation sequencing of reversed transcribed cDNA has several advantages over microarrays, including high specificity and sensitivity, greater dynamic range, and the capacity to identify new transcripts (Kukurba and Montgomery, 2015).

HTLV-1 integrates its viral genome into the host genome and exploits the transcriptional and translational machinery of the host cell to express the viral proteins. These viral proteins, particularly Tax, interact with multiple host factors (Boxus et al., 2008). HTLV-1 persistence and pathogenesis may be better understood if the mechanisms by which proviral expression modifies the host gene expression are understood. Several notable studies have used RNA-seq to study the changes in host gene expression during HTLV-1 infection and HTLV-1-associated diseases: In a study by Kataoka et al. involving transcriptome analysis of fifty-seven ATL patients, *tax* transcripts were detected only in one patient, while *HBZ* was detected in all patients (Kataoka et al., 2015). Also, in eleven instances where the provirus had integrated within a gene, resulted in the production of fusion transcripts and elevated host gene expression. Our group showed increased transcriptional activity in the genomic regions immediately flanking the HTLV-1 provirus (Melamed et al., 2018). There was also clone-specific evidence of altered transcriptional activity away from the proviral integration site, potentially through CTCF-mediated chromatin looping. In a recent study, Vandermeulen and colleagues reported HTLV-1-mediated altered host mRNA splicing, with Tax and HBZ having opposite effects: Tax facilitated exon retention, while HBZ promoted exon splicing (Vandermeulen et al., 2021). Mahgoub et al. showed altered transcriptional activity between Tax-expressing and non-Tax-expressing populations of the ATL cell line, MT1: Tax

expression was associated with the expression of apoptosis- and NF-κB-related genes (Mahgoub et al., 2018).

4.2.3 Fluorescence reporter system used to study host transcription during HTLV-1 plus-strand (Tax) expression

Using a conventional fluorescent protein such as GFP as the reporter protein in a proviral expression reporter system can only separate the proviral-expressing cells from proviral non-expressing cells. Each of these populations of cells is heterogeneous: The proviral-expressing population include cells that have just started expressing Tax and cells that have been expressing Tax for a while. The proviral non-expressing population consists of cells that have not expressed Tax for a while and ones that had recently terminated Tax expression. Analysis of these may not provide clues about the determinants of proviral expression initiation and termination. The use of a fluorescent timer protein circumvents the abovementioned limitations. Their time-dependent change in fluorescence allows the separation of proviral expression into four distinct stages when used in a proviral expression reporter system. Non-fluorescent cells belong to the "silent" stage. The cells that fluoresce only the first colour of the timer protein constitute the "early" phase. The cells that fluoresce both the first and the second colour of the timer protein form the "mid" stage, and the cells that fluoresce only the second colour of the fluorescent timer comprise the "late" stage.

I created an HTLV-1 proviral (Tax) expression reporter system by incorporating the *fast fluorescent timer* gene (Subach et al., 2009) under the control of a chimeric HTLV-1 promoter containing five tandem repeats of TRE type 2 and a truncated HTLV-1 LTR (Fujisawa et al., 1989).

4.3 Results

4.3.1 Timer protein-based Tax reporter system differentiates temporal phases of HTLV-1 plus-strand expression

I stably expressed the fast timer protein-based Tax reporter system (Figure 4-1A) in two naturally HTLV-1-infected T-cell clones through lentiviral transduction. Fast fluorescent timer protein reaches its maximal blue fluorescence intensity in 15 minutes, while the half maximal red fluorescence intensity is reached in 7.1 hours (Figure 4-1B) (Subach et al., 2009). Flow cytometry analysis of timer protein populations after staining with an anti-Tax antibody showed the presence of Tax protein in the majority of $Blue^{+}Red^{-}$ and $Blue^{+}Red^{+}$ (double positive – DP) cells of both clones (Figures 4-1C and 4-1D). Tax protein was hardly detectable among the $Blue^{-}Red^{-}$ (double negative – DN) cells, while only a minority of $Blue^{-}Red^{+}$ cells had Tax protein (Figures 4-1C and 4-1D).

The expression of the transcriptional transactivator protein Tax establishes a positive-feedback loop for HTLV-1 plus-strand expression and is often used as a surrogate for plus-strand expression (Billman et al., 2017). When expressed under the control of Tax, fast timer protein-expressing cells represent four distinct stages of plus-strand expression: non-fluorescent cells represent the silent stage; cells that fluoresce only blue constitute the early stage of plus-strand expression; cells with both blue and red fluorescence represent the mid stage of plus-strand expression; cells that fluoresce only red represent the late stage of plus-strand expression (Figure 4-1B)

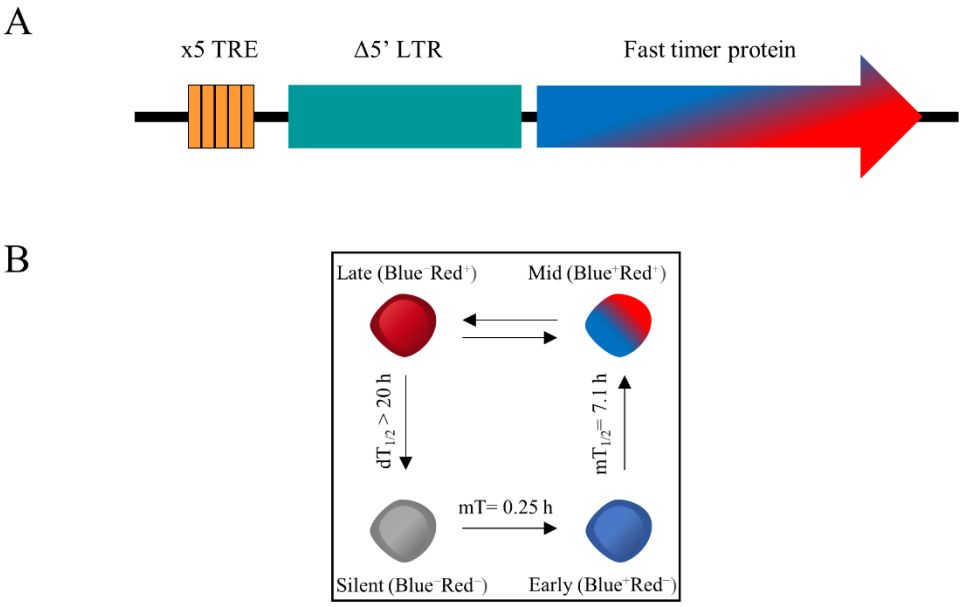
A
x5 TRE
Δ5' LTR
Fast timer protein
B
Late (Blue⁻Red⁺)
Mid (Blue⁺Red⁺)
dT1/2 > 20 h
mT1/2= 7.1 h
mT= 0.25 h
Silent (Blue⁻Red⁻)
Early (Blue⁺Red⁻)
C
Silent
(Blue⁻Red⁻)
Early
(Blue⁺Red⁻)
Mid
(Blue⁺Red⁺)
Late
(Blue⁻Red⁺)
Tax⁻ Tax⁺
98.7% 1.25%
35.6% 63.7%
17.4% 82.3%
82.8% 17.0%
SSC-A
Tax
D
% Tax⁺ cells
100
80
60
40
20
0
TBX4B
TBJ 3.60
Blue⁻Red⁻ (Silent)
Blue⁺Red⁻ (Early)
Blue⁺Red⁺ (Mid)
Blue⁻Red⁺ (Late)

Figure 4-1. The concept underlying Tax-mediated expression of timer protein.
(A) Schematic of the Tax reporter construct containing five tandem repeats of TRE type 2 and a truncated HTLV-1 LTR upstream of the *fast timer protein* gene. (B) Schematic of time-dependent fluorescence changes in timer protein-expressing cells showing successive stages of HTLV-1 plus-strand expression. (C) HTLV-1-infected T-cell clones TBX4B and TBJ 3.60 stably transduced with fast timer protein Tax reporter construct were analysed by flow cytometry after staining with an anti-Tax antibody. Representative flow cytometry plots showing Tax protein expression among different timer protein populations of clone TBJ 3.60. (D) The expression of Tax protein during different stages of HTLV-1 plus-strand burst in clones TBX4B and TBJ 3.60 as indicated by different timer protein populations. The data are from a single experiment.

4.3.2 RNA sequencing confirms the experimental design

We FACS sorted four populations of timer protein cells from duplicate parallel cultures of clones TBX4B and TBJ 3.60 stably transduced with the fast timer protein Tax reporter system. RNA extracted from FACS-sorted samples were subjected to polyA enrichment, sequencing library preparation, and subsequent next-generation sequencing. During the RNA-seq data analysis, we realised clone TBJ 3.60 had a 202 bp deletion corresponding to the *env* coding region and 3' untranslated region (UTR) of *sHBZ* of the plus- and minus-strands of the HTLV-1 provirus, respectively. I observed similar trajectories of HTLV-1 plus-strand and *fast timer* transcripts in both clones (Figures 4-2A, 4-2B and 4-2C). The expression trajectories of HTLV-1 minus-strand differed between the two clones and had no clear association with the plus-strand trajectory (Figure 4-2C). The transcript abundance of HTLV-1 plus-strand was substantially higher than that of HTLV-1 minus-strand (Figures 4-2B and 4-2D). Some genes that are known to be upregulated by Tax, including *interleukin-2 receptor alpha chain* (*ILR2A*) (Inoue et al., 1986), *ICAM-1* (Tanaka et al., 1995), *CCL22* (Hieshima et al., 2008), and *NF-κB* genes (Li and Gaynor, 1999) were upregulated at the start of the plus-strand burst (Figures 4-2E, 4-2F, 4-2G, 4-2H and 4-2I). Principal component analysis (PCA) confirmed distinct transcriptional activity during different phases of HTLV-1 plus-strand expression in both clones (Figures 4-2J and 4-2K).

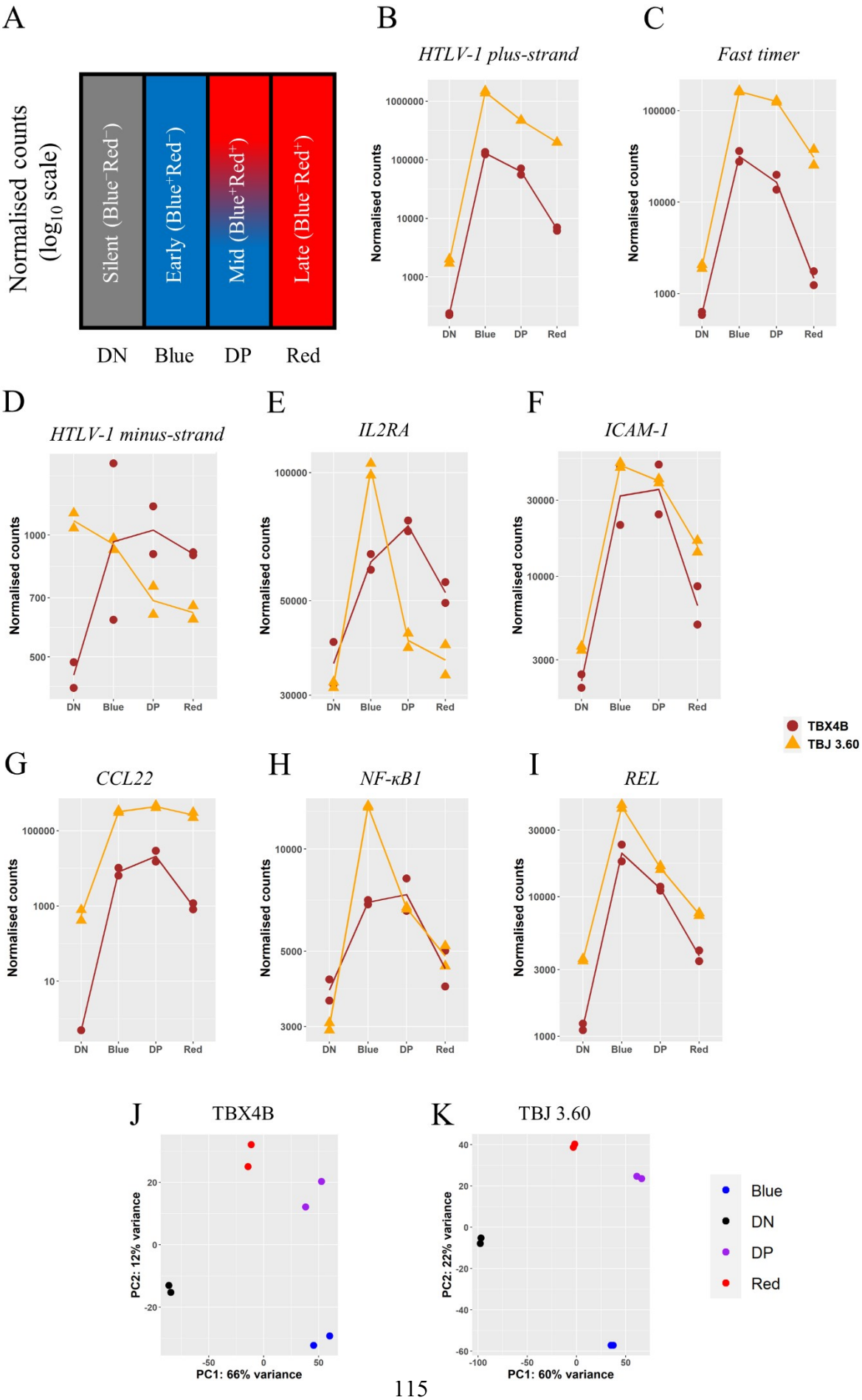
A
Normalised counts
(log10 scale)
Silent (Blue−Red−)
Early (Blue+Red−)
Mid (Blue+Red+)
Late (Blue−Red+)
DN
Blue
DP
Red
B
HTLV-1 plus-strand
C
Fast timer
D
HTLV-1 minus-strand
E
IL2RA
F
ICAM-1
TBX4B
TBJ 3.60
G
CCL22
H
NF-κB1
I
REL
Normalised counts
J
TBX4B
PC2: 12% variance
PC1: 66% variance
K
TBJ 3.60
PC2: 22% variance
PC1: 60% variance
Blue
DN
DP
Red

Figure 4-2. RNA-seq analysis validates Tax-associated timer protein expression.
(A) RNA sequencing was performed on FACS-sorted fast timer protein populations from clones TBX4B and TBJ 3.60. Schematic depicting different stages of HTLV-1 plus-strand expression based on the fluorescence of the fast timer protein-expressing cells. The transcript levels of (B) HTLV-1 plus-strand, (C) *Fast timer*, (D) HTLV-1 minus-strand, (E) *IL2RA*, (F) *ICAM-1*, (G) *CCL22*, (H) *NF-κB1*, and (I) *REL* during successive stages of HTLV-1 plus-strand burst. LRT with an FDR-adjusted p-value of less than 0.05 cut-off was used to determine the significantly differentially expressed genes. (J) Principal component analysis of transcripts counts of four duplicate timer protein populations of clones TBX4B and (K) TBJ 3.60.

4.3.3 Aryl hydrocarbon receptor signalling enhances HTLV-1 plus-strand expression

The most important populations the timer protein Tax reporter system allows to distinguish are the early ($Blue^{+}Red^{-}$) and late ($Blue^{-}Red^{+}$), which would otherwise be impossible to detect using a conventional fluorescent protein-based reporter system. These rare early and late populations represent the cells that had recently started expressing Tax (plus-strand) and ones that had recently terminated plus-strand expression, respectively. Pairwise comparison of early and late populations revealed 3028 and 5662 significantly differentially expressed genes for clones TBX4B and TBJ 3.60, respectively (Figure 4-3A). There were 1613 significantly differentially expressed genes that were common for both clones (Figure 4-3A).

I observed consistent and significant differential expression of *cytochrome P450 1A1* (*CYP1A1*), a product of the aryl hydrocarbon receptor (AhR) pathway between early and late populations in both clones (Figures 4-3B and 4-3C). AhR is a transcription factor whose activation in response to metabolic and environmental cues controls several biological processes (Harper et al., 2006; Rothhammer and Quintana, 2019). It was recently reported that AhR ligands augment HIV-1 proviral expression in *ex vivo* PBMCs of patients undergoing antiretroviral therapy (Zhou et al., 2019). While planning our experiments to investigate the effect of AhR signalling on HTLV-1 expression, it was reported that treatment with AhR ligands enhanced HTLV-1 plus-strand expression in transformed cell lines infected with

HTLV-1 (Hong et al., 2020). I wished to investigate the role of AhR signalling on HTLV-1 expression in naturally-infected, non-malignant T-cell clones.

Cell culture medium contains endogenous AhR ligands like tryptophan metabolites (Veldhoen et al., 2009). To investigate the effect of treatment with either additional AhR ligands or antagonists on HTLV-1 expression, I treated one hundred thousand cells from two naturally-infected T-cell clones with either AhR ligands or AhR antagonists or a CYP1A1 inhibitor for 48 hours. DMSO was used as the vehicle control. I quantified the percentage of Tax-expressing cells at the end of the treatment by flow cytometry analysis. Tax protein expression was significantly elevated by the treatment with ITE, an endogenous AhR ligand (Song et al., 2002) or FICZ, a tryptophan-derived AhR ligand (Rannug et al., 1995) (Figure 4-3D). Treatment AhR antagonists CH223191 or SR1 led to significantly diminished Tax protein expression (Figure 4-3D).

To evaluate the effect of AhR ligands and antagonists on HTLV-1 plus- and minus-strands transcription, I treated one hundred thousand cells from two HTLV-1-infected T-cell clones with either AhR ligands or antagonists or a CYP1A1 inhibitor for 24 hours and subsequently quantified *tax*, *sHBZ*, *CYP1A1*, and *CYP1B1* mRNA. DMSO served as the vehicle control. The expression of HTLV-1 plus-strand (*tax*) and target genes of AhR signalling (*CYP1A1* and *CYP1B1*) was significantly elevated and diminished by the treatment with AhR ligands and antagonists, respectively (Figures 4-3E, 4-3G and 4-3H). AhR ligands or antagonists did not affect HTLV-1 minus-strand expression (Figure 4-3F).

Given that *CYP1A1* was significantly upregulated in the late populations of both clones (Figures 4-3B and 4-3C), I wanted to know if CYP1A1 has a role in terminating HTLV-1 plus-strand expression. The treatment with Khellinoflavanone 4l (IIIM-517), a CYP1A1 enzymatic

activity inhibitor (Sharma et al., 2018) had no effect on HTLV-1 plus-strand expression (Figures 4-3D and 4-3E).

I then used one of the d2EGFP Tax reporter clones (d2EGFP TBW 11.50) to evaluate the effect of AhR ligands and antagonists on the reactivation and silencing dynamics of HTLV-1 plus-strand. I FACS-sorted proviral expressing ($d2EGFP^{+}$) and non-expressing ($d2EGFP^{-}$) cells, treated them with either AhR ligands or antagonists and performed live-cell imaging every 6 hours. The proportion of d2EGFP-expressing cells over time was quantified. AhR antagonists led to a greater proportion of cells terminating proviral expression than DMSO, the vehicle control (Figure 4-3I). However, AhR antagonists did not prevent the initial spontaneous proviral reactivation (Figure 4-3J). AhR ligands or CYP1A1 inhibitor did not have any appreciable effect on HTLV-1 proviral plus-strand silencing or reactivation dynamics (Figures 4-3I and 4-3J). These findings suggest that AhR signalling increases and sustains HTLV-1 plus-strand expression. However, AhR signalling is not the only factor determining the reactivation of latent HTLV-1 in naturally-infected T-cell clones.

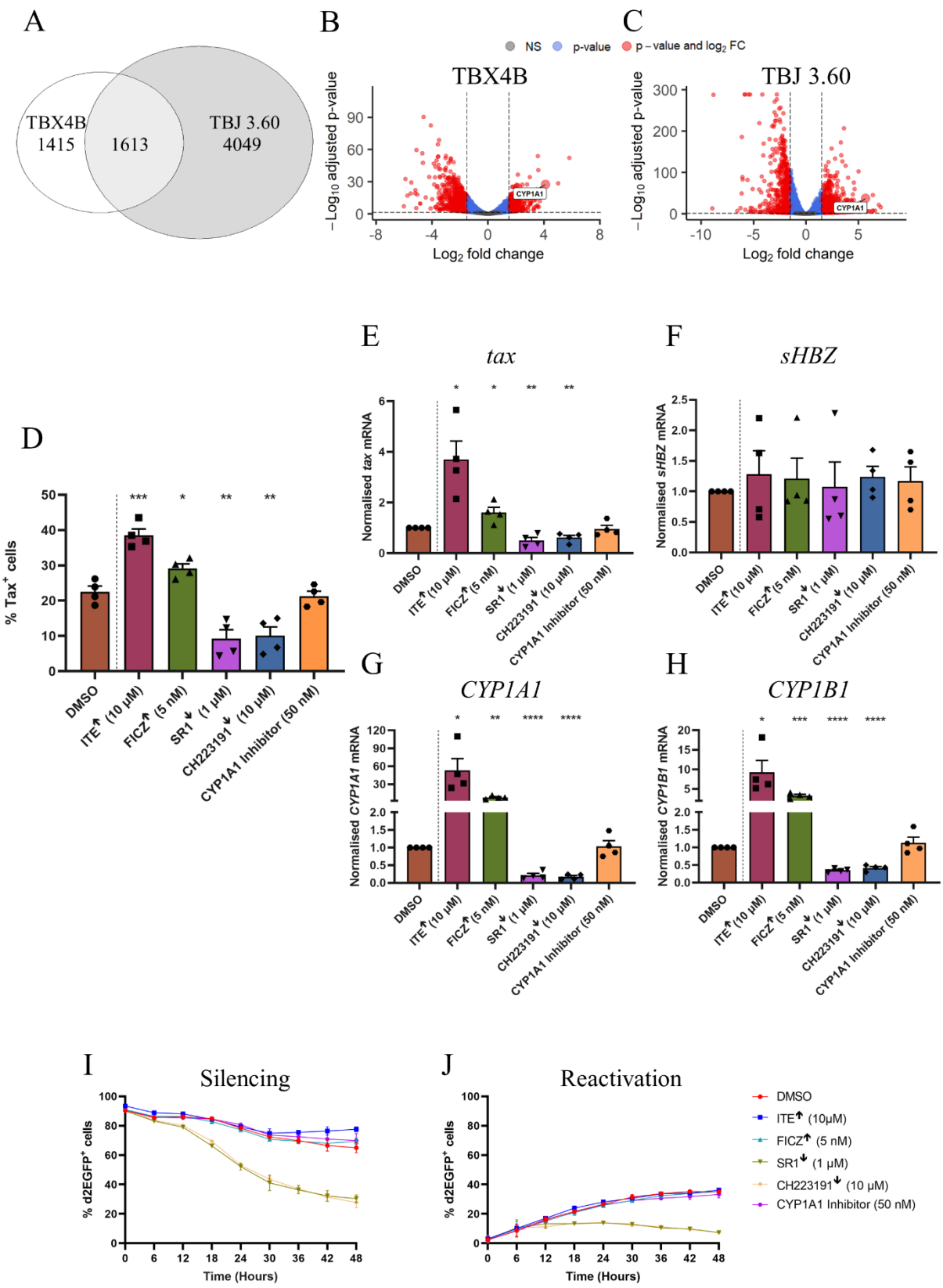
A
TBX4B
1415
1613
TBJ 3.60
4049
B
NS
p-value
p – value and log2 FC
TBX4B
−Log10 adjusted p-value
Log2 fold change
CYP1A1
C
TBJ 3.60
−Log10 adjusted p-value
Log2 fold change
CYP1A1
D
% Tax+ cells
DMSO
ITE↑ (10 μM)
FICZ↑ (5 nM)
SR1↓ (1 μM)
CH223191↓ (10 μM)
CYP1A1 Inhibitor (50 nM)
E
tax
Normalised tax mRNA
F
sHBZ
Normalised sHBZ mRNA
G
CYP1A1
Normalised CYP1A1 mRNA
H
CYP1B1
Normalised CYP1B1 mRNA
I
Silencing
% d2EGFP+ cells
Time (Hours)
J
Reactivation
% d2EGFP+ cells
Time (Hours)
DMSO
ITE↑ (10μM)
FICZ↑ (5 nM)
SR1↓ (1 μM)
CH223191↓ (10 μM)
CYP1A1 Inhibitor (50 nM)

Figure 4-3. AhR signalling augments HTLV-1 plus-strand expression.
(A) Venn diagram showing the distribution of significantly differentially expressed genes between the two clones from the pairwise comparison of early and late populations. (B) Volcano plots depicting the significant upregulation of *CYP1A* in the late population compared to the early population in TBX4B and (C) TBJ 3.60. (D) Two naturally HTLV-1-infected clones were treated with either AhR ligands or antagonists or a CYP1A1 inhibitor for 48 hours at indicated concentrations. DMSO treatment served as the vehicle control. The samples were analysed by flow cytometry to calculate the percentage of Tax-expressing cells under each treatment condition. The mean and SEM from two independent experiments are shown. Expression of (E) *tax* (plus-strand) (F) *sHBZ* (minus-strand) (G) *CYP1A1* (H) *CYP1B1* after 24-hour treatment with DMSO (vehicle control), AhR ligands, antagonists, or a CYP1A1 inhibitor quantified by real-time qRT-PCR. The mean and SEM from two independent experiments using two T-cell clones are shown. (I) HTLV-1 plus-strand silencing and (J) reactivation kinetics in response to the treatment with AhR ligands, antagonists, a CYP1A1 inhibitor, or DMSO (vehicle control). FACS-sorted proviral-expressing (d2EGFP^{+}) and non-expressing (d2EGFP^{-}) cells from clone d2EGFP TBW 11.50 were treated with the compounds at the indicated concentrations for 48 hours. The dead cells were labelled with YOYO-3 iodide. Time-lapse live-cell images in phase-contrast, green, and red channels were captured every 6 hours and the percentage of viable d2EGFP^{+} cells over time was calculated. The mean and SEM from two independent experiments using the clone d2EGFP TBW 11.50 are shown. ↑ and ↓ denote AhR ligands and antagonists, respectively. Wald test in DESeq2 was to determine the significantly differentially expressed genes between the early and late populations presented in Figures 4-3A, 4-3B, and 4-3C. FDR-adjusted p-value of less than 0.05 and LFC of greater than 0.58 cut-offs were used. Unpaired two-tailed t-tests were used to determine the significance of the difference between the vehicle control and treatment conditions in Figures 4-3D, 4-3E, 4-3F, 4-3G, and 4-3H. *P < 0.05, **P < 0.01, ***P < 0.001, ****P < 0.0001.

4.3.4 The expression of non-canonical subunits of the polycomb repressive complex 1 follows the plus-strand expression trajectory

I observed 6230 and 12249 significantly differentially expressed genes for clones TBX4B and TBJ 3.60, respectively, through differential expression analysis of RNA-seq data spanning the four stages of plus-strand expression described in section 2.6.3 (Figure 4-4A). There were 5266 significantly differentially expressed genes that were common to both clones (Figure 4-4A).

HTLV-1 latency is a multi-factorial phenomenon. Factors including hypoxia (Kulkarni et al., 2017), integration site (Melamed et al., 2013), AhR signalling (Hong et al., 2020), and cellular stress (Mahgoub et al., 2018) have been shown to impact proviral reactivation. Our group

recently reported the involvement of polycomb repressive complex 1 (PRC1) in HTLV-1 latency maintenance (Kulkarni et al., 2018): Repressive histone modification H2AK119ub1 deposited by PRC1 was enriched in freshly-thawed cryopreserved PBMCs from infected individuals. Short-term *in vitro* culture of infected PBMCs, which typically leads to spontaneous proviral plus-strand expression coincided with the reduction of H2AK119ub1 levels. A wide-spectrum deubiquitinase (DUB) inhibitor significantly decreased the spontaneous proviral plus-strand expression.

PRCs are a family of transcriptional repressor proteins that form two multi-subunit complexes: PRC1 and PRC2 (Margueron and Reinberg, 2011). PRC2 complex primarily facilitates the tri-methylation of lysine 27 on histone H3 to form the repressive histone mark H3K27me3 (Schuettengruber and Cavalli, 2009). The monoubiquitylation of lysine 119 on histone H2A – H2AK119ub1 that is associated with transcriptional repression is mediated by the PRC1 complex (Wang et al., 2004). PRC1 complex is sub-categorised into two groups, canonical PRC1 and non-canonical PRC1, depending on the composition of the subunits that form the complex.

The members of the canonical PRC1 complex, *B lymphoma Mo-MLV insertion region 1 homolog* (*BMI1*) and *polyhomeotic homolog 2* (*PHC2*) had their expression downregulated during the plus-strand burst (Figure 4-4B). The expression pattern of the subunits of the non-canonical PRC1 complex, *ring finger protein 1* (*RING1*), *RING1 and YY1 binding protein* (*RYBP*) and *lysine demethylase 2B* (KDM2B) followed the trajectory of the plus-strand (Figure 4-4C).

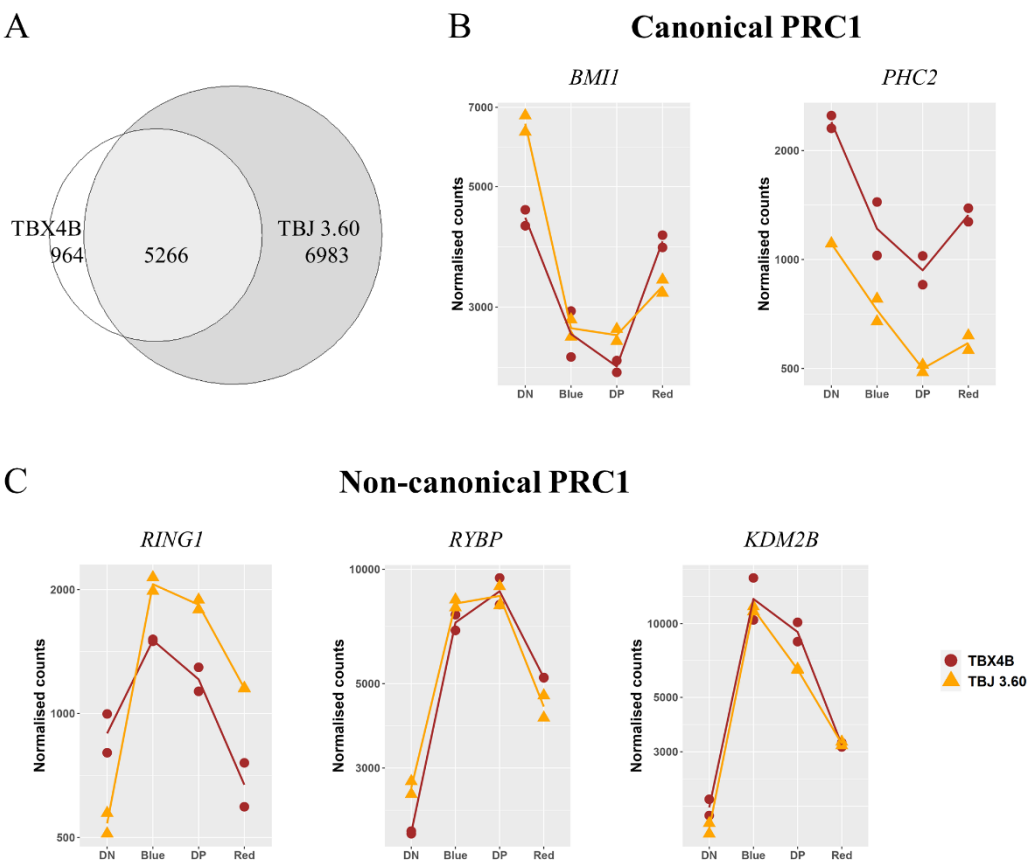

Figure 4-4. The expression patterns of the canonical and non-canonical PRC1 subunits. (A) Venn diagram depicting the distribution of significantly differentially expressed genes across two clones based on differential expression analysis of the four stages of plus-strand expression. (B) The expression patterns of the canonical and (C) non-canonical members of the PRC1 complex. The LRT in DESeq2 was used to determine the significantly differentially expressed genes across all four stages of plus-strand expression (timer protein populations). FDR-adjusted p-value of less than 0.05 was used as the cut-off.

4.3.5 Proviral expression correlates with the expression of cell cycle genes in a clone-dependent manner

Previous studies investigating the impact of Tax expression on cell cycle have observed that Tax both speeds up (Low et al., 1997; Lemoine and Marriott, 2001) and slows down (Yang et al., 2011; Mahgoub et al., 2018) the cell cycle progression. I investigated the expression pattern

of cyclin-dependent kinases (CDKs), proteins that regulate cell cycle progression and the cyclins, which activate CDKs, during successive stages of the HTLV-1 plus-strand expression.

The expression of G1 *cyclin-dependent kinase 6* (*CDK6*) and *Cyclin D1* (*CCND1*) and *Cyclin D3* (*CCND3*) followed a similar pattern during all stages of the proviral plus-strand expression in both clones (Figure 4-5A). The expression of the second G1 CDK, cyclin-*dependent kinase 4* (*CDK4*) was only significantly differentially expressed in clone TBJ 3.60 and showed a distinct expression pattern at the late (red) phase of proviral expression in the two clones (Figure 4-5A). *Cyclin D2* (*CCND2)* was differentially expressed in clone TBJ 3.60, and its expression pattern differed between the two clones at the mid phase of proviral expression (Figure 4-5A).

The *cyclin-dependent kinase 2* (*CDK2*) that mediates S phase entry upon its activation by Cyclin E (Ohtsubo et al., 1995) was differentially expressed and followed a similar pattern of expression in both clones (Figure 4-5B). The expression pattern of *Cyclin E1* (*CCNE1*) and *Cyclin E2* (*CCNE2*) was different between the two clones (Figure 4-5B). *CCNE1* was differentially expressed only in TBJ 3.60, while *CCNE2* was differentially expressed in only TBX4B.

Cyclin As that interact with CDK2 during the S phase (Girard et al., 1991) showed distinct expression patterns in the two clones during successive stages of proviral expression (Figure 4-5C). *Cyclin A1* (*CCNA1*) was differentially expressed in only TBJ 3.60, while *Cyclin A2* (*CCNA2*) had opposite patterns of expression in the two clones despite being differentially expressed in both (Figure 4-5C).

The *cyclin-dependent kinase 1* (*CDK1*) that regulates entry into the M phase through its interaction with Cyclin A (Arellano and Moreno, 1997) showed divergent patterns of expression in the two clones despite being differentially expressed (Figure 4-5D). Mitotic

cyclins, *Cyclin B1* (*CCNB1*) and *Cyclin B2* (*CCNB2*) were differentially expressed in both clones and showed distinct expression profiles in the two clones during successive stages of proviral expression (Figure 4-5D). The distinct expression patterns of cell cycle-associated genes during successive stages of plus-strand burst suggest clone-specific variations in response to the proviral plus-strand expression.

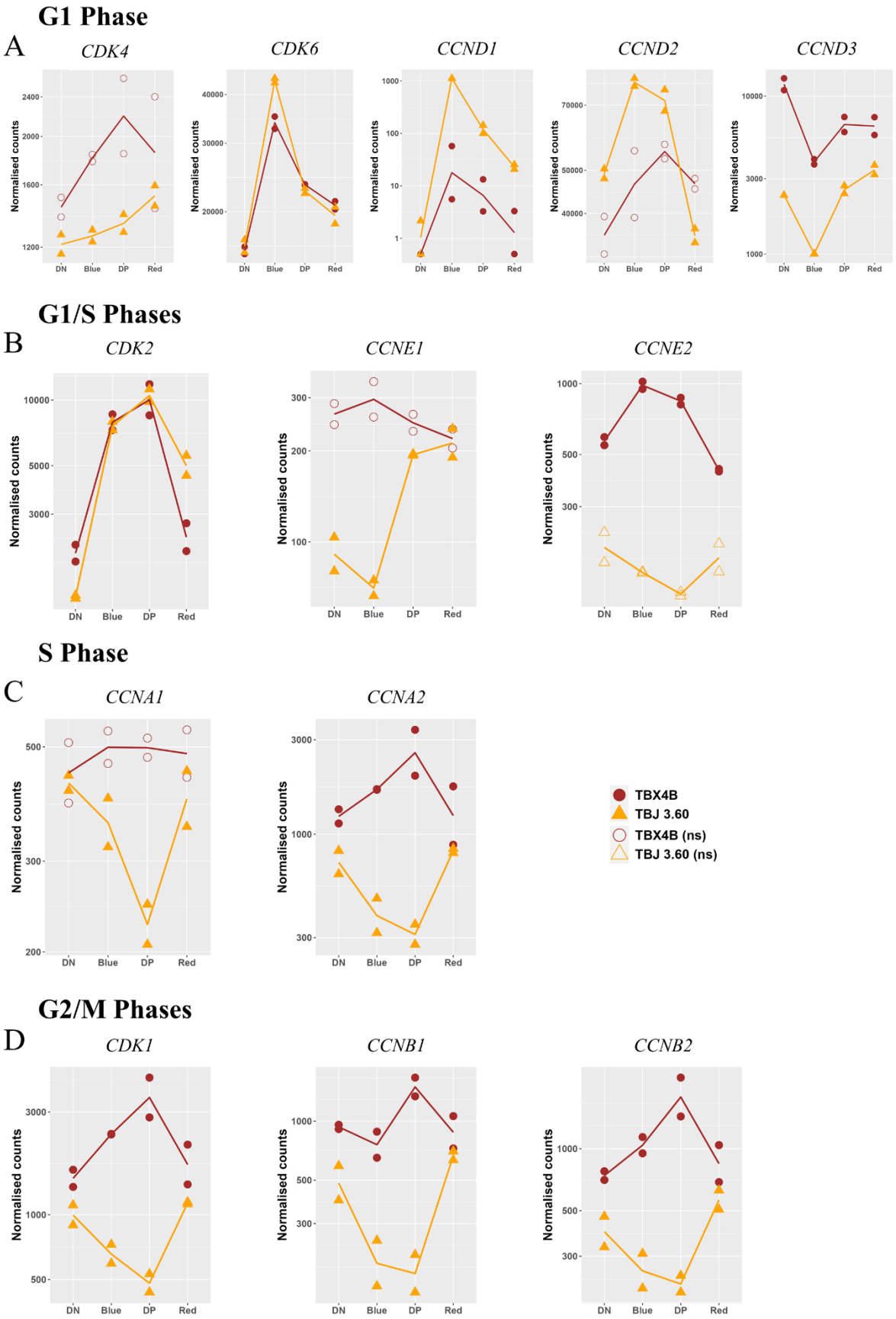
G1 Phase
A
CDK4
CDK6
CCND1
CCND2
CCND3
G1/S Phases
B
CDK2
CCNE1
CCNE2
S Phase
C
CCNA1
CCNA2
G2/M Phases
D
CDK1
CCNB1
CCNB2
Normalised counts
DN
Blue
DP
Red
TBX4B
TBJ 3.60
TBX4B (ns)
TBJ 3.60 (ns)

Figure 4-5. The distinct expression patterns of CDKs and cyclins during successive stages of HTLV-1 plus-stand burst.
(A) Expression levels of CDKs and cyclins that regulate G1, (B) G1/S, (C) S, and (D) G2/M phases of the cell cycle during different stages of HTLV-1 plus-strand expression. The LRT was to determine the significantly differentially expressed genes across all four stages of plus-strand expression. FDR-adjusted p-value of less than 0.05 was used as the cut-off. ns – not significant.

4.3.6 Upregulation of genes involved in DNA damage response during the plus-strand expression

There are multiple lines of evidence of Tax-induced DNA damage (Chandhasin et al., 2008; Durkin et al., 2008; Kinjo et al., 2010; Baydoun et al., 2015). I observed the upregulation of several genes involved in DNA damage repair as the cells started expressing the plus-strand (Figure 4-6A): DNA damage sensor, *xeroderma pigmentosum group C* (*XPC*) that activates nucleotide excision repair (Sugasawa et al., 1998), *Ku70* that forms a heterodimer to initiate DNA damage repair through the non-homologous end joining pathway (Fell and Schild-Poulter, 2015), *three prime exonuclease I* (*TREX1*) that mediates the removal of nucleoside monophosphates from the 3′ ends of DNA (Mazur and Perrino, 1999), and *proliferating cell nuclear antigen* (*PCNA*) that plays a vital role in multiple mechanisms of DNA damage repair (Essers et al., 2005).

p53 encoded by the gene *TP53* is an important tumour suppressor that is activated in response to multiple forms of stress, including DNA damage, activation of oncogenes, and hypoxia (Horn and Vousden, 2007). *TP53* was differentially expressed in both clones with diverging trajectories (Figure 4-6B). However, *tumour protein p63* (*TP63*), a member of the p53 family and p53 targets, including *growth arrest and DNA damage inducible alpha* (*GADD45A*) and *B-cell translocation gene 2* (*BTG2*) (Fischer, 2017) were upregulated at the beginning of the plus-strand expression in both clones (Figure 4-6B).

Ataxia telangiectasia mutated (*ATM*) and *ATM and Rad3-related* (*ATR*) kinases that act as sensors of the DNA damage response (DDR) pathways (Maréchal and Zou, 2013) showed distinct expression patterns: In both clones, *ATM* expression was downregulated at the beginning of the plus-strand burst, while *ATR* expression was upregulated (Figure 4-6C). These results demonstrate the activation of the DNA damage response pathways during the plus-strand burst.

DNA damage repair genes

A

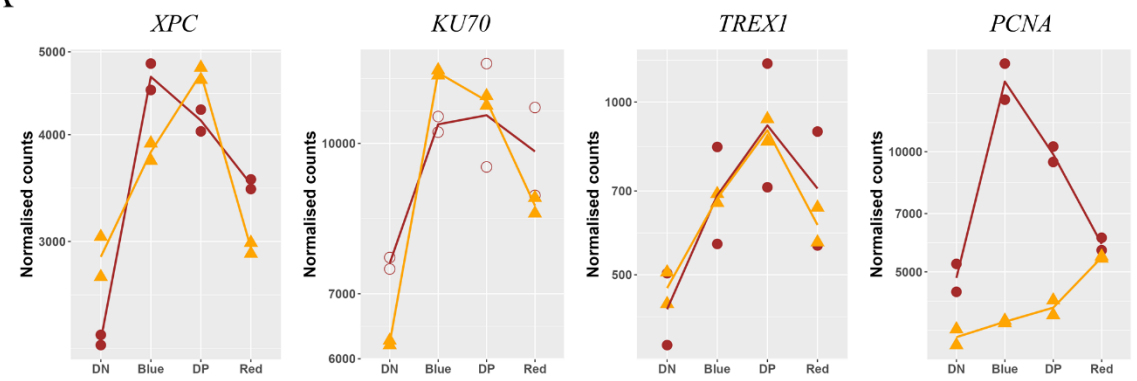

TP53 and target genes

B

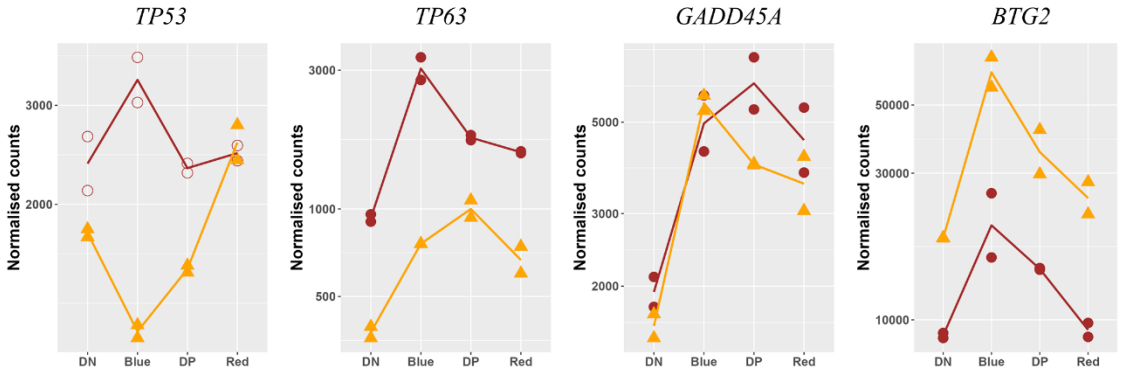

ATM and *ATR* kinases

C

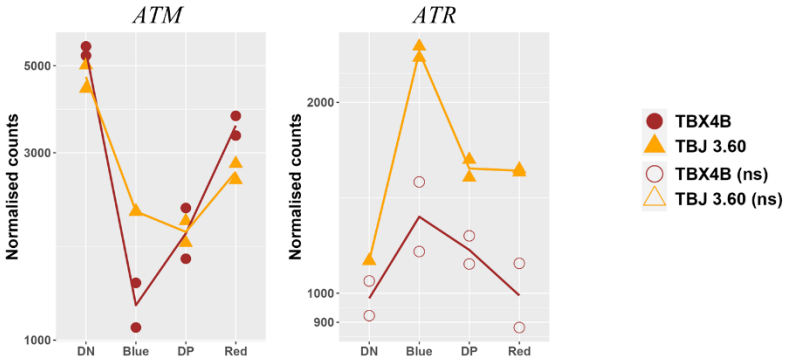

Figure 4-6. The expression pattern of genes regulating the DNA damage response during HTLV-1 plus-strand expression.
(A) Expression levels of genes involved in DNA damage repair, (B) *TP53* and its target genes, and (C) ATM and ATR kinases during successive stages of HTLV-1 plus-strand expression. The LRT was to determine the significantly differentially expressed genes across all four stages of plus-strand expression. FDR-adjusted p-value of less than 0.05 was used as the cut-off. ns – not significant.

4.3.7 Upregulation of apoptosis inhibitors and mediators during the plus-strand expression

Tax expression has been linked to both induction of (Kao et al., 2000; Rivera-Walsh et al., 2001; Takahashi et al., 2013) and protection from (Copeland et al., 1994; Mahgoub et al., 2018) apoptosis. Several important genes associated with the intrinsic and extrinsic apoptotic pathways were differentially expressed during successive stages of the HTLV-1 plus-strand burst (Figure 4-7). The equilibrium between pro- and anti-apoptotic members of the B-cell lymphoma protein 2 (Bcl-2) family of proteins regulates the intrinsic apoptosis pathway by modulating the mitochondrial membrane permeability (Leibowitz and Yu, 2010). Plus-strand expression was initially accompanied by an increase in the expression of the anti-apoptotic Bcl-2 family members *B-cell lymphoma 2* (*BCL2*) and *B-cell lymphoma 2 like 1* (*BCL2L1*) and a decrease in the expression of *Bcl-2-associated athanogene* (*BAG1*) and *myeloid cell leukaemia 1* (*MCL1*) (Figure 4-7A). The pro-apoptotic gene, *Bcl-2-associated X* (*BAX*) was downregulated, while pro-apoptotic genes, including *B-cell lymphoma/leukaemia 10* (*BCL10*), *phorbol-12-myristate-13-acetate-induced protein 1* (*PMAIP1*), and *B-cell lymphoma 2 like 11* (*BCL2L11*) were upregulated at the start of plus-strand burst (Figure 4-7B). *PMAIP1* and *BCL2L11* remained upregulated at the end of plus-strand burst.

Tumour necrosis factor (*TNF*), *Fas cell surface death receptor* (*FAS*) *ligand* (*FASLG*) and *tumour necrosis factor superfamily member 10* (*TNFSF10*), the ligands of the extrinsic apoptotic pathway were downregulated at the initiation of the plus-strand burst (Figure 4-7C). FAS, the receptor of FASLG, was upregulated at the initiation of the plus-strand transcription

(Figure 4-7C). In contrast, *tumour necrosis factor receptor superfamily member 10A (TNFRSF10A) and tumour necrosis factor receptor superfamily member 1A* (*TNFRSF1A*), the receptors of *TNFSF10 and TNF,* respectively, showed no clear trend in expression in the two clones (Figure 4-7C).

At the early stage of the plus-strand burst, *caspase 8* (*CASP8*) of the extrinsic pathway was downregulated in both clones, but *caspase 9* (*CASP9*) of the intrinsic pathway was elevated in clone TBJ 3.60. (Figure 4-7D). The expression of the execution caspases, *caspase 3* (*CASP3*) and *caspase 6* (*CASP6*) was attenuated, while *caspase 7* (*CASP7*) had a diverging expression pattern in the two clones at the start of the plus-strand burst (Figure 4-7D). These findings reveal that the expression of apoptosis inhibitors and mediators is dysregulated during HTLV-1 plus-strand expression.

Intrinsic apoptosis pathway – anti-apoptotic

A

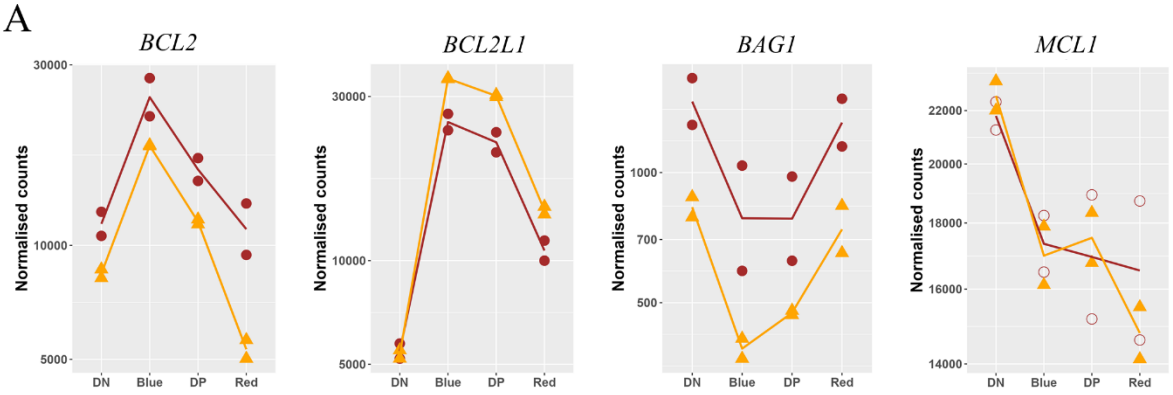

Intrinsic apoptosis pathway – pro-apoptotic

B

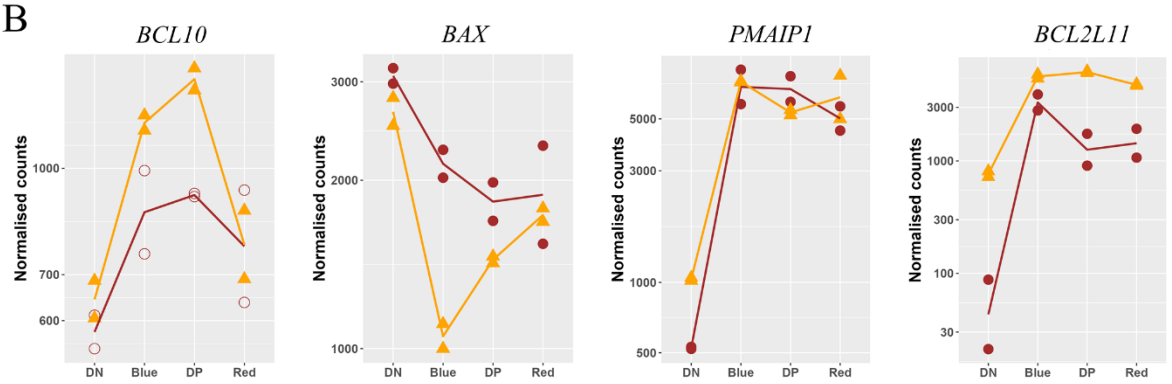

Extrinsic apoptosis pathway – receptors and ligands

C

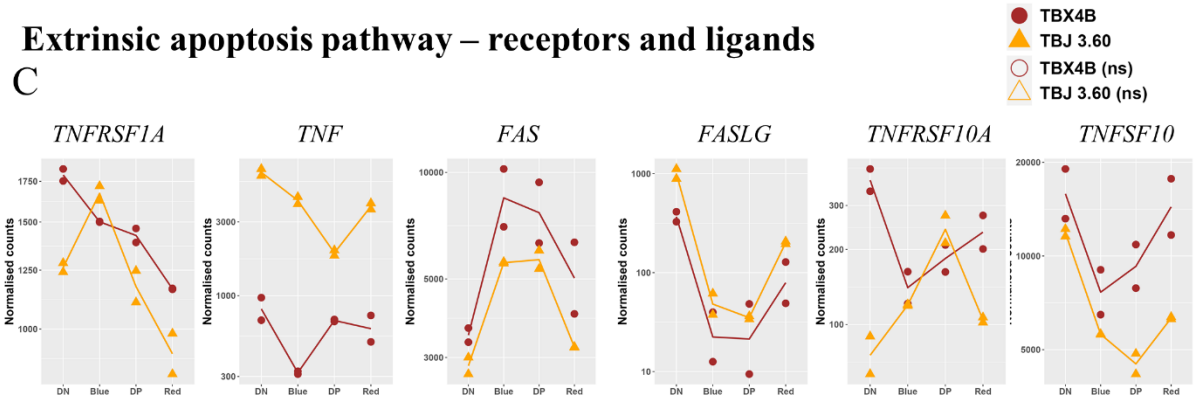

Caspases

D

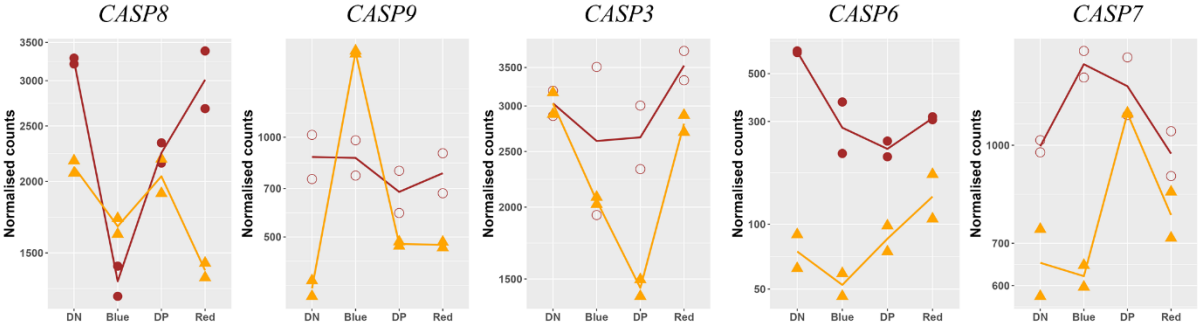

Figure 4-7. The expression of apoptosis-related genes during HTLV-1 plus-strand expression.
(A) Expression levels of anti-apoptotic genes of the intrinsic apoptosis pathway, (B) pro-apoptotic genes of the intrinsic apoptosis pathway, (C) receptor and ligands of the extrinsic apoptosis pathway, and (D) caspases during successive stages of HTLV-1 plus-strand expression. The LRT was used to determine the significantly differentially expressed genes across all four stages of plus-strand expression. FDR-adjusted p-value of less than 0.05 was used as the cut-off. ns – not significant.

4.4 Discussion

The expression of the plus-strand is crucial for *de novo* infection and pathogenesis of HTLV-1. Tax, through its binding to the TREs on the 5' LTR, enhances the transcriptional activity of the HTLV-1 plus-strand (Brady et al., 1987). The expression of Tax protein has been reported to alter the transcription pattern of hundreds of cellular genes (Ng et al., 2001). However, it is not clear if the effects of HTLV-1 plus-strand expression on host transcription are immediate, delayed, or secondary. I used a Tax protein- (a surrogate for HTLV-1 plus-strand expression) driven fluorescent timer protein reporter system that separated HTLV-1 plus-strand expression into four distinct temporal phases: silent, early, mid, and late (Figure 4-1) to study host transcription during different stages of plus-strand expression. I used two naturally HTLV-1-infected, non-transformed T-cell clones stably expressing the fast timer protein Tax reporter system, so avoiding the potentially aberrant gene expression patterns associated with HTLV-1-infected transformed cell lines and plasmid-based Tax expression systems in cells that are not typically associated with HTLV-1 infection. Both T-cell clones had timer protein expression profiles representing the four temporal stages of plus-strand expression.

Analysis of RNA sequencing data validated the Tax-mediated nature of timer protein expression, with HTLV-1 plus-strand and *Fast timer* transcripts showing similar expression patterns during successive stages of the plus-strand burst in both clones (Figures 4-2A and 4-2B). Several genes known to be upregulated by Tax, including *ILR2A* (Figure 4-2E), *ICAM-1* (Figure 4-2F), *CCL22* (Figure 4-2G), *NF-κB1* (Figure 4-2H), and *REL* (Figure 4-2I) were consistently upregulated following the initiation of plus-strand expression in both clones. While Tax expression is frequently used as a surrogate for HTLV-1 plus-strand expression (Billman et al., 2017; Miura et al., 2019), albeit potentially minor, the effects of other viral proteins of the plus-strand on host transcription cannot be excluded. Consistent with previous studies (Billman et al., 2017; Miura et al., 2019), the abundance of HTLV-1 minus-strand

transcripts was markedly lower compared to HTLV-1 plus-strand transcripts (Figures 4-2B and 4-2D). There was no clear association between plus-strand and minus-strand expression in both clones (Figures 4-2B and 4-2D), suggesting that Tax expression is unlikely to regulate HBZ expression or vice versa in these clones at the cell population level.

It has been shown that the ligand-activated transcription factor AhR is constitutively expressed in ATL cell lines and primary ATL cells in a Tax-dependent manner (Hayashibara et al., 2003). AhR signalling has also been shown to increase HIV-1 (Zhou et al., 2019) and HTLV-1 plus-strand (Hong et al., 2020) expression. Pairwise comparison between early and late populations showed consistent, significant upregulation of *CYP1A1*, an AhR product that exerts a negative feedback loop on AhR signalling through ligand degradation (Larigot et al., 2018) in the late populations of both clones (Figures 4-3B and 4-3C). The factors that terminate HTLV-1 plus-strand expression remain poorly characterised. The consistent upregulation of a negative regulator (*CYP1A1*) of the AhR pathway that is known to enhance HTLV-1 plus-strand expression in the late stage of plus-strand expression raised the possibility that *CYP1A1* may have a role in terminating HTLV-1 plus-strand transcription. Consistent with previous reports (Hayashibara et al., 2003; Hong et al., 2020), AhR ligands augmented plus-strand expression at protein and transcript levels, while AhR antagonists diminished plus-strand expression (Figures 4-3D and 4-3E). Inhibition of CYP1A1 enzymic activity had no effect on plus-strand expression, suggesting that elevated CYP1A1 levels in the late populations are simply an epiphenomenon of the active AhR pathway during the plus-strand expression.

Our group recently showed that HTLV-1 provirus in *ex vivo* PBMCs shows characteristics of an immediate early gene (IEG) (Kulkarni et al., 2018). IEGs are group of genes that rapidly increase their expression upon encountering a variety of stimuli, including stress. The expression of IEGs are typically driven by bivalent promoters containing both activatory – H3K4me3 and inhibitory – H3K27me3 histone modifications (Harikumar and Meshorer,

2015). IEG expression is characterised by an increase in H3K4me3 and a decrease in H3K27me3 levels (Bahrami and Drabløs, 2016). HTLV-1 reactivation is associated with an increase in H3K4me3 without a reduction in H3K27me3 (Kulkarni et al., 2017). The levels of PRC2, the HMT that catalyses the methylation of H3K27me3 is elevated during HTLV-1 reactivation, suggesting that PRC2 does not regulate HTLV-1 reactivation (Kulkarni et al., 2018). HTLV-1 reactivation is associated with decreased H2AK119ub1 levels, a histone mark deposited by PRC1. Our data showed the downregulation of canonical PRC1 genes *BMI1* and *PHC2* and the upregulation of non-canonical PRC1 genes *RING1, RYBP*, and *KDM2B* during HTLV-1 reactivation (Figure 4-4B and 4-4C). The elevated levels of *KDM2B* that directs PRC1 complex to non-methylated CpG islands (Farcas et al., 2012) and *RYBP* that enhances the enzymatic activity of PRC1 (Rose et al., 2016) during Tax expression suggest that they may have a role in terminating the HTLV-1 plus-strand expression. The epigenetic regulation of HTLV-1 latency by PRC1 contrasts HIV-1, in which PRC2 is a vital regulator of latency (Friedman et al., 2011). The difference in the frequency of CpG sites in LTRs may explain the differential epigenetic regulation between HTLV-1 and HIV-1: HTLV-1 LTR contains 47 CpG sites, while HIV-1 LTR contains only 9 CpG sites (Pluta et al., 2020).

The effects of HTLV-1 Tax on the cell cycle is contradictory, with some studies reporting Tax-mediated accelerated cell cycle progression (Low et al., 1997; Lemoine and Marriott, 2001), while some showing Tax-induced impaired cell cycle progression (Yang et al., 2011; Mahgoub et al., 2018). Our results showed a clone-specific effect between plus-strand and cell cycle-related gene expression (Figure 4-5). The upregulation of G1 *CDK6*, *CCND1*, and *CCND2* at the start of plus-strand expression and their decreased expression in the subsequent stages of plus-strand expression imply that early stage of Tax expression may promote cell cycle entry, while prolonged Tax expression may negate this effect (Figure 4-5A). Genes, including *CCNE1*, *CCNE2*, *CCNA1*, *CCNA2*, *CDK1*, *CCNB1*, and *CCNB2* that regulate subsequent

phases of the cell cycle diverged in expression between the two clones (Figures 4-5B, 4-5C and 4-5D). Our findings corroborate the study by Billman et al. that investigated the identical clones using smFISH (Billman et al., 2017): They showed clone-specific variation in the cell cycle phase distribution, with a high frequency of plus-strand-expressing cells of clones TBX4B and TBJ 3.60 in G2/M and G1, respectively. These results confirm cell-to-cell variation in naturally HTLV-1-infected T-cell clones and reconcile the opposing Tax-mediated effects on the cell cycle. However, studying the effects of Tax expression on cell cycle progression at the protein level is essential to understand the net effect of Tax expression on cell cycle progression. This has been investigated in chapter five.

Tax expression induces DNA damage through impeding DNA damage response pathways (Chandhasin et al., 2008; Durkin et al., 2008) and the production of genotoxic agents (Kinjo et al., 2010; Baydoun et al., 2015). In agreement with previous evidence of Tax-induced DNA damage, plus-strand expression was associated with strong upregulation of several mediators of DNA damage repair, including *XPC*, *Ku70*, and *TREX1* (Figure 4-6A). There are multiple lines of evidence of Tax-mediated inhibition of p53 activity (Mulloy et al., 1998; Pise-Masison et al., 2000). Our results showed divergent, dysregulated expression of *TP53* during plus-strand expression (Figure 4-6B). However, consistent upregulation of the p53 family member, *TP63* along with p53 target genes, *GADD45A* and *BTG2* during plus-strand expression provides further evidence of the activation of DNA damage response process resulting from plus-strand expression. There is evidence of Tax-mediated impairment of ATM activity (Chandhasin et al., 2008). The expression of ATM was downregulated, while *ATR* expression was upregulated during plus-strand expression (Figure 4-6C). These findings support the hypothesis that ATR-mediated DDR may be the predominant DNA damage response mechanism for Tax-induced DNA damage in naturally HTLV-1-infected T-cell clones.

The role of Tax protein in cellular apoptosis is unclear, with multiple studies reporting pro- (Kao et al., 2000; Rivera-Walsh et al., 2001; Takahashi et al., 2013) and anti- (Copeland et al., 1994; Mahgoub et al., 2018) apoptotic effects of Tax. Both pro- and anti-apoptotic genes of the intrinsic apoptosis pathway were upregulated during plus-strand expression (Figures 4-7A and 4-7B). Plus-strand expression was associated with the downregulation of the extrinsic apoptosis pathway ligands, upregulation of the FAS receptor (Figure 4-7C), and dysregulation of caspase expression (Figures 4-7D). These results agree with another gene expression analysis study, which reported dysregulated expression of both pro- and anti-apoptotic genes during HTLV-1 Tax expression (Ng et al., 2001), suggesting the complex association of Tax expression and apoptosis. While these results provide the evidence for immediate deregulation of genes of the intrinsic and extrinsic apoptosis pathways, perhaps in a direct Tax dependent manner, experimental evidence at the protein level is needed to decipher the net effect of Tax expression on apoptosis in naturally HTLV-1-infected T-cell clones. This is investigated in chapter five.

Chapter 5

5.1 Chapter Summary

In this chapter, I investigated the short- and longer-term implications of HTLV-1 plus-strand (Tax) expression using naturally HTLV-1-infected, non-malignant T-cell clones. Plus-strand expression was associated with decreased proliferation, an increase in the fraction of cells expressing the DNA damage marker – γH2AX, an increased frequency of apoptotic cells, and slower progression through G2/M of the cell cycle. Longer-term follow-up of FACS-sorted Tax positive and negative populations showed that the initial Tax positive population had a greater net overall expansion than the initial Tax negative population. This greater expansion was attributable to an increase in the fraction of proliferating cells and a decrease in the proportion of apoptotic cells as cells relaxed from a Tax positive to a Tax negative state. Tax-expressing cells showed clumping that was independent of ICAM-1 and CCR4 expression. Single-cell analysis revealed impaired cell motility among Tax-expressing cells. This work study was the first to investigate short- and longer-term consequences associated with HTLV-1 plus-strand expression in naturally HTLV-1-infected non-malignant T-cell clones.

Publication based on the data presented in this chapter:

Ramanayake S, Moulding DA, Tanaka Y, Singh A, Bangham CRM. Dynamics and consequences of the HTLV-1 proviral plus-strand burst. PLoS Pathog. 2022;18: e1010774.

5.2 Introduction

Tax engages with multiple cellular proteins to alter the activity of several key signalling pathways (Boxus et al., 2008). However, the impact of HTLV-1 proviral expression on the host cell is not conclusive, with multiple studies showing contradictory Tax-related effects such as proliferation (Akagi et al., 1995; Xie et al., 2006) and apoptosis (Rivera-Walsh et al., 2001; Takahashi et al., 2013). These contrasting consequences of Tax expression are probably attributable to the varying levels or duration of Tax expression observed in different cell models. A better understanding of the persistence and pathogenesis of HTLV-1 infection requires the study of the repercussions of Tax expression in naturally HTLV-1-infected cells.

5.2.1 Cell cycle

The cell cycle involves a series of biochemical reactions that ultimately form two identical daughter cells. The cell cycle comprises five different stages: G0, G1, S, G2, and M. The G0 stage is a resting phase where the cell awaits growth signals before entering the active phases of the cell cycle. The G1 phase is characterised by the preparation of the cell for DNA synthesis by increasing its size, making organelles, and synthesising proteins that regulate the cell cycle. DNA replication occurs during the S phase. The preparation for mitosis occurs during the second growth phase – G2, through mitotic protein expression and size increase. The Mitotic – M stage is characterised by the nuclear membrane breakdown, segregation of sister chromatids, and cytokinesis to form two identical daughter cells.

Progression through the cell cycle is tightly regulated through the activity of the CDK family of serine/threonine kinases and their binding partners, cyclins (Łukasik et al., 2021). The regulation of cell cycle progression through CDK activity ensures precise DNA replication and equal segregation between the two daughter cells. Upon activation during the early G1, cyclin

D-CDK4/6 complexes phosphorylate retinoblastoma (Rb) protein, causing the release of E2F transcription factor (Weintraub et al., 1995) to induce the expression of E2F target genes that are required for the cell cycle progression and DNA replication (Ren et al., 2002). In the late G1 phase, cyclin E-CDK2 complex further phosphorylates RB to further induce the expression of E2F targets. This facilitates progression beyond the G1-S checkpoint to commence the S phase. During the S phase, cyclin A complexes with CDK2 to promote DNA replication through the phosphorylation of proteins mediating DNA synthesis (Petersen et al., 1999). Cyclin A-CDK1 complex promotes the initiation of mitosis (Furuno et al., 1999), while cyclin B complexes with CDK1 to complete mitosis (Riabowol et al., 1989).

The cell cycle is further regulated by a group of proteins called CDK inhibitors (CKI) that inhibit CDK and cyclin-CDK activity. There are two families of CKIs: the INK4 family, which consists of $p16^{INK4a}$, $p15^{INK4b}$, $p18^{INK4c}$, and $p19^{INK4d}$ that inhibit the activity of CDK4 and CDK6, and the Cip/Kip family, which includes $p21^{Cip1/Waf1}$, $p27^{Kip1}$, and $p57^{Kip2}$ that inhibit the activity of multiple cyclin-CDK complexes including, cyclin A-CDK2, cyclin A- CDK1, cyclin E-CDK2, and cyclin B-CDK1 (Satyanarayana and Kaldis, 2009).

5.2.2 DNA damage response

Living cells are constantly exposed to a range of external and internal elements that have the potential to result in DNA damage. To prevent catastrophic results of DNA damage like cancer, cells deploy multiple DNA damage response mechanisms to either repair the DNA damage or if repair is not possible, to mediate irreversible growth arrest or apoptosis.

There are five DNA damage repair pathways: base excision repair (BER), nucleotide excision repair (NER), mismatch repair (MMR), homologous recombination (HR), and non-homologous end joining (NHEJ). BER is initiated by a DNA glycosylase removing the

damaged base to mediate the correction of single-base damages (Krokan and Bjørås, 2013). NER pathway corrects the bulky DNA lesions through the removal of the damaged lesion by the excision nuclease (Wood, 1997). MMR pathway corrects the nucleotide mismatches and repairs the insertions or deletions that occur during DNA replication (Li, 2008). The repair of deleterious double-strand breaks is mediated through either HR or NHEJ (Brandsma and Gent, 2012).

Four components make up the DNA damage checkpoints that halt cell cycle progression to allow DNA damage repair: sensors, mediators, transducers, and effectors. Sensors that initially detect DNA damage include members of the phosphoinositide 3-kinase-like kinase (PIKK) family, ATM and ATR (Maréchal and Zou, 2013). Mediator proteins, including the mediator of the DNA damage checkpoint protein 1 (MDC1) and p53 binding protein 1 (53BP1) interact with the sensors and checkpoint kinases 1 and 2 (ChK1 and ChK2) – the transducers to facilitate the signal transduction (Sancar et al., 2004). Checkpoint kinases phosphorylate the effector proteins, including p53 and cell division cycle 25 (CDC25) to inhibit cell cycle progression (Bartek and Lukas, 2003).

5.2.3 Apoptosis

Apoptosis or programmed cell death is mediated through two main pathways (Green, 1998). The extrinsic pathway that is facilitated through the "death domain"-containing receptors of the TNF receptor superfamily. The intrinsic pathway is mediated by the members of the Bcl-2 family proteins. The two pathways are not mutually exclusive and converge to activate the execution pathway through caspase 3 activation (Elmore, 2007).

Various internal and external stimuli, including the lack of growth cytokines, viral infections, oxidative stress, and radiation causes changes to the mitochondrial membrane potential that

results in the release of pro-apoptotic protein cytochrome C to the cytoplasm (Sprick and Walczak, 2004). Cytochrome c binds to the apoptosis activating factor 1 (APAF1) and recruits inactive initiator caspase 9 to form the apoptosome (Zou et al., 1999). Caspase 9, activated through ATP hydrolysis activates the executioner caspases through proteolytic cleavage to induce apoptosis through the intrinsic pathway.

The extrinsic apoptosis pathway is initiated through ligand binding to the death receptor. One of the best characterised receptor-ligand pairs is the FAS receptor and its ligand. FAS receptor-ligand binding recruits the cytoplasmic adaptor protein, FAS-associated death domain (FAAD) to the death domain of the receptor (Strasser et al., 2009). FAAD subsequently recruits the initiator caspase 8 to form the death-inducing signalling complex (DISC) (Wang et al., 2010). Auto-catalytic activation of caspase 8 activates the executioner caspases by proteolytic cleavage to mediate apoptosis.

The execution pathway that starts with the activation of executioner caspases forms the final stage of the intrinsic and extrinsic apoptotic pathways. Caspases 3, 6, and 7 function as executioner caspases and mediate the proteolytic cleavage of proteins that maintain the cellular integrity to induce apoptosis. Caspase 3, the most crucial among executioner caspases, activates the caspase-activated DNase (CAD) by cleaving the inhibitor of caspase-activated DNase (ICAD) to release CAD, which subsequently degrades DNA and induces chromatin condensation characteristic of apoptotic cells (Sakahira et al., 1998).

5.2.4 Cell motility

T-cells are a migratory population that frequently scan the cell surfaces in search of their cognate peptide antigen bound on the MHC molecule. T-cells exhibit different motility patterns in various body compartments. In lymph nodes, where T-cells are more likely to encounter antigen-presenting cells (APCs) with their cognate peptide-MHC complex, they exhibit Brownian random walk behaviour (Miller et al., 2002). In tissues where the probability of encountering APCs with cognate peptide-MHC complex is less, they display Levy random walk behaviour with intermittent longer jumps (Harris et al., 2012).

T-cells achieve motility using two main mechanisms – amoeboid and haptokinetic. Amoeboid migration relies on the sequential transient contacts with the surface. In amoeboid motility, the contact with the surface is brief and new contacts form at the front, while the old contacts terminate at the back. This allows the cell to jump from one position to another instead of crawling, resulting in faster motility (Krummel et al., 2014). The formation of protrusions through actin polymerisation and actomyosin-dependent contractions facilitate amoeboid migration (Gaylo et al., 2016). The haptokinetic motility during which cells form integrin-dependent focal adhesions with the surface is the slower form of motility (Smith et al., 2005). T-cells can promptly switch between amoeboid and haptokinetic motility patterns (Jacobelli et al., 2009).

5.3 Results

5.3.1 The immediate impact of Tax expression on the host cell

As shown in chapter four, the expression of genes associated with several processes, including cell cycle, DNA damage response, and apoptosis were dysregulated during HTLV-1 plus-strand expression. I investigated the effect of Tax protein expression on multiple cellular processes, including proliferation, DNA damage, cell cycle progression, and apoptosis using two naturally HTLV-1-infected non-malignant T-cell clones – TBX4B and TBW 11.50.

To study the association between Tax expression and cell proliferation, I performed flow cytometry analysis after co-staining the clones with an anti-Tax antibody and an antibody against the nuclear protein Ki-67, a marker of cell proliferation (Sun and Kaufman, 2018). The proportion of Ki-67^{+} cells was significantly lower in Tax-expressing cells compared to non-Tax-expressing cells (Figure 5-1A). This observation suggests that Tax expression is associated with diminished cell proliferation in naturally-infected T-cell clones.

It has been shown that Tax can induce DNA damage by interfering with DNA damage repair and producing genotoxic agents (Chandhasin et al., 2008; Durkin et al., 2008; Kinjo et al., 2010; Baydoun et al., 2015). This evidence is primarily based on experiments using recombinant plasmid-based expression systems or HTLV-1-infected cell lines that maintain high levels of Tax expression, unlike in naturally-infected $CD4^{+}$ T-cells. To investigate the association of Tax-expression with DNA damage, I co-stained Tax and γ-H2AX, a marker of DDR (Podhorecka et al., 2010). The percentage of γ-H2AX positive cells was significantly higher among Tax positive cells than in Tax negative cells, suggesting a larger fraction of Tax positive cells had undergone DNA damage than Tax negative cells (Figure 5-1B). Tax-induced production of reactive oxygen species (ROS) leads to DNA damage (Kinjo et al., 2010; Takahashi et al., 2013). To explore if ROS production could explain the higher proportion of

Tax-expressing cells with DNA damage, I analysed the proportion of ROS producing cells among d2EGFP (Tax) positive and d2EGFP negative cells by flow cytometry using a non-fluorescent probe that fluoresces upon its oxidation by ROS (Kinowaki et al., 2018). One hundred thousand cells from clones d2EGFP TBX4B and d2EGFP TBW 11.50 were subjected to different treatments: untreated, treated with a ROS inducer TBHP (positive control), or treated with a ROS inhibitor NAC (negative control) for one hour. The cells were subsequently stained with the ROS detection probe and analysed by flow cytometry. Compared to untreated and negative control samples, the percentage of ROS positive cells was significantly greater in the positive control group (Figure 5-1C). However, the proportion of ROS positive cells did not differ between d2EGFP positive and d2EGFP negative cells (Figure 5-1D), suggesting that ROS did not mediate the increased DNA damage observed among Tax-expressing cells in these clones.

The DDR is characterised by the activation of cell cycle checkpoints that halt advancement through the cell cycle, allowing for damage repair (Ciccia and Elledge, 2010). Given that a higher proportion of Tax-expressing cells experienced DNA damage, I investigated whether this increased DNA damage caused slower progression through the cell cycle using a flow cytometry-based assay that combined DNA labelling with the incorporation of a thymidine analogue, EdU (Mahgoub et al., 2018). Five hundred thousand cells from clones d2EGFP TBX4B and d2EGFP TBW 11.50 were pulsed with EdU for 1.5 hours, followed by washing to remove unincorporated EdU. Half of the EdU-pulsed cells were immediately fixed, while the other half were cultured for further 6.5 hours before fixation, staining, and flow cytometry acquisition (Figure 5-1E). At the end of the 1.5-hour pulse period, the distribution of EdU positive cells in the cell cycle phases was similar between d2EGFP positive and d2EGFP negative cells (Figure 5-1F). There was a significant difference in the cell cycle distribution of EdU positive cells at the end of the 8-hour (6.5-hour chase) period between d2EGFP positive

and d2EGFP negative populations, where most EdU positive cells of the d2EGFP positive population had accumulated in the G2/M (Figure 5-1F). There were twice as many EdU-tagged d2EGFP negative cells in the G1 phase of the subsequent cell cycle than EdU-tagged d2EGFP positive cells (Figures 5-1G and 5-1H), suggesting Tax expression is associated with impaired progression through the G2/M. EdU incorporation is an indicator of T-cell proliferation (Yu et al., 2009). Consistent with our Ki-67 analysis (Figure 5-1A), the proportion of EdU incorporated cells in the d2EGFP positive population at the end of the 1.5-hour pulse was significantly lower compared to the d2EGFP negative population (Figure 5-1I).

Apoptosis is a key outcome of permanent DNA damage (Roos and Kaina, 2006). Given that Tax expression was associated with increased DNA damage, I explored whether Tax also enhanced the likelihood of cellular apoptosis. Annexin-V is a recombinant phospholipid-binding protein that binds to phosphatidylserine exposed on the outer surface of the apoptotic cell membranes (Vermes et al., 1995). I FACS sorted viable apoptotic (annexin V^+) and viable non-apoptotic (annexin V^-) cells of clones TBX4B and TBW 11.50 and subsequently stained them with an anti-Tax antibody. A significantly higher portion of apoptotic cells than non-apoptotic cells expressed Tax, demonstrating that Tax expression was linked with a higher risk of apoptosis (Figure 5-1I).

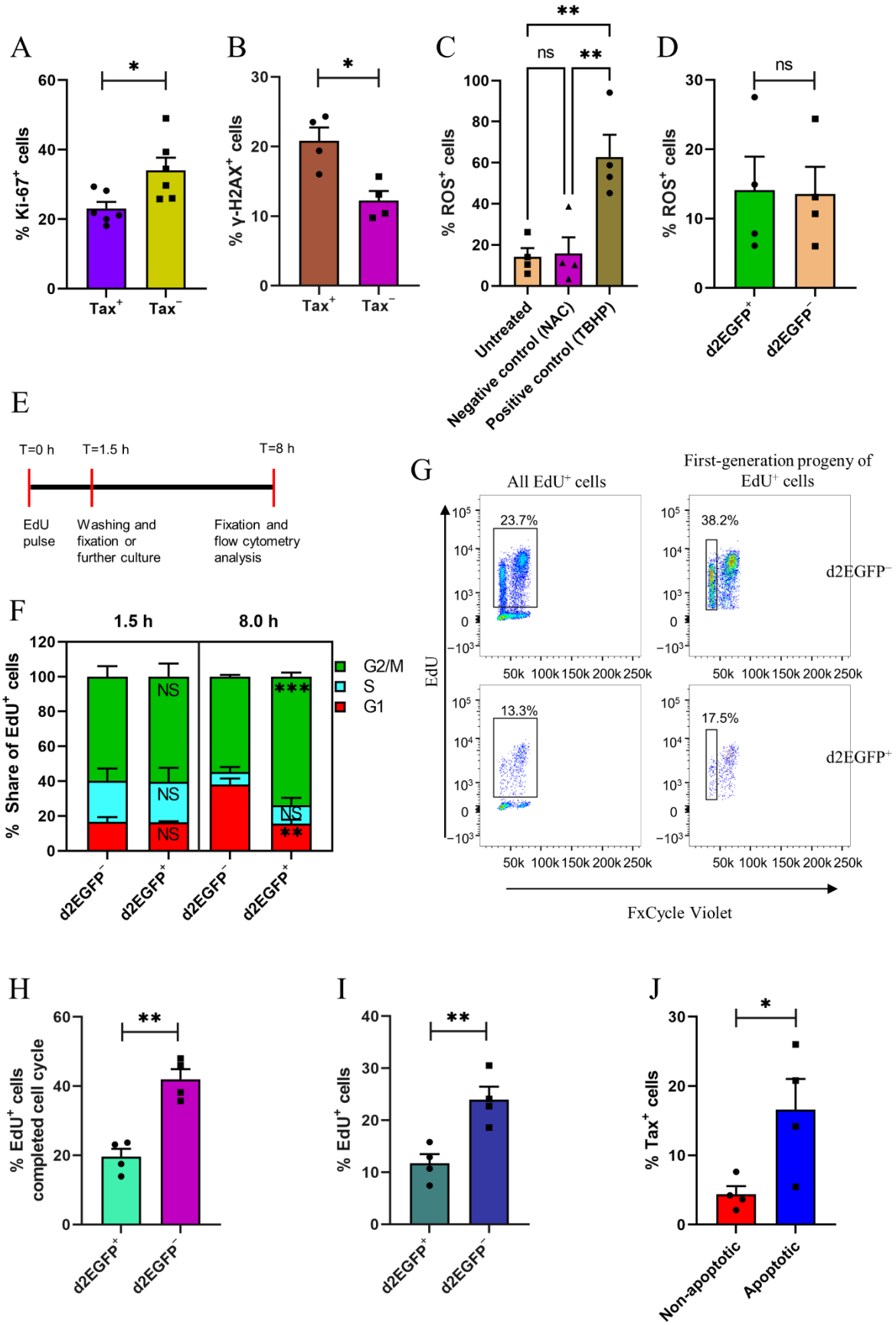
A
% Ki-67+ cells
Tax+
Tax−
B
% γ-H2AX+ cells
C
% ROS+ cells
ns
Untreated
Negative control (NAC)
Positive control (TBHP)
D
% ROS+ cells
d2EGFP+
d2EGFP−
E
T=0 h
T=1.5 h
T=8 h
EdU pulse
Washing and fixation or further culture
Fixation and flow cytometry analysis
F
1.5 h
8.0 h
% Share of EdU+ cells
G2/M
S
G1
NS
***
**
G
All EdU+ cells
First-generation progeny of EdU+ cells
23.7%
38.2%
13.3%
17.5%
EdU
FxCycle Violet
H
% EdU+ cells completed cell cycle
I
% EdU+ cells
J
% Tax+ cells
Non-apoptotic
Apoptotic

Figure 5-1. The short-term consequences of Tax expression on the host cell.
(A) Proportion of proliferating cells among Tax-expressing and non-Tax expressing cells. Clones TBX4B and TBW 11.50 were co-stained with anti-Ki-67 and anti-Tax antibodies. Percentage of Ki-67$^+$ cells among viable Tax$^+$ and Tax$^-$ cells were determined by flow cytometry. (B) Percentage of γ-H2AX$^+$ cells among Tax$^+$ and Tax$^-$ cells. Cells from clones TBX4B and TBW 11.50 were stained with anti-γ-H2AX and anti-Tax antibodies and analysed by flow cytometry to evaluate the percentage of γ-H2AX$^+$ cells among viable Tax$^+$ and Tax$^-$ cells. (C) Percentage of ROS positive cells under different treatment conditions. Clones d2EGFP TBX4B and d2EGFP TBW 11.50 were untreated, treated with either ROS scavenger, NAC or ROS inducer, TBHP for one hour and subsequently stained with a ROS detection probe before flow cytometry acquisition. (D) ROS expression among untreated d2EGFP$^+$ and d2EGFP$^-$ cells of clones d2EGFP TBX4B and d2EGFP TBW 11.50. (E) Schematic of the EdU pulse-chase assay used to determine the cell cycle progression. Clones d2EGFP TBX4B and d2EGFP TBW 11.50 were pulsed with EdU for 1.5 hours and washed. Half of the cells were fixed immediately, while the other half were cultured for further 6.5 hours before fixation, staining and subsequent flow cytometry analysis of both samples. (F) Distribution of EdU$^+$ cells in the cell cycle phases at the end of the 1.5-hour pulse and 8-hour assay. (G) Representative flow cytometry plots from d2EGFP TBX4B depicting the gating strategy used to determine the fraction of EdU-tagged cells that had completed the cell cycle after 8 hours. (H) Percentage of EdU$^+$ cells among d2EGFP$^+$ and d2EGFP$^-$ populations that had completed the cell cycle. (I) Percentage of EdU$^+$ cells within d2EGFP$^+$ and d2EGFP$^-$ cells. (J) Proportion of Tax-expressing cells among apoptotic and non-apoptotic cells. Viable apoptotic and viable non-apoptotic cells from clones TBX4B and TBW 11.50 were flow-sorted, stained with an anti-Tax antibody, and analysed by flow cytometry. Bar plots illustrate the mean and SEM from two to three independent experiments using two T-cell clones. Unpaired student's t-tests were used for statistical analysis. $^*P < 0.05$, $^{**}P < 0.01$, $^{***}P < 0.001$, ns – not significant.

5.3.2 The longer-term consequences of Tax expression on the host cell

Having observed immediate Tax-associated negative impact on the host cell, including diminished proliferation and an increased propensity for apoptosis, I next investigated the longer-term consequences of Tax expression on the host cell. I FACS sorted Tax-expressing (d2EGFP$^+$) and non-Tax-expressing (d2EGFP$^-$) cells from d2EGFP TBW 11.50 and quantified their Tax expression (d2EGFP), proliferation (Ki-67), apoptosis (annexin V) and expansion (cell count) on days 0, 4, 7, 11, and 14 post-sort (Figure 5-2A).

FACS-sorted d2EGFP$^+$ cells showed a steady decline of d2EGFP expression ($P = 0.0083$) to reach the equilibrium during the second-week post-sort, while d2EGFP$^-$ cells had reached the steady state by day 4 without showing a significant trend ($P = 0.408$) (Figure 5-2B). FACS-

sorted d2EGFP$^+$ population had a higher proportion of apoptotic cells during the first week, which fell below the levels observed in the d2EGFP$^-$ population during the second week of the culture by which most cells had ceased Tax expression (Figure 5-2C). Annexin V positivity among FACS-sorted d2EGFP$^+$ cells showed no significant trend (P = 0.592), while d2EGFP$^-$ cells displayed a monotonic increase (P = 0.0083) (Figure 5-2C).

At the conclusion of the 14-day culture, the fraction of Ki-67$^+$ cells in sorted Tax$^+$ cells was 4.5-fold greater than on day zero (Figure 5-2D). The proportion of Ki-67$^+$ cells among FACS-sorted Tax$^-$ cells decreased to 0.9-fold by day four and then progressively increased to 2.2-fold over the day 0 level by the end of the two-week culture (Figure 5-2D). Ki-67 expression among FACS-sorted Tax$^-$ cells exhibited a significant positive trend (P = 0.042), while Tax$^+$ cells displayed a significant upward trend during the first eleven days of the culture (P = 0.042) (Figure 5-2D). FACS-sorted Tax$^+$ population had a mean net expansion of 51-fold over the 14-day culture, while Tax$^-$ population had a mean net expansion of 28-fold (Figure 5-2E). Tax$^+$ and Tax$^-$ populations showed a significant upward trend in the net expansion (Figure 5-2E). These findings suggest that the immediate deleterious effects of the plus-strand expression are followed by a decrease in apoptosis levels and an increase in cell proliferation, resulting in a greater net expansion of the FACS-sorted Tax$^+$ population compared to the FACS-sorted Tax$^-$ population.

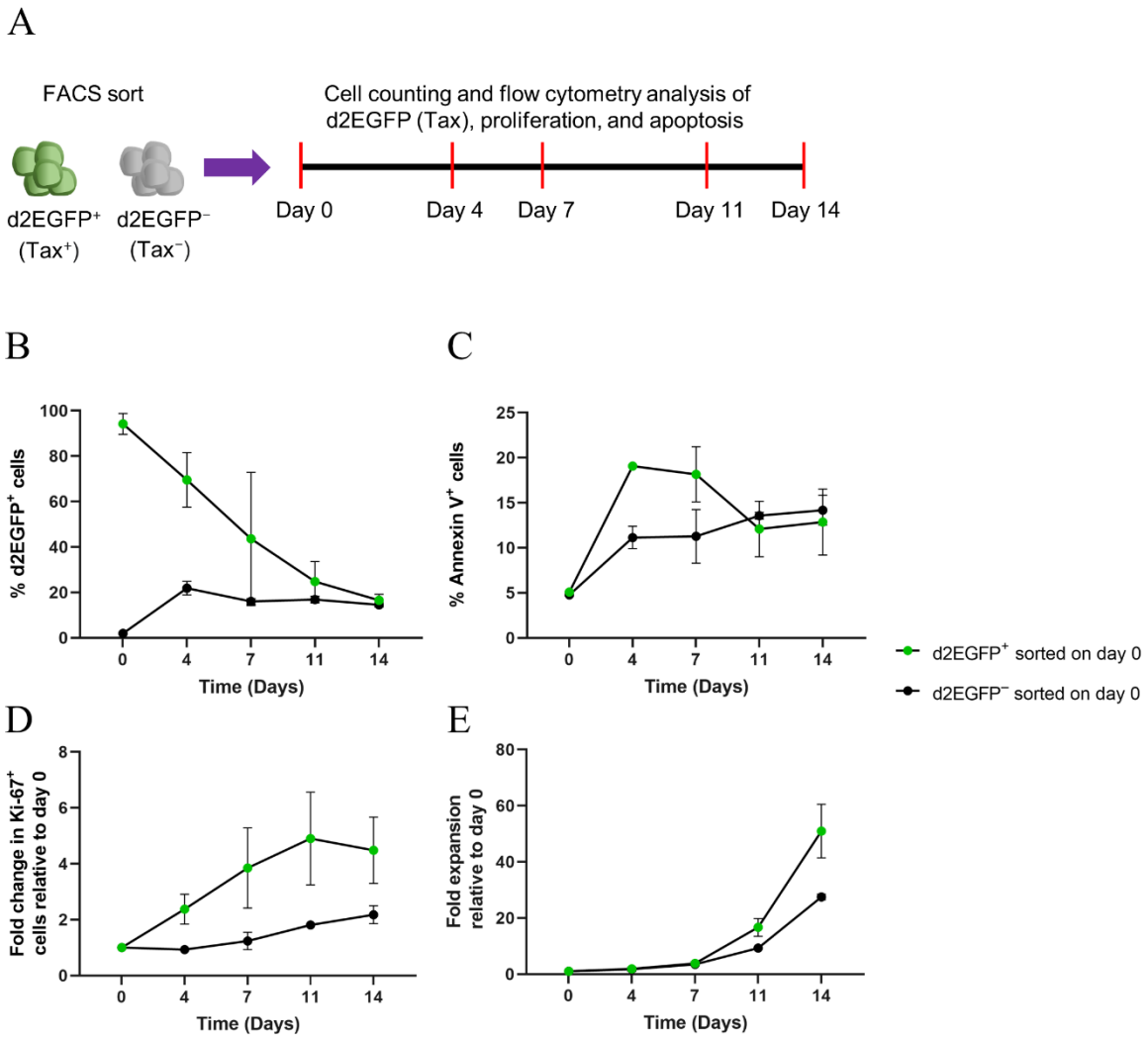

Figure 5-2. The longer-term consequences of Tax expression on the host cell.
(A) Schematic of the experimental design used to investigate the longer-term consequences of Tax expression on the host cell. FACS-sorted d2EGFP$^+$ (Tax$^+$) and d2EGFP$^-$ (Tax$^-$) cells from d2EGFP TBW 11.50 were cultured for up to 14 days. The proportion of d2EGFP$^+$, apoptotic (annexin V$^+$), and proliferating (Ki-67$^+$) cells were determined by flow cytometry analysis on days 0, 4, 7, 11, and 14 post-FACS sort. Cell counts were also performed on the days of flow cytometry analysis. The percentage of (B) d2EGFP and (C) annexin V positive cells among FACS-sorted populations. (D) Fold change in proliferating (Ki-67$^+$) cells and (E) net expansion of FACS-sorted d2EGFP positive and d2EGFP negative populations. The mean and SEM from two independent experiments using d2EGFP TBW 11.50 are shown. The Mann-Kendall test was used to assess the significance of the trend in figures B to E.

5.3.3 Tax expression is associated with the formation of cell clumps

I observed the formation of cell clusters (clumps) in the cultures of naturally HTLV-1-infected, non-malignant T-cell clones. There is evidence of Tax-mediated cell clump formation in rodent (Kitajima et al., 1996) and transformed (Takahashi et al., 2002) cell lines. I wanted to explore if the formation of cell clumps in our cultures was associated with Tax expression. I performed live-cell imaging on five thousand FACS-sorted d2EGFP^{+} (Tax^{+}) and d2EGFP^{-} (Tax^{-}) cells from clones d2EGFP TBX4B and d2EGFP TBW 11.50 at 4-hour frequency for 12 hours. Our assay also included a naturally HTLV-1-infected T-cell clone harbouring a single type 2 defective proviral copy that is incapable of expressing the plus-strand – TCX 8.13 and an uninfected T-cell clone –TBW 13.50.

The mean object area (average particle size) of FACS-sorted d2EGFP^{+} and d2EGFP^{-} populations was similar at the start of imaging, but the mean object area of the d2EGFP^{+} cultures was significantly larger than that of the d2EGFP^{-} cultures after 12 hours (Figures 5-3A, 5-3B, and 5-3C). The mean object area of d2EGFP^{-} cultures, type 2 defective TCX 8.13, and uninfected TBW 13.50 was similar at the beginning and remained steady at the end of the analysis period (Figure 5-3A). These results suggest that the clumps observed in naturally HTLV-1-infected T-cell cultures depended on the expression of the plus-strand.

I observed a significantly higher proportion of ICAM-1 positive cells among d2EGFP-expressing cells compared to non-d2EGFP-expressing cells (Figure 5-3D). A trigger for the cytoskeleton polarisation during virological synapse formation is the engagement of ICAM-1 on the infected cell with LFA-1 on the target cell (Barnard et al., 2005). I postulated that cell clumps (cell-to-cell adhesion) observed among Tax-expressing cells were due to the interaction between ICAM-1 and LFA-1. I investigated the effect of suppression of ICAM-1/LFA-1 interaction using pharmacological and non-pharmacological inhibitors. Pharmacological

inhibitors included an inhibitor of ICAM-1 expression – A205804 (Othumpangat et al., 2016) and an allosteric inhibitor of ICAM-1/LFA-1 engagement – A286982 (Keating et al., 2006). A monoclonal antibody directed towards a functional epitope of ICAM-1 (Jolly et al., 2007) and the cLAB.L cyclic peptide that blocks ICAM-1/LFA-1 interaction through its engagement with the D1 domain of ICAM-1 (Chittasupho et al., 2009). An isotype control antibody and a non-specific cyclic peptide – RD-LBEC were used as the negative controls for the anti-ICAM-1 antibody and cLAB.L peptide, respectively. DMSO served as the vehicle control for the pharmacological inhibitor treatment. Time-lapse whole-well live-cell images were captured at 4-hour frequency for 12 hours after pre-treating 5000 FACS-sorted d2EGFP^{+} cells from clone d2EGFP TBW 11.50 with either inhibitors or controls for one hour. FACS-sorted d2EGFP^{-} cells served as the negative control for cell clumping. The mean object area after 12-hour imaging was similar between cultures treated with LFA-1/ICAM-1 inhibitors and their negative controls, which was much higher than the mean object area of the d2EGFP negative culture (Figure 5-3F). These results indicate that LFA-1/ICAM-1 interaction did not mediate cell-to-cell adhesion among Tax-expressing cells.

There is evidence of Tax-expressing cell lines forming cell-to-cell adhesions with uninfected CCR4^{+} T-cells in a CCL22-dependent way (Hieshima et al., 2008). I observed a significantly higher percentage of CCR4^{+} cells among d2EGFP^{+} cells than in d2EGFP^{-} cells (Figure 5-3D). Real-time qRT-PCR analysis of FACS-sorted d2EGFP populations revealed elevated levels of *CCL22* gene expression among d2EGFP^{+} cells than among d2EGFP^{-} cells (Figure 5-3D). I investigated the hypothesis that the engagements between Tax^{+}CCR4^{+} and Tax^{+}CCL22^{+} cells are responsible for the clumps observed among Tax-expressing cells. Five thousand FACS-sorted d2EGFP-expressing cells from d2EGFP TBW 11.50 were pre-treated with either exogenous CCL22 – the positive control for clumping or C021 – a CCR4 antagonist (Yokoyama et al., 2009) or a combination of CCL22 and C021 for one hour and subsequently

imaged at 4-hour intervals for 12 hours. FACS-sorted d2EGFP^{-} cells served as the negative control for clumping. The mean object area of d2EGFP^{+} cells in all three treatment conditions remained similar and was substantially larger than the mean object area of d2EGFP^{-} cells at the end of 12-hour imaging (Figure 5-3F). These results prove that CCR4 expression does not mediate cell-to-cell adhesion among Tax-expressing cells.

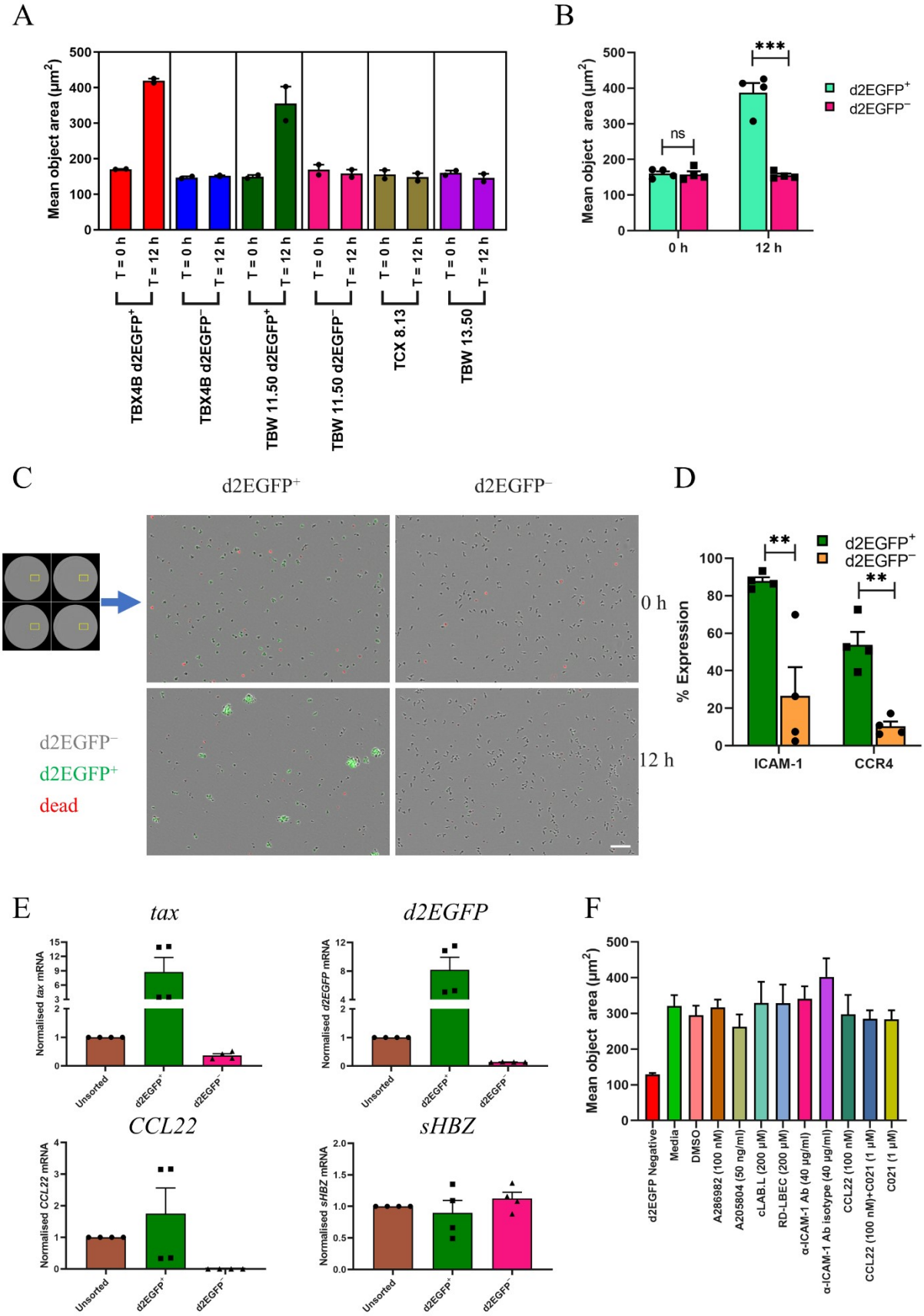
A
Mean object area (µm²)
T = 0 h
T = 12 h
TBX4B d2EGFP+
TBX4B d2EGFP−
TBW 11.50 d2EGFP+
TBW 11.50 d2EGFP−
TCX 8.13
TBW 13.50
B
Mean object area (µm²)
ns
***
d2EGFP+
d2EGFP−
0 h
12 h
C
d2EGFP+
d2EGFP−
0 h
12 h
d2EGFP−
d2EGFP+
dead
D
% Expression
**
**
d2EGFP+
d2EGFP−
ICAM-1
CCR4
E
tax
d2EGFP
CCL22
sHBZ
Normalised tax mRNA
Normalised d2EGFP mRNA
Normalised CCL22 mRNA
Normalised sHBZ mRNA
Unsorted
d2EGFP+
d2EGFP−
F
Mean object area (µm²)
d2EGFP Negative
Media
DMSO
A286982 (100 nM)
A205804 (50 ng/ml)
cLAB.L (200 µM)
RD-LBEC (200 µM)
α-ICAM-1 Ab (40 µg/ml)
α-ICAM-1 Ab isotype (40 µg/ml)
CCL22 (100 nM)
CCL22 (100 nM)+C021 (1 µM)
C021 (1 µM)

Figure 5-3. Tax-expressing cells form cell clumps.
(A) The mean object area at the beginning (0 h) and end (12 h) of imaging of each FACS-sorted cell population. FACS-sorted d2EGFP^{+} and d2EGFP^{-} cells from clones d2EGFP TBX4B and d2EGFP TBW 11.50 and FACS-sorted viable cells from clones TCX 8.13 and TBW 13.50 harbouring a single type 2 defective HTLV-1 proviral copy and uninfected, respectively were imaged at 4-hour intervals for 12 hours. Time-lapse whole-well live-cell images were captured in phase-contrast (d2EGFP^{-} cells), green (d2EGFP^{+} cells), and red (YOYO-3 Iodide – dead cells) channels using Incucyte S3 live-cell imaging system. The mean object area was calculated as described in section 2.4.5. The mean and SEM from two independent experiments are shown. (B) The mean object area of d2EGFP^{+} and d2EGFP^{-} populations of d2EGFP TBX4B and d2EGFP TBW 11.50 at the end of 12-hour imaging. The mean and SEM from two independent experiments are shown. (C) Representative images from d2EGFP TBX4B depicting the formation of cell clumps among d2EGFP^{+} cells after a 12-hour culture. The scale bar is 100 µm. (D) The percentage of ICAM-1^{+} or CCR4^{+} cells among d2EGFP^{+} and d2EGFP^{-} populations were determined by flow cytometry analysis. The mean and SEM from two independent experiments using d2EGFP TBX4B and d2EGFP TBW 11.50 are shown. (E) The expression levels of *tax*, *d2EGFP*, *CCL22*, and *sHBZ* transcripts in unsorted, FACS-sorted d2EGFP^{+}, and FACS-sorted d2EGFP^{-} populations were determined using real-time qRT-PCR. The mean and SEM of PCR technical duplicates from a single experiment using d2EGFP TBX4B and d2EGFP TBW 11.50 are shown. (F) The effect of inhibition of LFA-1/ICAM-1 engagement or CCR4 expression on clump formation. FACS-sorted d2EGFP^{+} cells from d2EGFP TBW 11.50 were pre-treated with agents for one hour at the indicated concentrations. FACS-sorted d2EGFP^{-} cells served as the negative control. Whole-well time-lapse live-cell cell images were captured in phase-contrast, green, and red channels every 4 hours for 12 hours. The mean object area under each treatment condition at the end of 12-hour imaging is shown. The mean and SEM from two independent experiments are depicted. Unpaired student's t-tests were used for statistical analysis. **$P < 0.01, ***$P < 0.001, ns – not significant.

5.3.4 Tax-expressing cells display impaired cell motility

T-cells are one of the most motile cell types that spend much of their time searching to engage their receptors with the cognate peptide-MHC ligands. T-cell motility also plays an important role in the initiation, propagation, and pathogenesis of HTLV-1 infection. There is evidence of enhanced migratory capacity among Tax-expressing cells (Varrin-Doyer et al., 2012; Chevalier et al., 2014). This evidence is based on studies that used cell population level transwell assays to quantify migration. I wished to compare the motility of Tax-expressing and non-Tax-expressing cells of naturally HTLV-1-infected T-cell clones at the single-cell resolution. Since HTLV-1 proviral-expressing cells grew in clumps and at any given time the fraction of non-Tax-expressing cells greatly outnumbered Tax-expressing cells, I FACS sorted d2EGFP^{+} and d2EGFP^{-} populations and subsequently mixed them at 1:1 to get single-cell suspension cultures that were had an approximately equal proportion of d2EGFP-expressing and d2EGFP-non-expressing cells. I seeded 10000 FACS-sorted and subsequently mixed cells from clones d2EGFP TBX4B and d2EGFP TBW 11.50 into wells of a 48 well plate pre-laid with a silicon membrane containing an array of 500 μm x 500 μm wells. This microwell membrane prevented the cells from moving out of the field of view during imaging. Phase-contrast (d2EGFP^{-}), green (d2EGFP^{+}), and red (non-viable) fluorescence time-lapse live-cell images were captured every 3 or 4 minutes for 1 hour.

Single-cell analysis revealed confined tracks among d2EGFP^{+} cells compared to d2EGFP^{-} cells in both clones (Figure 5-4A). The mean speed of d2EGFP^{+} cells in both clones was significantly lower than that of d2EGFP^{-} cells (Figure 5-4B). There was no difference between the two populations in the directionality, a metric of the linearity of the cell paths (Figure 5-4C). The d2EGFP negative population had a greater average MSD, a measure of a cell's displacement from its starting position, than the d2EGFP positive population (Figure 5-4D). Further analysis of MSD data to quantify the type of motion among the individual cells as

described in section 2.4.6 showed a significant difference between the d2EGFP^{+} and d2EGFP^{-} cells (Figure 5-4E): Most d2EGFP^{-} cells displayed superdiffusive motion, with a relatively lower proportion of cells showing diffusive motion. Among d2EGFP^{+} cells, roughly equal proportions of cells showed diffusive and superdiffusive motions. The subdiffusive motion was minimal among cells of both populations. These results show the reduced motility of the Tax-expressing cells relative to non-Tax-expressing cells at the single-cell level.

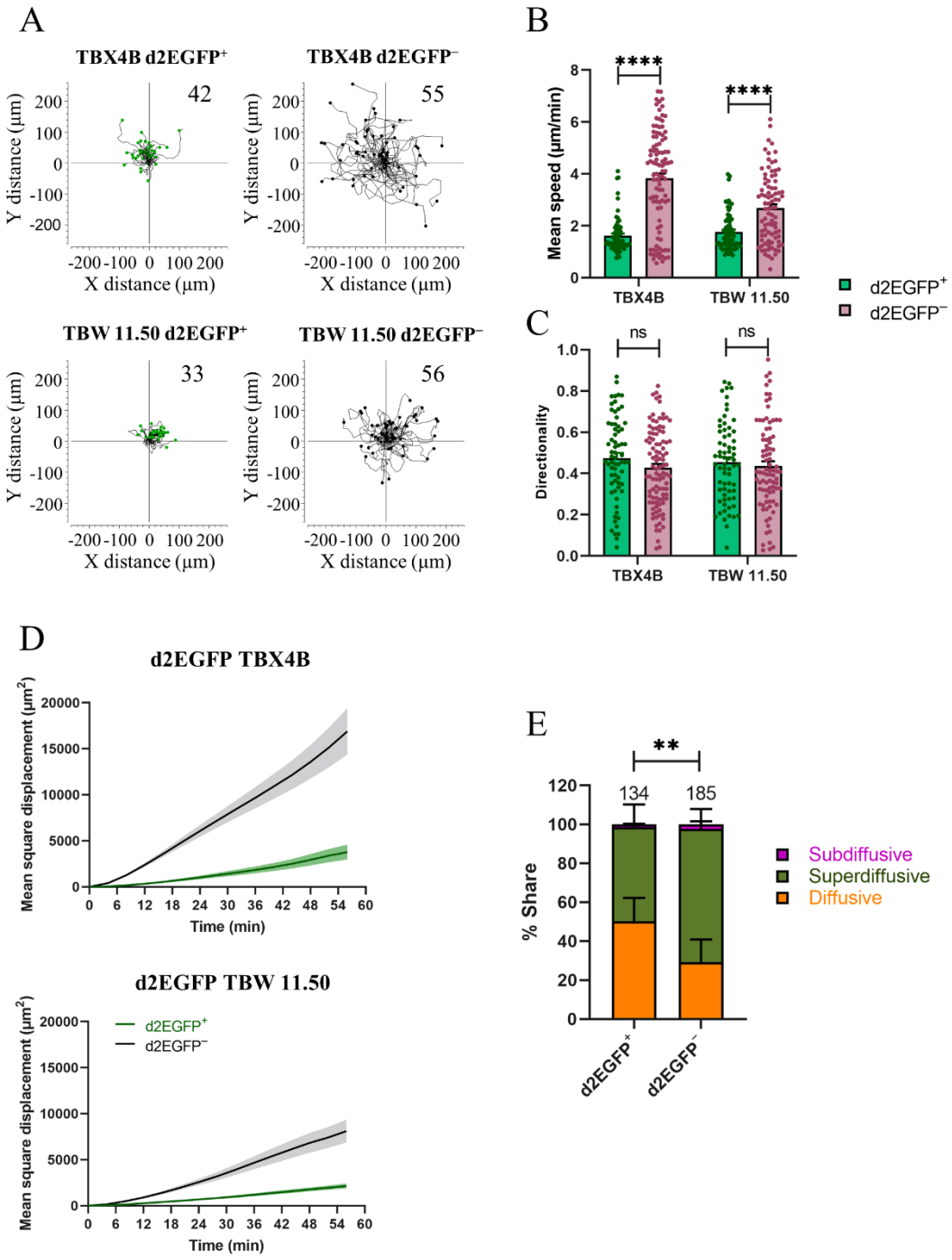
A
TBX4B d2EGFP+
TBX4B d2EGFP−
TBW 11.50 d2EGFP+
TBW 11.50 d2EGFP−
42
55
33
56
Y distance (µm)
X distance (µm)
B
Mean speed (µm/min)
****
****
TBX4B
TBW 11.50
d2EGFP+
d2EGFP−
C
Directionality
ns
ns
TBX4B
TBW 11.50
D
d2EGFP TBX4B
d2EGFP TBW 11.50
Mean square displacement (µm²)
Time (min)
d2EGFP+
d2EGFP−
E
**
134
185
% Share
Subdiffusive
Superdiffusive
Diffusive
d2EGFP+
d2EGFP−

Figure 5-4. Tax-expressing cells show reduced cell motility.
(A) Trajectory plots of d2EGFP$^+$ and d2EGFP$^-$ cells of d2EGFP TBX4B and d2EGFP TBW 11.50 after transforming the initial coordinates of all cells to a common (0,0) origin. Flow cytometry sorted d2EGFP$^+$ and d2EGFP$^-$ cells were mixed 1:1 and seeded into wells pre-laid with a silicon membrane containing an array of microwells. Time-lapse live-cell images were captured in phase-contrast (d2EGFP$^-$ cells), green (d2EGFP$^+$ cells), and red (YOYO-3 Iodide – dead cells) channels every 3 or 4 minutes for one hour. Single-cell tracking and quantitative analysis were performed as described in section 2.4.6. The data from a single representative experiment of two independent experiments are shown. The number within each plot depicts the number of trajectories. (B) Mean speed and (C) directionality of d2EGFP$^+$ and d2EGFP$^-$ cells. The number of cells analysed: TBX4B d2EGFP$^+$ – 68, TBX4B d2EGFP$^-$ – 101, TBW 11.50 d2EGFP$^+$ – 67, and TBW 11.50 d2EGFP$^-$ – 87. The mean and SEM from two independent experiments are shown. (D) MSD of d2EGFP$^+$ and d2EGFP$^-$ cells. The mean ± SEM of a single representative experiment from two independent experiments are shown. The number of cells analysed in the representative experiment: TBX4B d2EGFP$^+$ – 42, TBX4B d2EGFP$^-$ – 55, TBW 11.50 d2EGFP$^+$ – 33, and TBW 11.50 d2EGFP$^-$ – 56. (E) The distribution of different motion types among d2EGFP$^+$ and d2EGFP$^-$ cells. The mean and SEM of two independent experiments using d2EGFP TBX4B and d2EGFP TBW 11.50 are depicted. The numbers on top of the bars denote the number of cells analysed. The data on plots B and C were analysed using the Mann-Whitney test, while a Chi-square test was used to analyse the data presented in graph E. **$P < 0.01, ****$P < 0.0001, ns – not significant.

5.4 Discussion

The expression of the plus-strand is crucial for the persistence and pathogenesis of HTLV-1. The implications of plus-strand expression, in particular Tax protein, the transactivator of the plus-strand on the host cell are unclear. Several studies provide contrasting evidence of Tax-mediated effects on cellular events: Apoptosis promotion (Kao et al., 2000; Rivera-Walsh et al., 2001; Takahashi et al., 2013) or apoptosis inhibition (Copeland et al., 1994; Mahgoub et al., 2018); acceleration through the cell cycle (Low et al., 1997; Lemoine and Marriott, 2001) or impairment of cycle progression (Yang et al., 2011; Mahgoub et al., 2018). The likely cause of these contradictory effects of HTLV-1 Tax expression is the use of less-representative models such as transformed cell lines and recombinant plasmid-based expression systems in cell lines that are not naturally associated with HTLV-1 infection. Other implications of Tax expression such as cell motility and cell-to-cell adhesion remain insufficiently characterised. I studied the short- and longer-term effects of Tax expression on the host cell using naturally HTLV-1-infected, non-malignant T-cell clones to minimise the artefacts associated with recombinant plasmid-based expression systems and transformed cell lines,

A significantly higher proportion of Tax-expressing cells expressed γ-H2AX than non-Tax-expressing cells (Figure 5-1B). These results are consistent with previous studies showing Tax-mediated DNA damage (Chandhasin et al., 2008; Durkin et al., 2008; Kinjo et al., 2010; Baydoun et al., 2015). In addition to primarily being used as a molecular signature of double-strand breaks, the formation of γ-H2AX also occurs due to DNA replication stress (Ward and Chen, 2001). Given the lower frequency of proliferative (Figure 5-1A) and DNA synthesising (Figure 5-1I) cells among Tax-expressing cells, it is likely that the formation of γ-H2AX in Tax positive cells was primarily due to the double-strand breaks. The DDR activates cell cycle checkpoints that slow the advancement through the cell cycle (Houtgraaf et al., 2006). There is also evidence of Tax-mediated elongated cell cycle phases (Yang et al., 2011; Mahgoub et

al., 2018). In agreement with those studies, the passage of Tax-expressing cells through the G2/M transition of the cell cycle was impaired (Figures 5-1F and 5-1H). RNA sequencing results in chapter four showed that the mRNA levels of *ATR* followed that of the plus-strand transcripts, while *ATM* expression was downregulated at the start of the plus-strand expression. It has also been shown that Tax can impair ATM activity (Chandhasin et al., 2008), suggesting that ATR-mediated DDR may be the primary response mechanism to Tax-associated DNA damage observed in these naturally HTLV-1-infected T-cell clones. Apoptosis can be caused by irreparable DNA damage. The observation of a significantly higher percentage of apoptotic cells among Tax-expressing cells (Figure 5-1J) supports the idea that some Tax-expressing cells with irreversible DNA damage underwent apoptosis. In contrast to a previous study (Kinjo et al., 2010), there was no difference in the proportion of ROS positive cells among Tax-expressing and non-Tax-expressing cells (Figure 5-1D). Another genotoxic mediator such as nitric oxide that has been shown to induce DSBs in a Tax-dependent manner (Baydoun et al., 2015) could have accounted for the elevated DNA damage among Tax-expressing cells in these naturally HTLV-1-infected T-cell clones.

Longer-term follow-up of Tax positive and negative populations revealed that Tax negative population had reached the steady state by day four post-sort culture – the first point of analysis after the day of FACS sort, while Tax positive population only reached the equilibrium state during the second week of culture (Figure 5-2B). These observations highlight the differential dynamics of reaching the equilibrium state between the Tax positive and negative populations. The relatively rapid reactivation of non-Tax-expressing cells is consistent with a recent report showing that the reactivation of HTLV-1 plus-strand mimicked an immediate-early gene (Kulkarni et al., 2018). That is HTLV-1 plus-strand reactivation exhibits kinetics that resemble the expression of immediately early genes which are rapidly transcribed in response to a variety of stimuli, including cellular stress. The net expansion of the FACS-sorted Tax positive

population was higher owing to an increase in the fraction of proliferating cells and a decrease in the percentage of apoptotic cells as they terminated Tax expression (Figures 5-2C, 5-2D, and 5-2E). Apoptotic cells secrete growth-promoting proteins that activate signalling pathways in healthy cells promoting their proliferation and survival (Moreno-Celis et al., 2022). This phenomenon, known as apoptosis-induced cell proliferation has been described in insects (Ryoo et al., 2004), rodents (Valentin-Vega et al., 2008), and human cancers (Huang et al., 2011) and may account for the expansion of cells that survive the adverse effects of prolonged Tax expression.

There is evidence of Tax-mediated cell-to-cell adhesion in studies performed on rodent (Kitajima et al., 1996) and transformed human cell lines (Takahashi et al., 2002). Consistent with these studies, I observed significant cell-to-cell adhesion among Tax-expressing cells of naturally HTLV-1-infected, non-malignant T-cell clones. In contrast, non-Tax-expressing cells showed similar behaviour to an uninfected clone and a clone harbouring a provirus incapable of expressing the plus-strand by not forming substantial cell-to-cell adhesions during the observation period (Figures 5-3A, 5-3B, and 5-3C). Unlike HIV-1, cell-free virions of HTLV-1 are rare and poorly infectious (Mazurov et al., 2010). Cell-to-cell transmission occurs primarily through the formation of the virological synapse (Igakura et al., 2003). The interaction of ICAM-1 on the infected cell with LFA-1 on the target cell, resulting in the polarisation of the infected cell's cytoskeleton toward the cell-to-cell contact is a trigger in the formation of the virological synapse (Barnard et al., 2005). In agreement with a previous observation (Tanaka et al., 1995), ICAM-1 expression was upregulated among Tax-expressing cells (Figure 5-3D). Inhibition of ICAM-1/LFA-1 interaction did not inhibit the formation of clumps among Tax-expressing cells (Figure 5-3F), suggesting that ICAM-1/LFA-1 engagement did not mediate the cell-to-cell adhesion in Tax positive cells. Uninfected $CCR4^{+}$ cells form cell-to-cell adhesions with Tax-expressing cells in a CCL22-dependent manner

(Hieshima et al., 2008). CCR4 protein (Figure 5-3D) and *CCL22* transcripts (Figure 5-3E) were upregulated in Tax-expressing cells. Pharmacological inhibition of CCR4 had no effect on clump formation among Tax-expressing cells, implying that the interactions between $CCR4^+$ and CCL22-expressing cells did not mediate the clumps observed among Tax-expressing cells. There is novel evidence that the formation of cell clumps in HTLV-1-infected cells is attributable to the activation of the phospholipase C gamma 1 (PLCγ1) pathway with exogenous IL-2 enhancing this effect (Prawiro et al., 2023).

It has been shown that Tax directly enhances cell migration through the upregulation of Gem – a GFPase that promotes cytoskeletal remodelling to facilitate cell migration (Chevalier et al., 2014). Another study showed that the enhanced migratory capacity of HTLV-1-infected cells was only partially attributable to Tax, as it raised the levels of the cytoskeleton remodelling phosphoprotein – collapsing response mediator protein 2 (CRMP2) without inducing its phosphorylation that is required for CRMP2 function (Varrin-Doyer et al., 2012). Single-cell quantification showed reduced motility among Tax-expressing cells (Figures 5-4A, 5-4B, 5-4D, and 5-4E). The contrasting effects of Tax on cell migration observed between our study and the studies mentioned above could be attributable to the fundamental differences in the experimental design: I quantified random cell motility at the single-cell level in the 2D plane, while those studies quantified cell migration through a transwell membrane in response to a chemokine gradient.

Chapter 6

6.1 Discussion and future directions

The expression of the plus-strand is vital for the persistence and pathogenesis of HTLV-1. The kinetics of HTLV-1 expression remains insufficiently characterised. The impact of HTLV-1 expression on the host cell is less clear, with some studies reporting directly opposite consequences of HTLV-1 Tax on the host cell, potentially due to the use of different cell models. In this study, I used live-cell imaging, mathematical modelling, flow cytometry, and transcriptome analysis to study the kinetics, mechanisms, and consequences of HTLV-1 plus-strand expression in naturally HTLV-1-infected, non-malignant T-cell clones.

My significant findings were:

1. Multiple patterns of Tax (plus-strand) expression were observed among individual T-cell clones and the distribution of these Tax expression patterns was significantly different between the clones. The mean duration of Tax expression was also markedly different between the T-cell clones.
2. PKC agonists, bryostatin-1 and prostratin induced the highest level of proviral expression among the LRAs and the frequency of spontaneous proviral reactivation differed noticeably between the T-cell clones.
3. Genes regulating cellular processes, including cell cycle, DNA damage response, and apoptosis were dysregulated during the plus-strand expression.
4. The increase of AhR signalling resulted in enhanced proviral expression and the inhibition of AhR signalling was insufficient to prevent the spontaneous proviral reactivation.
5. HTLV-1 plus-strand expression was associated with decreased proliferation, increased DNA damage and apoptosis, and slower progression through the cell cycle in the short-

term. In the longer-term, Tax expression was followed by a post-expression compensatory proliferative burst.

6. Tax expression was associated with cell-to-cell adhesion and decreased cell motility.

Gene expression is inherently stochastic even among an isoclonal population of cells owing to the fluctuations in the biochemical reactions, ultimately giving rise to cell-to-cell heterogeneity (Blake et al., 2003). Single-cell analysis revealed five different patterns of plus-strand (Tax) expression within the clonal cell populations. Since the integration site, a factor known to regulate HTLV-1 proviral expression remained uniform across all clonal cells, multiple patterns of proviral expression within clonal cells may have been attributable to either the extrinsic factors such as the epigenetic modifications at the proviral promoter, cell size, and cell cycle stage or the stochasticity in gene expression. Stochastic changes in the levels of Tat drive the decision between latency and proviral expression in HIV-1 (Weinberger et al., 2005). The stochastic fluctuations in Tax protein levels that drive the expression of the d2EGFP reporter may have accounted for the observed phenotypic differences in the clonal populations.

The long duration of Tax expression observed in naturally HTLV-1-infected T-cell clones comes as a surprise. Given the highly immunogenic nature of the Tax protein, one would expect the cells to minimise its expression to short bursts, thus allowing a narrow window of opportunity for the proviral replication and *de novo* infection. Indeed, it has been shown using the mathematical modelling of smFISH data from *ex vivo* PBMCS of an ATL patient with a single dominant clone, that the spontaneous, intense plus-strand bursts on average last for less than an hour (Miura et al., 2019). This estimate is vastly different to the mean duration of Tax protein expression of 19 hours reported in the ATL cell line – MT1 through live-cell imaging (Mahgoub et al., 2018) and our estimate of >90 hours based on the mathematical modelling of

the live-cell imaging data. In the study of Miura et al., it may have been possible that the initial plus-strand transcriptional burst was terminated in the presence of Tax protein in the cell. However, given the long half-life of Tax protein (Hemelaar et al., 2001), repeated transcriptional bursts may occur before Tax is entirely degraded, thus "replenishing" the depleting Tax protein levels, resulting in a much longer duration of Tax expression in the protein level studies.

Clone-specific factors including the proviral viral integration site that regulate proviral gene expression may have accounted for the difference in the Tax expression duration between the clones. Significant clone-to-clone variation was also evident in the frequency of spontaneous and maximal reactivation of latent HTLV-1, which again is most likely attributable to the genomic environment surrounding the proviral promotor.

Proteins of several chronic human viruses activate the NF-κB pathway: HTLV-1 Tax; HIV-1 Tat; Epstein-Barr virus (EBV) latent membrane protein 1 (LMP1) (Hiscott et al., 2001), suggesting an important role of the NF-κB pathway in chronic viral infections. It has been shown that the knockdown of IκBs induces HIV-1 proviral reactivation (Fernandez et al., 2013), indicating the importance of the NF-κB pathway in HIV-1 latency maintenance. The PKC activators bryostatin-1 (Díaz et al., 2015) and prostratin (Williams et al., 2004) induce HIV-1 expression by activating the NF-κB pathway through PKC-mediated IκB degradation. Consistent with the analogy in HIV-1, bryostatin-1 and prostratin proved to be potent inducers of HTLV-1 proviral expression in non-malignant T-cell clones, suggesting a role of NF-κB pathway in HTLV-1 latency preservation. However, given the multifactorial nature of retroviral latency, multi-pronged reactivation and kill strategies are likely to be needed to successfully implement the "shock and kill" in HTLV-1 and HIV-1 infections.

Microbial infections mediate changes in host gene expression, which may be the cause or effect of their pathogenesis. Infection with HTLV-1 alters the host gene expression (Ng et al., 2001; Mahgoub et al., 2018), primarily through the regulatory protein Tax that is known to interact with hundreds of cellular proteins (Boxus et al., 2008). The use of a novel fluorescent timer protein-based Tax reporter system that allowed temporal separation of the plus-strand burst paved the way to distinguish immediate and delayed effects of the plus-strand expression. The dysregulated expression of genes regulating multiple cellular processes, including cell cycle, DNA damage response, and apoptosis immediately following the initiation of the plus-strand expression suggests a direct role of Tax in altering these cellular processes. The divergent expression pattern of some cell cycle-related genes in the two clones suggests some effects of the plus-strand expression, at least at the mRNA level are clone specific. The upregulation of pro-apoptotic genes suggests the toxicity of sustained Tax expression on the host cell, while the upregulation of anti-apoptotic genes may counteract this effect.

The hypothesis that negative regulation of AhR signalling may terminate the plus-strand expression proved invalid. Crucially, the importance of AhR signalling in modulating HTLV-1 plus-strand expression was confirmed in naturally HTLV-1-infected T-cell clones. AhR also plays a role in HIV-1 reactivation, where HIV-1 Tat recruits the positive transcription elongation factor b (P-TEFb) to the promoter in an AhR-dependent manner (Zhou et al., 2019). In HTLV-1, AhR binds to the LTR's dioxin response element (DRE) to activate plus-strand expression (Hong et al., 2020). Endogenous AhR ligands such as tryptophan metabolites accumulate in the tissue culture medium, contributing to basal AhR signalling (Veldhoen et al., 2009). *In vivo* however, the levels of endogenous ligands are likely to be significantly lower due to excretion, making background AhR signalling negligible. Indeed, the lack of detectable AhR activity has been demonstrated in the peripheral blood of ATL patients despite high AhR expression (Hayashibara et al., 2003). This might explain the lack of detectable proviral

expression in peripheral blood *in vivo* and the spontaneous proviral reactivation during short-term *ex vivo* culture. However, other factors such as stress that are known to induce proviral expression are also likely to contribute to the *ex vivo* spontaneous proviral reactivation. The possibility of using exogenous AhR ligands such as indoles and flavonoids to induce *in vivo* proviral reactivation through the increased AhR signalling to augment the effect of "shock and kill" should be investigated.

Although extensively studied, the experimental consequences of HTLV-1 plus-strand (Tax) expression are sometimes contradictory: Tax expression has been linked to promotion (Kao et al., 2000; Takahashi et al., 2013) and prevention (Copeland et al., 1994; Mahgoub et al., 2018) of apoptosis; Tax has also been linked to proliferation (Akagi et al., 1995; Xie et al., 2006) and impaired cell cycle progression (Yang et al., 2011; Mahgoub et al., 2018). The contrasting effects associated with Tax expression are potentially due to the different cellular systems used. The intensity and duration of Tax expression in various cell models are substantially different – for example, in the MT2 cell line that harbours multiple copies of the HTLV-1 provirus, Tax is constitutively expressed in all cells at high levels (Kobayashi et al., 1984). In contrast, in the ATL cell line, MT1 that contains multiple copies of the HTLV-1 provirus, Tax expression is limited to short intermittent bursts, with only a minority of cells expressing Tax at any given time (Mahgoub et al., 2018). The recombinant plasmid-based expression systems that use strong promoters induce high and sustained levels of transgene expression. The use of naturally HTLV-1-infected T-cell clones provided a physiologically appropriate model for investigating the effect of Tax expression on the host cell.

Given that prolonged Tax expression is harmful to the cells and the observation of long duration of Tax expression through live-cell imaging and mathematical modelling, the immediate adverse effects associated with Tax expression, including reduced proliferation, impaired cell cycle progression, and increased DNA damage and apoptosis are not surprising. Tax, through

its prolonged expression may have promoted DNA damage as indicated by elevated γ-H2AX positivity. In an attempt to repair the DNA damage, the cell cycle progression may have been impaired, with irreversible DNA damage leading to more apoptotic cells, as observed among the Tax-expressing cells. Permanent growth arrest or cellular senescence is another major outcome of irreversible DNA damage (Chen et al., 2007), which has also been liked to HTLV-1 Tax expression (Zhi et al., 2011). Future studies should investigate if cellular senescence is also an outcome of Tax expression in naturally HTLV-1-infected T-cells.

The immediate adverse effects associated with Tax expression were followed by a decrease in the frequency of apoptotic cells and an increase in the fraction of proliferating cells as cells gradually switched off Tax expression, leading to a greater net expansion of the original Tax positive population. This observation implies that the cells that survive the adverse effects associated with long Tax bursts have a survival and growth advantage. Apoptosis-induced cell proliferation, discussed in chapter five, could have mediated this post-Tax expression proliferative burst. Another possibility is the expression of HBZ protein that binds to CREB to suppress plus-strand expression (Lemasson et al., 2007). HBZ has also been shown to enhance cellular proliferation at the transcript (Satou et al., 2006) and protein (Sugata et al., 2016) levels and to suppress apoptosis at the transcript level (Mitobe et al., 2015).

The epigenetic modifications of the proviral genome play a significant role in latency maintenance in HIV-1 (Khan et al., 2018) and HTLV-1 (Ratner, 2021). The relatively-speedy proviral reactivation to reach the steady-state observed among silent cells agrees with stress-induced, p38-MAPK-dependent immediate-early gene response (Kulkarni et al., 2018). In contrast, the longer duration taken to reach the steady-state by the proviral-expressing cells suggests that the epigenetic modifications that sustain the proviral latency are not rapidly re-stored upon proviral reactivation. Chromatin immunoprecipitation (ChIP) assays on FACS-

sorted fluorescent timer protein-expressing cells representing different stages of HTLV-1 plus-strand expression will help test this hypothesis.

The expression of HTLV-1 plus-strand is obligatory for *de novo* infections. Virological synapse formation triggered through ICAM-1/LFA-1 engagement (Barnard et al., 2005) plays a major role in cell-to-cell transmission of HTLV-1, where cell-free virions are rare and poorly infectious (Mazurov et al., 2010). Although less critical than HTLV-1, cell-to-cell transmission remains an important mode of *de novo* HIV-1 infections facilitated by ICAM-3/LFA-1 interactions forming the HIV-1 virological synapse (Jolly et al., 2007). Tax-expressing cells formed cell-to-cell adhesions despite the inhibition of ICAM-1/LFA-1 interactions implying that clump formation was independent of ICAM-1/LFA-1 engagement. According to a recent study (Prawiro et al., 2023), cell clumping was related to increased PLCγ1 activity driven by the missense mutation S345F in the *PLCG1*, a gene that is mutated in 36% of ATL cases (Kataoka et al., 2015). T-cell clones used in our study were non-malignant. Therefore, they were unlikely to have the abovementioned mutation in the *PLCG1.* The formation of clumps was observed between Tax-expressing cells, but not among non-Tax-expressing cells. These pieces of evidence suggest that the clumping was mediated through one or more receptors – for example, CADM-1 or E-cadherin upregulated by Tax, something that the future studies should investigate.

As described in chapter five, Tax-expressing cells are "sticky" by nature, attaching to each other independent of certain adhesion molecules and receptors. It is plausible that transient attachments of Tax-expressing cells to the polymer surface slowed their motility, resulting in decreased speed and displacement. This hypothesis can be tested by coating the PDMS surface with a layer of hydrophilic gel that has been shown to minimise non-specific cell attachment (Shen and Horbett, 2001). Regulatory proteins Tax and HBZ alter the expression of several chemokines and their receptors that have important implications in HTLV-1 infection and

pathogenesis (Zargari et al., 2020). CCR4 is one such receptor that is frequently expressed in ATL cells and may have a role in the skin and lymph node infiltration of ATL cells (Yoshie et al., 2002). Given that Tax expression was associated with increased CCR4 expression, it is important to quantify the chemotactic potential of Tax positive and negative cells in response to the CCR4 ligands CCL17 and CCL22 in transwell migration assays. It would also be interesting to investigate if the random motility of Tax-expressing cells changes in response to the treatment with exogenous CCL17 and CCL22.

The primary role of proviral expression is to establish *de novo* infections. Plus-strand expression was associated with increased cell-to-cell adhesion and decreased motility. These observations suggest that the primary objective of the proviral-expressing cells is to increase the chances of contacting the nearby cells to maximise the likelihood of *de novo* infections instead of travelling over long distances in search of cells. Indeed, most lymphocytes occupy the lymphoid organs, with only a minority (~2%) in the peripheral blood at a given time (Battaglia et al., 2003). This means proviral-expressing cells in these organs do not have to move long distances to encounter uninfected cells, as cells are more densely populated than in the peripheral blood. Proviral expression is rarely detected in peripheral circulation, while lymphoid organs are hypoxic (Tsai et al., 2004), a condition known to increase the plus-strand expression (Kulkarni et al., 2017). All these factors may work in concert to increase the efficiency of *de novo* infections in the lymphoid organs.

This study was based on two naturally HTLV-1-infected T-cell clones isolated from two HAM/TSP patients. While most plus-strand-associated consequences were consistent between the two clones, there were fundamental differences regarding the duration and distribution of the plus-strand expression patterns. Also, clone-specific divergence was observed in the dysregulation of cell cycle-related genes. While it may be impractical to study hundreds or

even tens of clones, using more clones from individuals representing diverse disease status would strengthen the inferences.

Tax protein is a surrogate for the plus-strand expression. However, given the expression of other plus-strand-encoded viral proteins transactivated by Tax, some consequences reported in this thesis may be attributable to the plus-strand viral proteins other than Tax. I aimed to understand the changes in the host cell at the transcript and protein levels in response to the plus-strand expression of the unmanipulated HTLV-1 provirus, and understanding the precisely coordinated consequences of the viral life cycle requires the study of the provirus in naturally-infected cells.

In summary, this study was the first to quantify the duration of Tax (plus-strand) expression in naturally HTLV-1-infected non-malignant T-cell clones. Multiple patterns of Tax expression were observed among clonal cells, and the distribution of these patterns was different between the two clones tested. The frequency of spontaneous proviral reactivation was different between the clones. PKC agonists, bryostatin-1 and prostratin were the most potent inducers of HTLV-1 plus-strand expression among the LRAs. The study of host gene expression during successive stages of the proviral plus-strand expression for the first time revealed the dysregulation in the expression of genes associated with multiple cellar processes, including cell cycle, DNA damage response, and apoptosis immediately following the HTLV-1 proviral reactivation. Increased AhR signalling enhanced proviral expression and inhibiting AhR signalling could not prevent the spontaneous proviral reactivation. Tax expression was associated with immediate, but transient adverse effects, including increased apoptosis, decreased proliferation, upregulation of a DNA damage marker, and impaired cell cycle progression. However, in the longer term, these negative effects were counterbalanced by decreased apoptosis and enhanced proliferation upon the cessation of Tax expression resulting

in a greater net expansion. Tax expression was associated with enhanced cell-to-cell adhesion and reduced motility at the single-cell level.

These data demonstrate the intra- and inter-clonal heterogeneity in the patterns and kinetics of HTLV-1 plus-strand expression, the changes to the host gene transcription resulting from HTLV-1 proviral reactivation, and the equilibrium between the favourable and detrimental consequences of the plus-strand expression on the host cell.

References

Akagi, T., Ono, H. & Shimotohno, K. 1995. Characterization of T cells immortalized by Tax1 of human T-cell leukemia virus type 1. *Blood,* 86**,** 4243-9.

Alais, S., Dutartre, H. & Mahieux, R. 2017. Quantitative Analysis of Human T-Lymphotropic Virus Type 1 (HTLV-1) Infection Using Co-Culture with Jurkat LTR-Luciferase or Jurkat LTR-GFP Reporter Cells. *Methods Mol Biol,* 1582**,** 47-55.

Andresen, V., Pise-Masison, C. A., Sinha-Datta, U., Bellon, M., Valeri, V., et al. 2011. Suppression of HTLV-1 replication by Tax-mediated rerouting of the p13 viral protein to nuclear speckles. *Blood,* 118**,** 1549-59.

Arellano, M. & Moreno, S. 1997. Regulation of CDK/cyclin complexes during the cell cycle. *Int J Biochem Cell Biol,* 29**,** 559-73.

Arisawa, K., Soda, M., Endo, S., Kurokawa, K., Katamine, S., et al. 2000. Evaluation of adult T-cell leukemia/lymphoma incidence and its impact on non-Hodgkin lymphoma incidence in southwestern Japan. *Int J Cancer,* 85**,** 319-24.

Arnold, J., Yamamoto, B., Li, M., Phipps, A. J., Younis, I., et al. 2006. Enhancement of infectivity and persistence in vivo by HBZ, a natural antisense coded protein of HTLV-1. *Blood,* 107**,** 3976-82.

Asquith, B., Mosley, A. J., Barfield, A., Marshall, S. E. F., Heaps, A., et al. 2005. A functional CD8+ cell assay reveals individual variation in CD8+ cell antiviral efficacy and explains differences in human T-lymphotropic virus type 1 proviral load. *J Gen Virol,* 86**,** 1515-1523.

Assil, S., Futsch, N., Décembre, E., Alais, S., Gessain, A., et al. 2019. Sensing of cell-associated HTLV by plasmacytoid dendritic cells is regulated by dense β-galactoside glycosylation. *PLoS Pathog,* 15**,** e1007589.

Atsaves, V., Leventaki, V., Rassidakis, G. Z. & Claret, F. X. 2019. AP-1 Transcription Factors as Regulators of Immune Responses in Cancer. *Cancers (Basel),* 11.

Azakami, K., Sato, T., Araya, N., Utsunomiya, A., Kubota, R., et al. 2009. Severe loss of invariant NKT cells exhibiting anti-HTLV-1 activity in patients with HTLV-1-associated disorders. *Blood,* 114**,** 3208-15.

Bahrami, S. & Drabløs, F. 2016. Gene regulation in the immediate-early response process. *Adv Biol Regul,* 62**,** 37-49.

Ballard, D. W., Böhnlein, E., Lowenthal, J. W., Wano, Y., Franza, B. R., et al. 1988. HTLV-I tax induces cellular proteins that activate the kappa B element in the IL-2 receptor alpha gene. *Science,* 241**,** 1652-5.

Bangham, C. R. 2009. CTL quality and the control of human retroviral infections. *Eur J Immunol,* 39**,** 1700-12.

Bangham, C. R., Araujo, A., Yamano, Y. & Taylor, G. P. 2015. HTLV-1-associated myelopathy/tropical spastic paraparesis. *Nat Rev Dis Primers,* 1**,** 15012.

Barnard, A. L., Igakura, T., Tanaka, Y., Taylor, G. P. & Bangham, C. R. 2005. Engagement of specific T-cell surface molecules regulates cytoskeletal polarization in HTLV-1-infected lymphocytes. *Blood,* 106**,** 988-95.

Bartek, J. & Lukas, J. 2003. Chk1 and Chk2 kinases in checkpoint control and cancer. *Cancer Cell,* 3**,** 421-9.

Basbous, J., Bazarbachi, A., Granier, C., Devaux, C. & Mesnard, J. M. 2003. The central region of human T-cell leukemia virus type 1 Tax protein contains distinct domains involved in subunit dimerization. *J Virol,* 77**,** 13028-35.

Battaglia, A., Ferrandina, G., Buzzonetti, A., Malinconico, P., Legge, F., et al. 2003. Lymphocyte populations in human lymph nodes. Alterations in CD4+ CD25+ T regulatory cell phenotype and T-cell receptor Vbeta repertoire. *Immunology,* 110**,** 304-12.

Baydoun, H. H., Cherian, M. A., Green, P. & Ratner, L. 2015. Inducible nitric oxide synthase mediates DNA double strand breaks in Human T-Cell Leukemia Virus Type 1-induced leukemia/lymphoma. *Retrovirology,* 12**,** 71.

Bazarbachi, A., Plumelle, Y., Carlos Ramos, J., Tortevoye, P., Otrock, Z., et al. 2010. Meta-analysis on the use of zidovudine and interferon-alfa in adult T-cell leukemia/lymphoma showing improved survival in the leukemic subtypes. *J Clin Oncol,* 28**,** 4177-83.

Bellon, M., Baydoun, H. H., Yao, Y. & Nicot, C. 2010. HTLV-I Tax-dependent and -independent events associated with immortalization of human primary T lymphocytes. *Blood,* 115**,** 2441-8.

Belrose, G., Gross, A., Olindo, S., Lézin, A., Dueymes, M., et al. 2011. Effects of valproate on Tax and HBZ expression in HTLV-1 and HAM/TSP T lymphocytes. *Blood,* 118**,** 2483-91.

Bending, D., Paduraru, A., Ducker, C. B., Prieto Martín, P., Crompton, T., et al. 2018. A temporally dynamic Foxp3 autoregulatory transcriptional circuit controls the effector Treg programme. *Embo j,* 37.

Berg, S., Kutra, D., Kroeger, T., Straehle, C. N., Kausler, B. X., et al. 2019. ilastik: interactive machine learning for (bio)image analysis. *Nat Methods,* 16**,** 1226-1232.

Bertrand, E., Chartrand, P., Schaefer, M., Shenoy, S. M., Singer, R. H., et al. 1998. Localization of ASH1 mRNA particles in living yeast. *Mol Cell,* 2**,** 437-45.

Bex, F., Murphy, K., Wattiez, R., Burny, A. & Gaynor, R. B. 1999. Phosphorylation of the human T-cell leukemia virus type 1 transactivator tax on adjacent serine residues is critical for tax activation. *J Virol,* 73**,** 738-45.

Billman, M. R., Rueda, D. & Bangham, C. R. M. 2017. Single-cell heterogeneity and cell-cycle-related viral gene bursts in the human leukaemia virus HTLV-1. *Wellcome Open Res,* 2**,** 87.

Blake, W. J., M, K. A., Cantor, C. R. & Collins, J. J. 2003. Noise in eukaryotic gene expression. *Nature,* 422**,** 633-7.

Boelen, L., Debebe, B., Silveira, M., Salam, A., Makinde, J., et al. 2018. Inhibitory killer cell immunoglobulin-like receptors strengthen CD8(+) T cell-mediated control of HIV-1, HCV, and HTLV-1. *Sci Immunol,* 3.

Boxus, M., Twizere, J. C., Legros, S., Dewulf, J. F., Kettmann, R., et al. 2008. The HTLV-1 Tax interactome. *Retrovirology,* 5**,** 76.

Boxus, M. & Willems, L. 2009. Mechanisms of HTLV-1 persistence and transformation. *Br J Cancer,* 101**,** 1497-501.

Brady, J., Jeang, K. T., Duvall, J. & Khoury, G. 1987. Identification of p40x-responsive regulatory sequences within the human T-cell leukemia virus type I long terminal repeat. *J Virol,* 61**,** 2175-81.

Brandsma, I. & Gent, D. C. 2012. Pathway choice in DNA double strand break repair: observations of a balancing act. *Genome Integr,* 3**,** 9.

Brunetto, G. S., Massoud, R., Leibovitch, E. C., Caruso, B., Johnson, K., et al. 2014. Digital droplet PCR (ddPCR) for the precise quantification of human T-lymphotropic virus 1 proviral loads in peripheral blood and cerebrospinal fluid of HAM/TSP patients and identification of viral mutations. *J Neurovirol,* 20**,** 341-51.

Cachat, A., Alais, S., Chevalier, S. A., Journo, C., Fusil, F., et al. 2014. ADAR1 enhances HTLV-1 and HTLV-2 replication through inhibition of PKR activity. *Retrovirology,* 11**,** 93.

Cachat, A., Chevalier, S. A., Alais, S., Ko, N. L., Ratner, L., et al. 2013. Alpha interferon restricts human T-lymphotropic virus type 1 and 2 de novo infection through PKR activation. *J Virol,* 87**,** 13386-96.

Chandhasin, C., Ducu, R. I., Berkovich, E., Kastan, M. B. & Marriott, S. J. 2008. Human T-cell leukemia virus type 1 tax attenuates the ATM-mediated cellular DNA damage response. *J Virol,* 82**,** 6952-61.

Chao, J. A., Patskovsky, Y., Almo, S. C. & Singer, R. H. 2008. Structural basis for the coevolution of a viral RNA-protein complex. *Nat Struct Mol Biol,* 15**,** 103-5.

Charoenthongtrakul, S., Zhou, Q., Shembade, N., Harhaj, N. S. & Harhaj, E. W. 2011. Human T cell leukemia virus type 1 Tax inhibits innate antiviral signaling via NF-kappaB-dependent induction of SOCS1. *J Virol,* 85**,** 6955-62.

Chen, J. H., Hales, C. N. & Ozanne, S. E. 2007. DNA damage, cellular senescence and organismal ageing: causal or correlative? *Nucleic Acids Res,* 35**,** 7417-28.

Cheng, X., Joseph, A., Castro, V., Chen-Liaw, A., Skidmore, Z., et al. 2021. Epigenomic regulation of human T-cell leukemia virus by chromatin-insulator CTCF. *PLoS Pathog,* 17**,** e1009577.

Chevalier, S. A., Turpin, J., Cachat, A., Afonso, P. V., Gessain, A., et al. 2014. Gem-induced cytoskeleton remodeling increases cellular migration of HTLV-1-infected cells, formation of infected-to-target T-cell conjugates and viral transmission. *PLoS Pathog,* 10**,** e1003917.

Chittasupho, C., Xie, S. X., Baoum, A., Yakovleva, T., Siahaan, T. J., et al. 2009. ICAM-1 targeting of doxorubicin-loaded PLGA nanoparticles to lung epithelial cells. *Eur J Pharm Sci,* 37**,** 141-50.

Chu, Z. L., DiDonato, J. A., Hawiger, J. & Ballard, D. W. 1998. The tax oncoprotein of human T-cell leukemia virus type 1 associates with and persistently activates IkappaB kinases containing IKKalpha and IKKbeta. *J Biol Chem,* 273**,** 15891-4.

Ciccia, A. & Elledge, S. J. 2010. The DNA damage response: making it safe to play with knives. *Mol Cell,* 40**,** 179-204.

Cikos, S., Bukovská, A. & Koppel, J. 2007. Relative quantification of mRNA: comparison of methods currently used for real-time PCR data analysis. *BMC Mol Biol,* 8**,** 113.

Clerc, I., Polakowski, N., André-Arpin, C., Cook, P., Barbeau, B., et al. 2008. An interaction between the human T cell leukemia virus type 1 basic leucine zipper factor (HBZ) and the KIX domain of p300/CBP contributes to the down-regulation of tax-dependent viral transcription by HBZ. *J Biol Chem,* 283**,** 23903-13.

Colisson, R., Barblu, L., Gras, C., Raynaud, F., Hadj-Slimane, R., et al. 2010. Free HTLV-1 induces TLR7-dependent innate immune response and TRAIL relocalization in killer plasmacytoid dendritic cells. *Blood,* 115**,** 2177-85.

Cook, L. B., Melamed, A., Demontis, M. A., Laydon, D. J., Fox, J. M., et al. 2016. Rapid dissemination of human T-lymphotropic virus type 1 during primary infection in transplant recipients. *Retrovirology,* 13**,** 3.

Cook, L. B., Melamed, A., Niederer, H., Valganon, M., Laydon, D., et al. 2014. The role of HTLV-1 clonality, proviral structure, and genomic integration site in adult T-cell leukemia/lymphoma. *Blood,* 123**,** 3925-31.

Cook, L. B., Rowan, A. G., Melamed, A., Taylor, G. P. & Bangham, C. R. 2012. HTLV-1-infected T cells contain a single integrated provirus in natural infection. *Blood,* 120**,** 3488-90.

Copeland, K. F., Haaksma, A. G., Goudsmit, J., Krammer, P. H. & Heeney, J. L. 1994. Inhibition of apoptosis in T cells expressing human T cell leukemia virus type I Tax. *AIDS Res Hum Retroviruses,* 10**,** 1259-68.

Cubitt, A. B., Heim, R., Adams, S. R., Boyd, A. E., Gross, L. A., et al. 1995. Understanding, improving and using green fluorescent proteins. *Trends Biochem Sci,* 20**,** 448-55.

Currer, R., Van Duyne, R., Jaworski, E., Guendel, I., Sampey, G., et al. 2012. HTLV tax: a fascinating multifunctional co-regulator of viral and cellular pathways. *Front Microbiol,* 3**,** 406.

Danhier, P., Krishnamachary, B., Bharti, S., Kakkad, S., Mironchik, Y., et al. 2015. Combining Optical Reporter Proteins with Different Half-lives to Detect Temporal Evolution of Hypoxia and Reoxygenation in Tumors. *Neoplasia,* 17**,** 871-881.

Dar, R. D., Razooky, B. S., Singh, A., Trimeloni, T. V., McCollum, J. M., et al. 2012. Transcriptional burst frequency and burst size are equally modulated across the human genome. *Proc Natl Acad Sci U S A,* 109**,** 17454-9.

Darcis, G., Kula, A., Bouchat, S., Fujinaga, K., Corazza, F., et al. 2015. An In-Depth Comparison of Latency-Reversing Agent Combinations in Various In Vitro and Ex Vivo HIV-1 Latency Models Identified Bryostatin-1+JQ1 and Ingenol-B+JQ1 to Potently Reactivate Viral Gene Expression. *PLoS Pathog,* 11**,** e1005063.

de Thé, G. & Kazanji, M. 1996. An HTLV-I/II vaccine: from animal models to clinical trials? *J Acquir Immune Defic Syndr Hum Retrovirol,* 13 Suppl 1**,** S191-8.

Delamarre, L., Rosenberg, A. R., Pique, C., Pham, D., Callebaut, I., et al. 1996. The HTLV-I envelope glycoproteins: structure and functions. *J Acquir Immune Defic Syndr Hum Retrovirol,* 13 Suppl 1**,** S85-91.

Demontis, M. A., Sadiq, M. T., Golz, S. & Taylor, G. P. 2015. HTLV-1 viral RNA is detected rarely in plasma of HTLV-1 infected subjects. *J Med Virol,* 87**,** 2130-4.

Díaz, L., Martínez-Bonet, M., Sánchez, J., Fernández-Pineda, A., Jiménez, J. L., et al. 2015. Bryostatin activates HIV-1 latent expression in human astrocytes through a PKC and NF-κB-dependent mechanism. *Sci Rep,* 5**,** 12442.

Dobin, A., Davis, C. A., Schlesinger, F., Drenkow, J., Zaleski, C., et al. 2013. STAR: ultrafast universal RNA-seq aligner. *Bioinformatics,* 29**,** 15-21.

Durkin, S. S., Guo, X., Fryrear, K. A., Mihaylova, V. T., Gupta, S. K., et al. 2008. HTLV-1 Tax oncoprotein subverts the cellular DNA damage response via binding to DNA-dependent protein kinase. *J Biol Chem,* 283**,** 36311-20.

Eden, E., Geva-Zatorsky, N., Issaeva, I., Cohen, A., Dekel, E., et al. 2011. Proteome half-life dynamics in living human cells. *Science,* 331**,** 764-8.

Elmore, S. 2007. Apoptosis: a review of programmed cell death. *Toxicol Pathol,* 35**,** 495-516.

Essers, J., Theil, A. F., Baldeyron, C., van Cappellen, W. A., Houtsmuller, A. B., et al. 2005. Nuclear dynamics of PCNA in DNA replication and repair. *Mol Cell Biol,* 25**,** 9350-9.

Farcas, A. M., Blackledge, N. P., Sudbery, I., Long, H. K., McGouran, J. F., et al. 2012. KDM2B links the Polycomb Repressive Complex 1 (PRC1) to recognition of CpG islands. *Elife,* 1**,** e00205.

Fell, V. L. & Schild-Poulter, C. 2015. The Ku heterodimer: function in DNA repair and beyond. *Mutat Res Rev Mutat Res,* 763**,** 15-29.

Fernandez, G., Zaikos, T. D., Khan, S. Z., Jacobi, A. M., Behlke, M. A., et al. 2013. Targeting IκB proteins for HIV latency activation: the role of individual IκB and NF-κB proteins. *J Virol,* 87**,** 3966-78.

Fischer, M. 2017. Census and evaluation of p53 target genes. *Oncogene,* 36**,** 3943-3956.

Friedman, J., Cho, W. K., Chu, C. K., Keedy, K. S., Archin, N. M., et al. 2011. Epigenetic silencing of HIV-1 by the histone H3 lysine 27 methyltransferase enhancer of Zeste 2. *J Virol,* 85**,** 9078-89.

Fryrear, K. A., Guo, X., Kerscher, O. & Semmes, O. J. 2012. The Sumo-targeted ubiquitin ligase RNF4 regulates the localization and function of the HTLV-1 oncoprotein Tax. *Blood,* 119**,** 1173-81.

Fujisawa, J., Toita, M. & Yoshida, M. 1989. A unique enhancer element for the trans activator (p40tax) of human T-cell leukemia virus type I that is distinct from cyclic AMP- and 12-O-tetradecanoylphorbol-13-acetate-responsive elements. *J Virol,* 63**,** 3234-9.

Furukawa, Y., Fujisawa, J., Osame, M., Toita, M., Sonoda, S., et al. 1992. Frequent clonal proliferation of human T-cell leukemia virus type 1 (HTLV-1)-infected T cells in HTLV-1-associated myelopathy (HAM-TSP). *Blood,* 80**,** 1012-6.

Furukawa, Y., Kubota, R., Tara, M., Izumo, S. & Osame, M. 2001. Existence of escape mutant in HTLV-I tax during the development of adult T-cell leukemia. *Blood,* 97**,** 987-93.

Furuno, N., den Elzen, N. & Pines, J. 1999. Human cyclin A is required for mitosis until mid prophase. *J Cell Biol,* 147**,** 295-306.

Furuta, R., Yasunaga, J. I., Miura, M., Sugata, K., Saito, A., et al. 2017. Human T-cell leukemia virus type 1 infects multiple lineage hematopoietic cells in vivo. *PLoS Pathog,* 13**,** e1006722.

Gaudray, G., Gachon, F., Basbous, J., Biard-Piechaczyk, M., Devaux, C., et al. 2002. The complementary strand of the human T-cell leukemia virus type 1 RNA genome encodes a bZIP transcription factor that down-regulates viral transcription. *J Virol,* 76**,** 12813-22.

Gaylo, A., Schrock, D. C., Fernandes, N. R. & Fowell, D. J. 2016. T Cell Interstitial Migration: Motility Cues from the Inflamed Tissue for Micro- and Macro-Positioning. *Front Immunol,* 7**,** 428.

Gessain, A., Barin, F., Vernant, J. C., Gout, O., Maurs, L., et al. 1985. Antibodies to human T-lymphotropic virus type-I in patients with tropical spastic paraparesis. *Lancet,* 2**,** 407-10.

Gessain, A. & Cassar, O. 2012. Epidemiological Aspects and World Distribution of HTLV-1 Infection. *Front Microbiol,* 3**,** 388.

Gessain, A., Gallo, R. C. & Franchini, G. 1992. Low degree of human T-cell leukemia/lymphoma virus type I genetic drift in vivo as a means of monitoring viral transmission and movement of ancient human populations. *J Virol,* 66**,** 2288-95.

Ghez, D., Lepelletier, Y., Lambert, S., Fourneau, J. M., Blot, V., et al. 2006. Neuropilin-1 is involved in human T-cell lymphotropic virus type 1 entry. *J Virol,* 80**,** 6844-54.

Giam, C. Z. & Xu, Y. L. 1989. HTLV-I tax gene product activates transcription via pre-existing cellular factors and cAMP responsive element. *J Biol Chem,* 264**,** 15236-41.

Gillet, N. A., Malani, N., Melamed, A., Gormley, N., Carter, R., et al. 2011. The host genomic environment of the provirus determines the abundance of HTLV-1-infected T-cell clones. *Blood,* 117**,** 3113-22.

Girard, F., Strausfeld, U., Fernandez, A. & Lamb, N. J. 1991. Cyclin A is required for the onset of DNA replication in mammalian fibroblasts. *Cell,* 67**,** 1169-79.

Goon, P. K., Biancardi, A., Fast, N., Igakura, T., Hanon, E., et al. 2004a. Human T cell lymphotropic virus (HTLV) type-1-specific CD8+ T cells: frequency and immunodominance hierarchy. *J Infect Dis,* 189**,** 2294-8.

Goon, P. K., Igakura, T., Hanon, E., Mosley, A. J., Barfield, A., et al. 2004b. Human T cell lymphotropic virus type I (HTLV-I)-specific CD4+ T cells: immunodominance hierarchy and preferential infection with HTLV-I. *J Immunol,* 172**,** 1735-43.

Goren, I., Semmes, O. J., Jeang, K. T. & Moelling, K. 1995. The amino terminus of Tax is required for interaction with the cyclic AMP response element binding protein. *J Virol,* 69**,** 5806-11.

Grassmann, R., Aboud, M. & Jeang, K. T. 2005. Molecular mechanisms of cellular transformation by HTLV-1 Tax. *Oncogene,* 24**,** 5976-85.

Green, D. R. 1998. Apoptotic pathways: the roads to ruin. *Cell,* 94**,** 695-8.

Gross, C. & Thoma-Kress, A. K. 2016. Molecular Mechanisms of HTLV-1 Cell-to-Cell Transmission. *Viruses,* 8**,** 74.

Grossman, W. J., Kimata, J. T., Wong, F. H., Zutter, M., Ley, T. J., et al. 1995. Development of leukemia in mice transgenic for the tax gene of human T-cell leukemia virus type I. *Proc Natl Acad Sci U S A,* 92**,** 1057-61.

Hajj, H. E., Nasr, R., Kfoury, Y., Dassouki, Z., Nasser, R., et al. 2012. Animal models on HTLV-1 and related viruses: what did we learn? *Front Microbiol,* 3**,** 333.

Hakata, Y., Umemoto, T., Matsushita, S. & Shida, H. 1998. Involvement of human CRM1 (exportin 1) in the export and multimerization of the Rex protein of human T-cell leukemia virus type 1. *J Virol,* 72**,** 6602-7.

Halasi, M., Wang, M., Chavan, T. S., Gaponenko, V., Hay, N., et al. 2013. ROS inhibitor N-acetyl-L-cysteine antagonizes the activity of proteasome inhibitors. *Biochem J,* 454**,** 201-8.

Hall, W. W. & Fujii, M. 2005. Deregulation of cell-signaling pathways in HTLV-1 infection. *Oncogene,* 24**,** 5965-75.

Hanon, E., Hall, S., Taylor, G. P., Saito, M., Davis, R., et al. 2000. Abundant tax protein expression in CD4+ T cells infected with human T-cell lymphotropic virus type I (HTLV-I) is prevented by cytotoxic T lymphocytes. *Blood,* 95**,** 1386-92.

Harikumar, A. & Meshorer, E. 2015. Chromatin remodeling and bivalent histone modifications in embryonic stem cells. *EMBO Rep,* 16**,** 1609-19.

Harper, P. A., Riddick, D. S. & Okey, A. B. 2006. Regulating the regulator: factors that control levels and activity of the aryl hydrocarbon receptor. *Biochem Pharmacol,* 72**,** 267-79.

Harris, T. H., Banigan, E. J., Christian, D. A., Konradt, C., Tait Wojno, E. D., et al. 2012. Generalized Lévy walks and the role of chemokines in migration of effector CD8+ T cells. *Nature,* 486**,** 545-8.

Hattori, S., Kiyokawa, T., Imagawa, K., Shimizu, F., Hashimura, E., et al. 1984. Identification of gag and env gene products of human T-cell leukemia virus (HTLV). *Virology,* 136**,** 338-47.

Hayashibara, T., Yamada, Y., Mori, N., Harasawa, H., Sugahara, K., et al. 2003. Possible involvement of aryl hydrocarbon receptor (AhR) in adult T-cell leukemia (ATL) leukemogenesis: constitutive activation of AhR in ATL. *Biochem Biophys Res Commun,* 300**,** 128-34.

Hemelaar, J., Bex, F., Booth, B., Cerundolo, V., McMichael, A., et al. 2001. Human T-cell leukemia virus type 1 Tax protein binds to assembled nuclear proteasomes and enhances their proteolytic activity. *J Virol,* 75**,** 11106-15.

Hidaka, M., Inoue, J., Yoshida, M. & Seiki, M. 1988. Post-transcriptional regulator (rex) of HTLV-1 initiates expression of viral structural proteins but suppresses expression of regulatory proteins. *Embo j,* 7**,** 519-23.

Hieshima, K., Nagakubo, D., Nakayama, T., Shirakawa, A. K., Jin, Z., et al. 2008. Tax-inducible production of CC chemokine ligand 22 by human T cell leukemia virus type 1 (HTLV-1)-infected T cells promotes preferential transmission of HTLV-1 to CCR4-expressing CD4+ T cells. *J Immunol,* 180**,** 931-9.

Hilburn, S., Rowan, A., Demontis, M. A., MacNamara, A., Asquith, B., et al. 2011. In vivo expression of human T-lymphotropic virus type 1 basic leucine-zipper protein generates specific CD8+ and CD4+ T-lymphocyte responses that correlate with clinical outcome. *J Infect Dis,* 203**,** 529-36.

Hino, S. 2011. Establishment of the milk-borne transmission as a key factor for the peculiar endemicity of human T-lymphotropic virus type 1 (HTLV-1): the ATL Prevention Program Nagasaki. *Proc Jpn Acad Ser B Phys Biol Sci,* 87**,** 152-66.

Hinuma, Y., Nagata, K., Hanaoka, M., Nakai, M., Matsumoto, T., et al. 1981. Adult T-cell leukemia: antigen in an ATL cell line and detection of antibodies to the antigen in human sera. *Proc Natl Acad Sci U S A,* 78**,** 6476-80.

Hirai, H., Suzuki, T., Fujisawa, J., Inoue, J. & Yoshida, M. 1994. Tax protein of human T-cell leukemia virus type I binds to the ankyrin motifs of inhibitory factor kappa B and induces nuclear translocation of transcription factor NF-kappa B proteins for transcriptional activation. *Proc Natl Acad Sci U S A,* 91**,** 3584-8.

Hiscott, J., Kwon, H. & Génin, P. 2001. Hostile takeovers: viral appropriation of the NF-kappaB pathway. *J Clin Invest,* 107**,** 143-51.

Hishizawa, M., Imada, K., Kitawaki, T., Ueda, M., Kadowaki, N., et al. 2004. Depletion and impaired interferon-alpha-producing capacity of blood plasmacytoid dendritic cells in human T-cell leukaemia virus type I-infected individuals. *Br J Haematol,* 125**,** 568-75.

Hivin, P., Frédéric, M., Arpin-André, C., Basbous, J., Gay, B., et al. 2005. Nuclear localization of HTLV-I bZIP factor (HBZ) is mediated by three distinct motifs. *J Cell Sci,* 118**,** 1355-62.

Hong, W., Cheng, W., Zheng, T., Jiang, N. & Xu, R. 2020. AHR is a tunable knob that controls HTLV-1 latency-reactivation switching. *PLoS Pathog,* 16**,** e1008664.

Horn, H. F. & Vousden, K. H. 2007. Coping with stress: multiple ways to activate p53. *Oncogene,* 26**,** 1306-16.

Houtgraaf, J. H., Versmissen, J. & van der Giessen, W. J. 2006. A concise review of DNA damage checkpoints and repair in mammalian cells. *Cardiovasc Revasc Med,* 7**,** 165-72.

Hu, W. S. & Hughes, S. H. 2012. HIV-1 reverse transcription. *Cold Spring Harb Perspect Med,* 2.

Huang, Q., Li, F., Liu, X., Li, W., Shi, W., et al. 2011. Caspase 3-mediated stimulation of tumor cell repopulation during cancer radiotherapy. *Nat Med,* 17**,** 860-6.

Igakura, T., Stinchcombe, J. C., Goon, P. K., Taylor, G. P., Weber, J. N., et al. 2003. Spread of HTLV-I between lymphocytes by virus-induced polarization of the cytoskeleton. *Science,* 299**,** 1713-6.

Inoue, J., Seiki, M., Taniguchi, T., Tsuru, S. & Yoshida, M. 1986. Induction of interleukin 2 receptor gene expression by p40x encoded by human T-cell leukemia virus type 1. *Embo j,* 5**,** 2883-8.

Izaki, M., Yasunaga, J. I., Nosaka, K., Sugata, K., Utsunomiya, H., et al. 2021. In vivo dynamics and adaptation of HTLV-1-infected clones under different clinical conditions. *PLoS Pathog,* 17**,** e1009271.

Jacobelli, J., Bennett, F. C., Pandurangi, P., Tooley, A. J. & Krummel, M. F. 2009. Myosin-IIA and ICAM-1 regulate the interchange between two distinct modes of T cell migration. *J Immunol,* 182**,** 2041-50.

Jacobson, S., Shida, H., McFarlin, D. E., Fauci, A. S. & Koenig, S. 1990. Circulating CD8+ cytotoxic T lymphocytes specific for HTLV-I pX in patients with HTLV-I associated neurological disease. *Nature,* 348**,** 245-8.

Jain, P., Manuel, S. L., Khan, Z. K., Ahuja, J., Quann, K., et al. 2009. DC-SIGN mediates cell-free infection and transmission of human T-cell lymphotropic virus type 1 by dendritic cells. *J Virol,* 83**,** 10908-21.

Jeang, K. T., Boros, I., Brady, J., Radonovich, M. & Khoury, G. 1988. Characterization of cellular factors that interact with the human T-cell leukemia virus type I p40x-responsive 21-base-pair sequence. *J Virol,* 62**,** 4499-509.

Jeffery, K. J., Usuku, K., Hall, S. E., Matsumoto, W., Taylor, G. P., et al. 1999. HLA alleles determine human T-lymphotropic virus-I (HTLV-I) proviral load and the risk of HTLV-I-associated myelopathy. *Proc Natl Acad Sci U S A,* 96**,** 3848-53.

Jin, D. Y., Giordano, V., Kibler, K. V., Nakano, H. & Jeang, K. T. 1999. Role of adapter function in oncoprotein-mediated activation of NF-kappaB. Human T-cell leukemia virus type I Tax interacts directly with IkappaB kinase gamma. *J Biol Chem,* 274**,** 17402-5.

Johnson, J. M., Nicot, C., Fullen, J., Ciminale, V., Casareto, L., et al. 2001. Free major histocompatibility complex class I heavy chain is preferentially targeted for degradation by human T-cell leukemia/lymphotropic virus type 1 p12(I) protein. *J Virol,* 75**,** 6086-94.

Jolly, C., Mitar, I. & Sattentau, Q. J. 2007. Adhesion molecule interactions facilitate human immunodeficiency virus type 1-induced virological synapse formation between T cells. *J Virol,* 81**,** 13916-21.

Jones, K. S., Lambert, S., Bouttier, M., Bénit, L., Ruscetti, F. W., et al. 2011. Molecular aspects of HTLV-1 entry: functional domains of the HTLV-1 surface subunit (SU) and their relationships to the entry receptors. *Viruses,* 3**,** 794-810.

Jones, K. S., Petrow-Sadowski, C., Bertolette, D. C., Huang, Y. & Ruscetti, F. W. 2005. Heparan sulfate proteoglycans mediate attachment and entry of human T-cell leukemia virus type 1 virions into CD4+ T cells. *J Virol,* 79**,** 12692-702.

Jones, K. S., Petrow-Sadowski, C., Huang, Y. K., Bertolette, D. C. & Ruscetti, F. W. 2008. Cell-free HTLV-1 infects dendritic cells leading to transmission and transformation of CD4(+) T cells. *Nat Med,* 14**,** 429-36.

Journo, C. & Mahieux, R. 2011. HTLV-1 and innate immunity. *Viruses,* 3**,** 1374-94.

Kajiyama, W., Kashiwagi, S., Ikematsu, H., Hayashi, J., Nomura, H., et al. 1986. Intrafamilial transmission of adult T cell leukemia virus. *J Infect Dis,* 154**,** 851-7.

Kao, S. Y., Lemoine, F. J. & Mariott, S. J. 2000. HTLV-1 Tax protein sensitizes cells to apoptotic cell death induced by DNA damaging agents. *Oncogene,* 19**,** 2240-8.

Kataoka, K., Nagata, Y., Kitanaka, A., Shiraishi, Y., Shimamura, T., et al. 2015. Integrated molecular analysis of adult T cell leukemia/lymphoma. *Nat Genet,* 47**,** 1304-15.

Katsuya, H., Ishitsuka, K., Utsunomiya, A., Hanada, S., Eto, T., et al. 2015. Treatment and survival among 1594 patients with ATL. *Blood,* 126**,** 2570-7.

Kattan, T., MacNamara, A., Rowan, A. G., Nose, H., Mosley, A. J., et al. 2009. The avidity and lytic efficiency of the CTL response to HTLV-1. *J Immunol,* 182**,** 5723-9.

Keating, S. M., Clark, K. R., Stefanich, L. D., Arellano, F., Edwards, C. P., et al. 2006. Competition between intercellular adhesion molecule-1 and a small-molecule antagonist for a common binding site on the alphal subunit of lymphocyte function-associated antigen-1. *Protein Sci,* 15**,** 290-303.

Khan, S., Iqbal, M., Tariq, M., Baig, S. M. & Abbas, W. 2018. Epigenetic regulation of HIV-1 latency: focus on polycomb group (PcG) proteins. *Clin Epigenetics,* 10**,** 14.

Kim, Y. M., Ramírez, J. A., Mick, J. E., Giebler, H. A., Yan, J. P., et al. 2007. Molecular characterization of the Tax-containing HTLV-1 enhancer complex reveals a prominent role for CREB phosphorylation in Tax transactivation. *J Biol Chem,* 282**,** 18750-7.

Kimata, J. T. & Ratner, L. 1991. Temporal regulation of viral and cellular gene expression during human T-lymphotropic virus type I-mediated lymphocyte immortalization. *J Virol,* 65**,** 4398-407.

Kinjo, T., Ham-Terhune, J., Peloponese, J. M., Jr. & Jeang, K. T. 2010. Induction of reactive oxygen species by human T-cell leukemia virus type 1 tax correlates with DNA damage and expression of cellular senescence marker. *J Virol,* 84**,** 5431-7.

Kinowaki, Y., Kurata, M., Ishibashi, S., Ikeda, M., Tatsuzawa, A., et al. 2018. Glutathione peroxidase 4 overexpression inhibits ROS-induced cell death in diffuse large B-cell lymphoma. *Lab Invest,* 98**,** 609-619.

Kinpara, S., Kijiyama, M., Takamori, A., Hasegawa, A., Sasada, A., et al. 2013. Interferon-α (IFN-α) suppresses HTLV-1 gene expression and cell cycling, while IFN-α combined with zidovudine induces p53 signaling and apoptosis in HTLV-1-infected cells. *Retrovirology,* 10**,** 52.

Kinter, A. L., Poli, G., Maury, W., Folks, T. M. & Fauci, A. S. 1990. Direct and cytokine-mediated activation of protein kinase C induces human immunodeficiency virus expression in chronically infected promonocytic cells. *J Virol,* 64**,** 4306-12.

Kirk, P. D., Huvet, M., Melamed, A., Maertens, G. N. & Bangham, C. R. 2016. Retroviruses integrate into a shared, non-palindromic DNA motif. *Nat Microbiol,* 2**,** 16212.

Kitajima, I., Kawahara, K., Hanyu, N., Shin, H., Tokioka, T., et al. 1996. Enhanced E-cadherin expression and increased calcium-dependent cell-cell adhesion in human T-cell leukemia virus type I Tax-expressing PC12 cells. *J Cell Sci,* 109 (Pt 3)**,** 609-17.

Kiyokawa, T., Seiki, M., Iwashita, S., Imagawa, K., Shimizu, F., et al. 1985. p27x-III and p21x-III, proteins encoded by the pX sequence of human T-cell leukemia virus type I. *Proc Natl Acad Sci U S A,* 82**,** 8359-63.

Kobayashi, N., Konishi, H., Sabe, H., Shigesada, K., Noma, T., et al. 1984. Genomic structure of HTLV (human T-cell leukemia virus): detection of defective genome and its amplification in MT-2 cells. *Embo j,* 3**,** 1339-43.

Koyanagi, Y., Itoyama, Y., Nakamura, N., Takamatsu, K., Kira, J., et al. 1993. In vivo infection of human T-cell leukemia virus type I in non-T cells. *Virology,* 196**,** 25-33.

Krokan, H. E. & Bjørås, M. 2013. Base excision repair. *Cold Spring Harb Perspect Biol,* 5**,** a012583.

Krummel, M. F., Friedman, R. S. & Jacobelli, J. 2014. Modes and mechanisms of T cell motility: roles for confinement and Myosin-IIA. *Curr Opin Cell Biol,* 30**,** 9-16.

Kubota, R., Nagai, M., Kawanishi, T., Osame, M. & Jacobson, S. 2000. Increased HTLV type 1 tax specific CD8+ cells in HTLV type 1-asociated myelopathy/tropical spastic paraparesis: correlation with HTLV type 1 proviral load. *AIDS Res Hum Retroviruses,* 16**,** 1705-9.

Kubota, R., Umehara, F., Izumo, S., Ijichi, S., Matsumuro, K., et al. 1994. HTLV-I proviral DNA amount correlates with infiltrating CD4+ lymphocytes in the spinal cord from patients with HTLV-I-associated myelopathy. *J Neuroimmunol,* 53**,** 23-9.

Kukurba, K. R. & Montgomery, S. B. 2015. RNA Sequencing and Analysis. *Cold Spring Harb Protoc,* 2015**,** 951-69.

Kulkarni, A. & Bangham, C. R. M. 2018. HTLV-1: Regulating the Balance Between Proviral Latency and Reactivation. *Front Microbiol,* 9**,** 449.

Kulkarni, A., Mateus, M., Thinnes, C. C., McCullagh, J. S., Schofield, C. J., et al. 2017. Glucose Metabolism and Oxygen Availability Govern Reactivation of the Latent Human Retrovirus HTLV-1. *Cell Chem Biol,* 24**,** 1377-1387.e3.

Kulkarni, A., Taylor, G. P., Klose, R. J., Schofield, C. J. & Bangham, C. R. 2018. Histone H2A monoubiquitylation and p38-MAPKs regulate immediate-early gene-like reactivation of latent retrovirus HTLV-1. *JCI Insight,* 3.

Kuramitsu, M., Sekizuka, T., Yamochi, T., Firouzi, S., Sato, T., et al. 2017. Proviral Features of Human T Cell Leukemia Virus Type 1 in Carriers with Indeterminate Western Blot Analysis Results. *J Clin Microbiol,* 55**,** 2838-2849.

Kwok, R. P., Laurance, M. E., Lundblad, J. R., Goldman, P. S., Shih, H., et al. 1996. Control of cAMP-regulated enhancers by the viral transactivator Tax through CREB and the co-activator CBP. *Nature,* 380**,** 642-6.

Laird, G. M., Bullen, C. K., Rosenbloom, D. I., Martin, A. R., Hill, A. L., et al. 2015. Ex vivo analysis identifies effective HIV-1 latency-reversing drug combinations. *J Clin Invest,* 125**,** 1901-12.

Lal, R. B., Giam, C. Z., Coligan, J. E. & Rudolph, D. L. 1994. Differential immune responsiveness to the immunodominant epitopes of regulatory proteins (tax and rex) in human T cell lymphotropic virus type I-associated myelopathy. *J Infect Dis,* 169**,** 496-503.

Landry, C. R., Lemos, B., Rifkin, S. A., Dickinson, W. J. & Hartl, D. L. 2007. Genetic properties influencing the evolvability of gene expression. *Science,* 317**,** 118-21.

Larigot, L., Juricek, L., Dairou, J. & Coumoul, X. 2018. AhR signaling pathways and regulatory functions. *Biochim Open,* 7**,** 1-9.

Laydon, D. J., Melamed, A., Sim, A., Gillet, N. A., Sim, K., et al. 2014. Quantification of HTLV-1 clonality and TCR diversity. *PLoS Comput Biol,* 10**,** e1003646.

Laydon, D. J., Sunkara, V., Boelen, L., Bangham, C. R. M. & Asquith, B. 2020. The relative contributions of infectious and mitotic spread to HTLV-1 persistence. *PLoS Comput Biol,* 16**,** e1007470.

Leibowitz, B. & Yu, J. 2010. Mitochondrial signaling in cell death via the Bcl-2 family. *Cancer Biol Ther,* 9**,** 417-22.

Lemasson, I., Lewis, M. R., Polakowski, N., Hivin, P., Cavanagh, M. H., et al. 2007. Human T-cell leukemia virus type 1 (HTLV-1) bZIP protein interacts with the cellular transcription factor CREB to inhibit HTLV-1 transcription. *J Virol,* 81**,** 1543-53.

Lemasson, I., Polakowski, N. J., Laybourn, P. J. & Nyborg, J. K. 2002. Transcription factor binding and histone modifications on the integrated proviral promoter in human T-cell leukemia virus-I-infected T-cells. *J Biol Chem,* 277**,** 49459-65.

Lemasson, I., Polakowski, N. J., Laybourn, P. J. & Nyborg, J. K. 2006. Tax-dependent displacement of nucleosomes during transcriptional activation of human T-cell leukemia virus type 1. *J Biol Chem,* 281**,** 13075-13082.

Lemoine, F. J. & Marriott, S. J. 2001. Accelerated G(1) phase progression induced by the human T cell leukemia virus type I (HTLV-I) Tax oncoprotein. *J Biol Chem,* 276**,** 31851-7.

Lenstra, T. L., Rodriguez, J., Chen, H. & Larson, D. R. 2016. Transcription Dynamics in Living Cells. *Annu Rev Biophys,* 45**,** 25-47.

Lezin, A., Gillet, N., Olindo, S., Signaté, A., Grandvaux, N., et al. 2007. Histone deacetylase mediated transcriptional activation reduces proviral loads in HTLV-1 associated myelopathy/tropical spastic paraparesis patients. *Blood,* 110**,** 3722-8.

Li, B. & Dewey, C. N. 2011. RSEM: accurate transcript quantification from RNA-Seq data with or without a reference genome. *BMC Bioinformatics,* 12**,** 323.

Li, G. M. 2008. Mechanisms and functions of DNA mismatch repair. *Cell Res,* 18**,** 85-98.

Li, J., Chen, H., Tang, M. S., Shi, X., Amin, S., et al. 2004. PI-3K and Akt are mediators of AP-1 induction by 5-MCDE in mouse epidermal Cl41 cells. *J Cell Biol,* 165**,** 77-86.

Li, M., Kesic, M., Yin, H., Yu, L. & Green, P. L. 2009. Kinetic analysis of human T-cell leukemia virus type 1 gene expression in cell culture and infected animals. *J Virol,* 83**,** 3788-97.

Li, X., Zhao, X., Fang, Y., Jiang, X., Duong, T., et al. 1998. Generation of destabilized green fluorescent protein as a transcription reporter. *J Biol Chem,* 273**,** 34970-5.

Li, X. H. & Gaynor, R. B. 1999. Regulation of NF-kappaB by the HTLV-1 Tax protein. *Gene Expr,* 7**,** 233-45.

Lin, P., Hu, S. W. & Chang, T. H. 2003. Correlation between gene expression of aryl hydrocarbon receptor (AhR), hydrocarbon receptor nuclear translocator (Arnt), cytochromes P4501A1 (CYP1A1) and 1B1 (CYP1B1), and inducibility of CYP1A1 and CYP1B1 in human lymphocytes. *Toxicol Sci,* 71**,** 20-6.

Liu, R., Simonetti, F. R. & Ho, Y. C. 2020. The forces driving clonal expansion of the HIV-1 latent reservoir. *Virol J,* 17**,** 4.

Liu, T., Zhang, L., Joo, D. & Sun, S. C. 2017. NF-κB signaling in inflammation. *Signal Transduct Target Ther,* 2**,** 17023-.

Liu, Y., Wang, Y., Yamakuchi, M., Masuda, S., Tokioka, T., et al. 2001. Phosphoinositide-3 kinase-PKB/Akt pathway activation is involved in fibroblast Rat-1 transformation by human T-cell leukemia virus type I tax. *Oncogene,* 20**,** 2514-26.

Lodewick, J., Lamsoul, I., Polania, A., Lebrun, S., Burny, A., et al. 2009. Acetylation of the human T-cell leukemia virus type 1 Tax oncoprotein by p300 promotes activation of the NF-kappaB pathway. *Virology,* 386**,** 68-78.

Love, M. I., Huber, W. & Anders, S. 2014. Moderated estimation of fold change and dispersion for RNA-seq data with DESeq2. *Genome Biol,* 15**,** 550.

Low, K. G., Dorner, L. F., Fernando, D. B., Grossman, J., Jeang, K. T., et al. 1997. Human T-cell leukemia virus type 1 Tax releases cell cycle arrest induced by p16INK4a. *J Virol,* 71**,** 1956-62.

Lu, H., Pise-Masison, C. A., Fletcher, T. M., Schiltz, R. L., Nagaich, A. K., et al. 2002. Acetylation of nucleosomal histones by p300 facilitates transcription from tax-responsive human T-cell leukemia virus type 1 chromatin template. *Mol Cell Biol,* 22**,** 4450-62.

Łukasik, P., Załuski, M. & Gutowska, I. 2021. Cyclin-Dependent Kinases (CDK) and Their Role in Diseases Development-Review. *Int J Mol Sci,* 22.

Lundblad, J. R., Kwok, R. P., Laurance, M. E., Huang, M. S., Richards, J. P., et al. 1998. The human T-cell leukemia virus-1 transcriptional activator Tax enhances cAMP-responsive element-binding protein (CREB) binding activity through interactions with the DNA minor groove. *J Biol Chem,* 273**,** 19251-9.

Lyngdoh, D. L., Shukla, H., Sonkar, A., Anupam, R. & Tripathi, T. 2019. Portrait of the Intrinsically Disordered Side of the HTLV-1 Proteome. *ACS Omega,* 4**,** 10003-10018.

Ma, G., Yasunaga, J. I., Shimura, K., Takemoto, K., Watanabe, M., et al. 2021. Human retroviral antisense mRNAs are retained in the nuclei of infected cells for viral persistence. *Proc Natl Acad Sci U S A,* 118.

Macatonia, S. E., Cruickshank, J. K., Rudge, P. & Knight, S. C. 1992. Dendritic cells from patients with tropical spastic paraparesis are infected with HTLV-1 and stimulate autologous lymphocyte proliferation. *AIDS Res Hum Retroviruses,* 8**,** 1699-706.

Macnamara, A., Rowan, A., Hilburn, S., Kadolsky, U., Fujiwara, H., et al. 2010. HLA class I binding of HBZ determines outcome in HTLV-1 infection. *PLoS Pathog,* 6**,** e1001117.

Maeda, M., Shimizu, A., Ikuta, K., Okamoto, H., Kashihara, M., et al. 1985. Origin of human T-lymphotrophic virus I-positive T cell lines in adult T cell leukemia. Analysis of T cell receptor gene rearrangement. *J Exp Med,* 162**,** 2169-74.

Maertens, G. N. 2016. B'-protein phosphatase 2A is a functional binding partner of delta-retroviral integrase. *Nucleic Acids Res,* 44**,** 364-76.

Mahgoub, M., Yasunaga, J. I., Iwami, S., Nakaoka, S., Koizumi, Y., et al. 2018. Sporadic on/off switching of HTLV-1 Tax expression is crucial to maintain the whole population of virus-induced leukemic cells. *Proc Natl Acad Sci U S A,* 115**,** E1269-e1278.

Manel, N., Battini, J. L., Taylor, N. & Sitbon, M. 2005. HTLV-1 tropism and envelope receptor. *Oncogene,* 24**,** 6016-25.

Manel, N., Kim, F. J., Kinet, S., Taylor, N., Sitbon, M., et al. 2003. The ubiquitous glucose transporter GLUT-1 is a receptor for HTLV. *Cell,* 115**,** 449-59.

Manns, A., Murphy, E. L., Wilks, R., Haynes, G., Figueroa, J. P., et al. 1991. Detection of early human T-cell lymphotropic virus type I antibody patterns during seroconversion among transfusion recipients. *Blood,* 77**,** 896-905.

Maréchal, A. & Zou, L. 2013. DNA damage sensing by the ATM and ATR kinases. *Cold Spring Harb Perspect Biol,* 5.

Margueron, R. & Reinberg, D. 2011. The Polycomb complex PRC2 and its mark in life. *Nature,* 469**,** 343-9.

Martinat, C., Bacci, J. J., Leete, T., Kim, J., Vanti, W. B., et al. 2006. Cooperative transcription activation by Nurr1 and Pitx3 induces embryonic stem cell maturation to the midbrain dopamine neuron phenotype. *Proc Natl Acad Sci U S A,* 103**,** 2874-9.

Matsumoto, J., Ohshima, T., Isono, O. & Shimotohno, K. 2005. HTLV-1 HBZ suppresses AP-1 activity by impairing both the DNA-binding ability and the stability of c-Jun protein. *Oncogene,* 24**,** 1001-10.

Matsuoka, M. & Green, P. L. 2009. The HBZ gene, a key player in HTLV-1 pathogenesis. *Retrovirology,* 6**,** 71.

Matsuoka, M. & Jeang, K. T. 2007. Human T-cell leukaemia virus type 1 (HTLV-1) infectivity and cellular transformation. *Nat Rev Cancer,* 7**,** 270-80.

Matsuoka, M. & Mesnard, J. M. 2020. HTLV-1 bZIP factor: the key viral gene for pathogenesis. *Retrovirology,* 17**,** 2.

Mazur, D. J. & Perrino, F. W. 1999. Identification and expression of the TREX1 and TREX2 cDNA sequences encoding mammalian 3'-->5' exonucleases. *J Biol Chem,* 274**,** 19655-60.

Mazurov, D., Ilinskaya, A., Heidecker, G., Lloyd, P. & Derse, D. 2010. Quantitative comparison of HTLV-1 and HIV-1 cell-to-cell infection with new replication dependent vectors. *PLoS Pathog,* 6**,** e1000788.

Mbonye, U. & Karn, J. 2017. The Molecular Basis for Human Immunodeficiency Virus Latency. *Annu Rev Virol,* 4**,** 261-285.

McGuire, K. L., Curtiss, V. E., Larson, E. L. & Haseltine, W. A. 1993. Influence of human T-cell leukemia virus type I tax and rex on interleukin-2 gene expression. *J Virol,* 67**,** 1590-9.

McKimpson, W. M. & Accili, D. 2019. A fluorescent reporter assay of differential gene expression response to insulin in hepatocytes. *Am J Physiol Cell Physiol,* 317**,** C143-c151.

Melamed, A., Fitzgerald, T. W., Wang, Y., Ma, J., Birney, E., et al. 2022. Selective clonal persistence of human retroviruses in vivo: Radial chromatin organization, integration site, and host transcription. *Sci Adv,* 8**,** eabm6210.

Melamed, A., Laydon, D. J., Al Khatib, H., Rowan, A. G., Taylor, G. P., et al. 2015. HTLV-1 drives vigorous clonal expansion of infected CD8(+) T cells in natural infection. *Retrovirology,* 12**,** 91.

Melamed, A., Laydon, D. J., Gillet, N. A., Tanaka, Y., Taylor, G. P., et al. 2013. Genome-wide determinants of proviral targeting, clonal abundance and expression in natural HTLV-1 infection. *PLoS Pathog,* 9**,** e1003271.

Melamed, A., Yaguchi, H., Miura, M., Witkover, A., Fitzgerald, T. W., et al. 2018. The human leukemia virus HTLV-1 alters the structure and transcription of host chromatin in cis. *Elife,* 7.

Miller, M. J., Wei, S. H., Parker, I. & Cahalan, M. D. 2002. Two-photon imaging of lymphocyte motility and antigen response in intact lymph node. *Science,* 296**,** 1869-73.

Mitobe, Y., Yasunaga, J., Furuta, R. & Matsuoka, M. 2015. HTLV-1 bZIP Factor RNA and Protein Impart Distinct Functions on T-cell Proliferation and Survival. *Cancer Res,* 75**,** 4143-52.

Miura, M., Dey, S., Ramanayake, S., Singh, A., Rueda, D. S., et al. 2019. Kinetics of HTLV-1 reactivation from latency quantified by single-molecule RNA FISH and stochastic modelling. *PLoS Pathog,* 15**,** e1008164.

Miura, M., Miyazato, P., Satou, Y., Tanaka, Y. & Bangham, C. R. M. 2018. Epigenetic changes around the pX region and spontaneous HTLV-1 transcription are CTCF-independent. *Wellcome Open Res,* 3**,** 105.

Miyoshi, I., Kubonishi, I., Sumida, M., Hiraki, S., Tsubota, T., et al. 1980. A novel T-cell line derived from adult T-cell leukemia. *Gan,* 71**,** 155-6.

Miyoshi, I., Kubonishi, I., Yoshimoto, S., Akagi, T., Ohtsuki, Y., et al. 1981. Type C virus particles in a cord T-cell line derived by co-cultivating normal human cord leukocytes and human leukaemic T cells. *Nature,* 294**,** 770-1.

Mohammadi, P., di Iulio, J., Muñoz, M., Martinez, R., Bartha, I., et al. 2014. Dynamics of HIV latency and reactivation in a primary CD4+ T cell model. *PLoS Pathog,* 10**,** e1004156.

Montes, M., Sanchez, C., Verdonck, K., Lake, J. E., Gonzalez, E., et al. 2009. Regulatory T cell expansion in HTLV-1 and strongyloidiasis co-infection is associated with reduced IL-5 responses to Strongyloides stercoralis antigen. *PLoS Negl Trop Dis,* 3**,** e456.

Montgomery, R. D., Cruickshank, E. K., Robertson, W. B. & McMenemey, W. H. 1964. CLINICAL AND PATHOLOGICAL OBSERVATIONS ON JAMAICAN NEUROPATHY; A REPORT ON 206 CASES. *Brain,* 87**,** 425-62.

Moreno-Celis, U., García-Gasca, T. & Mejía, C. 2022. Apoptosis-Induced Compensatory Proliferation in Cancer. *In:* Sergi, C. M. (ed.) *Metastasis.* Brisbane (AU): Exon Publications

Mulloy, J. C., Crownley, R. W., Fullen, J., Leonard, W. J. & Franchini, G. 1996. The human T-cell leukemia/lymphotropic virus type 1 p12I proteins bind the interleukin-2 receptor beta and gammac chains and affects their expression on the cell surface. *J Virol,* 70**,** 3599-605.

Mulloy, J. C., Kislyakova, T., Cereseto, A., Casareto, L., LoMonico, A., et al. 1998. Human T-cell lymphotropic/leukemia virus type 1 Tax abrogates p53-induced cell cycle arrest and apoptosis through its CREB/ATF functional domain. *J Virol,* 72**,** 8852-60.

Nagai, M., Usuku, K., Matsumoto, W., Kodama, D., Takenouchi, N., et al. 1998. Analysis of HTLV-I proviral load in 202 HAM/TSP patients and 243 asymptomatic HTLV-I carriers: high proviral load strongly predisposes to HAM/TSP. *J Neurovirol,* 4**,** 586-93.

Nagasaka, M., Yamagishi, M., Yagishita, N., Araya, N., Kobayashi, S., et al. 2020. Mortality and risk of progression to adult T cell leukemia/lymphoma in HTLV-1-associated myelopathy/tropical spastic paraparesis. *Proc Natl Acad Sci U S A,* 117**,** 11685-11691.

Nagata, K., Ohtani, K., Nakamura, M. & Sugamura, K. 1989. Activation of endogenous c-fos proto-oncogene expression by human T-cell leukemia virus type I-encoded p40tax protein in the human T-cell line, Jurkat. *J Virol,* 63**,** 3220-6.

Nakagawa, M., Shaffer, A. L., 3rd, Ceribelli, M., Zhang, M., Wright, G., et al. 2018. Targeting the HTLV-I-Regulated BATF3/IRF4 Transcriptional Network in Adult T Cell Leukemia/Lymphoma. *Cancer Cell,* 34**,** 286-297.e10.

Nam, S. H., Copeland, T. D., Hatanaka, M. & Oroszlan, S. 1993. Characterization of ribosomal frameshifting for expression of pol gene products of human T-cell leukemia virus type I. *J Virol,* 67**,** 196-203.

Napolitano, M., Modi, W. S., Cevario, S. J., Gnarra, J. R., Seuanez, H. N., et al. 1991. The gene encoding the Act-2 cytokine. Genomic structure, HTLV-I/Tax responsiveness of 5' upstream sequences, and chromosomal localization. *J Biol Chem,* 266**,** 17531-6.

Nasr, R., Marçais, A., Hermine, O. & Bazarbachi, A. 2017. Overview of Targeted Therapies for Adult T-Cell Leukemia/Lymphoma. *Methods Mol Biol,* 1582**,** 197-216.

Nethe, M., Berkhout, B. & van der Kuyl, A. C. 2005. Retroviral superinfection resistance. *Retrovirology,* 2**,** 52.

Ng, P. W., Iha, H., Iwanaga, Y., Bittner, M., Chen, Y., et al. 2001. Genome-wide expression changes induced by HTLV-1 Tax: evidence for MLK-3 mixed lineage kinase involvement in Tax-mediated NF-kappaB activation. *Oncogene,* 20**,** 4484-96.

Nicolas, D., Phillips, N. E. & Naef, F. 2017. What shapes eukaryotic transcriptional bursting? *Mol Biosyst,* 13**,** 1280-1290.

Nicot, C., Dundr, M., Johnson, J. M., Fullen, J. R., Alonzo, N., et al. 2004. HTLV-1-encoded p30II is a post-transcriptional negative regulator of viral replication. *Nat Med,* 10**,** 197-201.

Norris, P. J., Hirschkorn, D. F., DeVita, D. A., Lee, T. H. & Murphy, E. L. 2010. Human T cell leukemia virus type 1 infection drives spontaneous proliferation of natural killer cells. *Virulence,* 1**,** 19-28.

Ohtsubo, M., Theodoras, A. M., Schumacher, J., Roberts, J. M. & Pagano, M. 1995. Human cyclin E, a nuclear protein essential for the G1-to-S phase transition. *Mol Cell Biol,* 15**,** 2612-24.

Okochi, K., Sato, H. & Hinuma, Y. 1984. A retrospective study on transmission of adult T cell leukemia virus by blood transfusion: seroconversion in recipients. *Vox Sang,* 46**,** 245-53.

Ong, C. T. & Corces, V. G. 2014. CTCF: an architectural protein bridging genome topology and function. *Nat Rev Genet,* 15**,** 234-46.

Osame, M., Usuku, K., Izumo, S., Ijichi, N., Amitani, H., et al. 1986. HTLV-I associated myelopathy, a new clinical entity. *Lancet,* 1**,** 1031-2.

Othumpangat, S., Noti, J. D., McMillen, C. M. & Beezhold, D. H. 2016. ICAM-1 regulates the survival of influenza virus in lung epithelial cells during the early stages of infection. *Virology,* 487**,** 85-94.

Pais-Correia, A. M., Sachse, M., Guadagnini, S., Robbiati, V., Lasserre, R., et al. 2010. Biofilm-like extracellular viral assemblies mediate HTLV-1 cell-to-cell transmission at virological synapses. *Nat Med,* 16**,** 83-9.

Parker, C. E., Daenke, S., Nightingale, S. & Bangham, C. R. 1992. Activated, HTLV-1-specific cytotoxic T-lymphocytes are found in healthy seropositives as well as in patients with tropical spastic paraparesis. *Virology,* 188**,** 628-36.

Parslow, A., Cardona, A. & Bryson-Richardson, R. J. 2014. Sample drift correction following 4D confocal time-lapse imaging. *J Vis Exp*.

Pätzold, S., Schneider, J., Rudolph, C., Marmé, D. & Schächtele, C. 1993. Novel indolocarbazole protein kinase C inhibitors prevent reactivation of HIV-1 in latently infected cells. *Antiviral Res,* 22**,** 273-83.

Pearson, R., Kim, Y. K., Hokello, J., Lassen, K., Friedman, J., et al. 2008. Epigenetic silencing of human immunodeficiency virus (HIV) transcription by formation of restrictive chromatin structures at the viral long terminal repeat drives the progressive entry of HIV into latency. *J Virol,* 82**,** 12291-303.

Peloponese, J. M., Jr. & Jeang, K. T. 2006. Role for Akt/protein kinase B and activator protein-1 in cellular proliferation induced by the human T-cell leukemia virus type 1 tax oncoprotein. *J Biol Chem,* 281**,** 8927-38.

Petersen, B. O., Lukas, J., Sørensen, C. S., Bartek, J. & Helin, K. 1999. Phosphorylation of mammalian CDC6 by cyclin A/CDK2 regulates its subcellular localization. *Embo j,* 18**,** 396-410.

Phillips, E. H., Hodson, A., Hermine, O., Bazarbachi, A. & Cwynarski, K. 2016. Striving to cure adult T-cell leukaemia/lymphoma: a role for allogeneic stem cell transplant? *Bone Marrow Transplant,* 51**,** 1549-1555.

Pise-Masison, C. A., Mahieux, R., Jiang, H., Ashcroft, M., Radonovich, M., et al. 2000. Inactivation of p53 by human T-cell lymphotropic virus type 1 Tax requires activation of the NF-kappaB pathway and is dependent on p53 phosphorylation. *Mol Cell Biol,* 20**,** 3377-86.

Pluta, A., Jaworski, J. P. & Douville, R. N. 2020. Regulation of Expression and Latency in BLV and HTLV. *Viruses,* 12.

Podhorecka, M., Skladanowski, A. & Bozko, P. 2010. H2AX Phosphorylation: Its Role in DNA Damage Response and Cancer Therapy. *J Nucleic Acids,* 2010.

Poiesz, B. J., Ruscetti, F. W., Gazdar, A. F., Bunn, P. A., Minna, J. D., et al. 1980. Detection and isolation of type C retrovirus particles from fresh and cultured lymphocytes of a patient with cutaneous T-cell lymphoma. *Proc Natl Acad Sci U S A,* 77**,** 7415-9.

Prawiro, C., Bunney, T. D., Kampyli, C., Yaguchi, H., Katan, M., et al. 2023. A frequent PLCγ1 mutation in adult T-cell leukemia/lymphoma determines functional properties of the malignant cells. *Biochim Biophys Acta Mol Basis Dis,* 1869**,** 166601.

Proietti, F. A., Carneiro-Proietti, A. B., Catalan-Soares, B. C. & Murphy, E. L. 2005. Global epidemiology of HTLV-I infection and associated diseases. *Oncogene,* 24**,** 6058-68.

Raj, A., Peskin, C. S., Tranchina, D., Vargas, D. Y. & Tyagi, S. 2006. Stochastic mRNA synthesis in mammalian cells. *PLoS Biol,* 4**,** e309.

Raj, A., van den Bogaard, P., Rifkin, S. A., van Oudenaarden, A. & Tyagi, S. 2008. Imaging individual mRNA molecules using multiple singly labeled probes. *Nat Methods,* 5**,** 877-9.

Raj, A. & van Oudenaarden, A. 2008. Nature, nurture, or chance: stochastic gene expression and its consequences. *Cell,* 135**,** 216-26.

Ramírez, J. A. & Nyborg, J. K. 2007. Molecular characterization of HTLV-1 Tax interaction with the KIX domain of CBP/p300. *J Mol Biol,* 372**,** 958-969.

Rannug, U., Rannug, A., Sjöberg, U., Li, H., Westerholm, R., et al. 1995. Structure elucidation of two tryptophan-derived, high affinity Ah receptor ligands. *Chem Biol,* 2**,** 841-5.

Ratner, L. 2021. Epigenetic Regulation of Human T-Cell Leukemia Virus Gene Expression. *Microorganisms,* 10.

Ren, B., Cam, H., Takahashi, Y., Volkert, T., Terragni, J., et al. 2002. E2F integrates cell cycle progression with DNA repair, replication, and G(2)/M checkpoints. *Genes Dev,* 16**,** 245-56.

Rende, F., Cavallari, I., Corradin, A., Silic-Benussi, M., Toulza, F., et al. 2011. Kinetics and intracellular compartmentalization of HTLV-1 gene expression: nuclear retention of HBZ mRNAs. *Blood,* 117**,** 4855-9.

Riabowol, K., Draetta, G., Brizuela, L., Vandre, D. & Beach, D. 1989. The cdc2 kinase is a nuclear protein that is essential for mitosis in mammalian cells. *Cell,* 57**,** 393-401.

Richardson, J. H., Edwards, A. J., Cruickshank, J. K., Rudge, P. & Dalgleish, A. G. 1990. In vivo cellular tropism of human T-cell leukemia virus type 1. *J Virol,* 64**,** 5682-7.

Rivera-Walsh, I., Waterfield, M., Xiao, G., Fong, A. & Sun, S. C. 2001. NF-kappaB signaling pathway governs TRAIL gene expression and human T-cell leukemia virus-I Tax-induced T-cell death. *J Biol Chem,* 276**,** 40385-8.

Rodari, A., Darcis, G. & Van Lint, C. M. 2021. The Current Status of Latency Reversing Agents for HIV-1 Remission. *Annu Rev Virol,* 8**,** 491-514.

Roos, W. P. & Kaina, B. 2006. DNA damage-induced cell death by apoptosis. *Trends Mol Med,* 12**,** 440-50.

Rose, N. R., King, H. W., Blackledge, N. P., Fursova, N. A., Ember, K. J., et al. 2016. RYBP stimulates PRC1 to shape chromatin-based communication between Polycomb repressive complexes. *Elife,* 5.

Rosenblatt, J. D., Cann, A. J., Slamon, D. J., Smalberg, I. S., Shah, N. P., et al. 1988. HTLV-II transactivation is regulated by the overlapping tax/rex nonstructural genes. *Science,* 240**,** 916-9.

Ross, I. L., Browne, C. M. & Hume, D. A. 1994. Transcription of individual genes in eukaryotic cells occurs randomly and infrequently. *Immunol Cell Biol,* 72**,** 177-85.

Rothhammer, V. & Quintana, F. J. 2019. The aryl hydrocarbon receptor: an environmental sensor integrating immune responses in health and disease. *Nat Rev Immunol,* 19**,** 184-197.

Rullas, J., Bermejo, M., García-Pérez, J., Beltán, M., González, N., et al. 2004. Prostratin induces HIV activation and downregulates HIV receptors in peripheral blood lymphocytes. *Antivir Ther,* 9**,** 545-54.

Ryoo, H. D., Gorenc, T. & Steller, H. 2004. Apoptotic cells can induce compensatory cell proliferation through the JNK and the Wingless signaling pathways. *Dev Cell,* 7**,** 491-501.

Saito, M., Matsuzaki, T., Satou, Y., Yasunaga, J., Saito, K., et al. 2009. In vivo expression of the HBZ gene of HTLV-1 correlates with proviral load, inflammatory markers and disease severity in HTLV-1 associated myelopathy/tropical spastic paraparesis (HAM/TSP). *Retrovirology,* 6**,** 19.

Saito, M., Nakagawa, M., Kaseda, S., Matsuzaki, T., Jonosono, M., et al. 2004. Decreased human T lymphotropic virus type I (HTLV-I) provirus load and alteration in T cell phenotype after interferon-alpha therapy for HTLV-I-associated myelopathy/tropical spastic paraparesis. *J Infect Dis,* 189**,** 29-40.

Sakahira, H., Enari, M. & Nagata, S. 1998. Cleavage of CAD inhibitor in CAD activation and DNA degradation during apoptosis. *Nature,* 391**,** 96-9.

Sancar, A., Lindsey-Boltz, L. A., Unsal-Kaçmaz, K. & Linn, S. 2004. Molecular mechanisms of mammalian DNA repair and the DNA damage checkpoints. *Annu Rev Biochem,* 73**,** 39-85.

Sato, T., Coler-Reilly, A. L. G., Yagishita, N., Araya, N., Inoue, E., et al. 2018. Mogamulizumab (Anti-CCR4) in HTLV-1-Associated Myelopathy. *N Engl J Med,* 378**,** 529-538.

Satou, Y., Miyazato, P., Ishihara, K., Yaguchi, H., Melamed, A., et al. 2016. The retrovirus HTLV-1 inserts an ectopic CTCF-binding site into the human genome. *Proc Natl Acad Sci U S A,* 113**,** 3054-9.

Satou, Y., Yasunaga, J., Yoshida, M. & Matsuoka, M. 2006. HTLV-I basic leucine zipper factor gene mRNA supports proliferation of adult T cell leukemia cells. *Proc Natl Acad Sci U S A,* 103**,** 720-5.

Satyanarayana, A. & Kaldis, P. 2009. Mammalian cell-cycle regulation: several Cdks, numerous cyclins and diverse compensatory mechanisms. *Oncogene,* 28**,** 2925-39.

Schierhout, G., McGregor, S., Gessain, A., Einsiedel, L., Martinello, M., et al. 2020. Association between HTLV-1 infection and adverse health outcomes: a systematic review and meta-analysis of epidemiological studies. *Lancet Infect Dis,* 20**,** 133-143.

Schneider-Poetsch, T., Ju, J., Eyler, D. E., Dang, Y., Bhat, S., et al. 2010. Inhibition of eukaryotic translation elongation by cycloheximide and lactimidomycin. *Nat Chem Biol,* 6**,** 209-217.

Schneider, C. A., Rasband, W. S. & Eliceiri, K. W. 2012. NIH Image to ImageJ: 25 years of image analysis. *Nat Methods,* 9**,** 671-5.

Schnell, A. P., Kohrt, S., Aristodemou, A., Taylor, G. P., Bangham, C. R. M., et al. 2022. HDAC inhibitors Panobinostat and Romidepsin enhance tax transcription in HTLV-1-infected cell lines and freshly isolated patients' T-cells. *Front Immunol,* 13**,** 978800.

Schoggins, J. W., Wilson, S. J., Panis, M., Murphy, M. Y., Jones, C. T., et al. 2011. A diverse range of gene products are effectors of the type I interferon antiviral response. *Nature,* 472**,** 481-5.

Schröder, A. R., Shinn, P., Chen, H., Berry, C., Ecker, J. R., et al. 2002. HIV-1 integration in the human genome favors active genes and local hotspots. *Cell,* 110**,** 521-9.

Schuettengruber, B. & Cavalli, G. 2009. Recruitment of polycomb group complexes and their role in the dynamic regulation of cell fate choice. *Development,* 136**,** 3531-42.

Semmes, O. J. & Jeang, K. T. 1995. Definition of a minimal activation domain in human T-cell leukemia virus type I Tax. *J Virol,* 69**,** 1827-33.

Semmes, O. J. & Jeang, K. T. 1996. Localization of human T-cell leukemia virus type 1 tax to subnuclear compartments that overlap with interchromatin speckles. *J Virol,* 70**,** 6347-57.

Sharma, N. & Nyborg, J. K. 2008. The coactivators CBP/p300 and the histone chaperone NAP1 promote transcription-independent nucleosome eviction at the HTLV-1 promoter. *Proc Natl Acad Sci U S A,* 105**,** 7959-63.

Sharma, R., Williams, I. S., Gatchie, L., Sonawane, V. R., Chaudhuri, B., et al. 2018. Khellinoflavanone, a Semisynthetic Derivative of Khellin, Overcomes Benzo[a]pyrene Toxicity in Human Normal and Cancer Cells That Express CYP1A1. *ACS Omega,* 3**,** 8553-8566.

Shembade, N., Harhaj, N. S., Yamamoto, M., Akira, S. & Harhaj, E. W. 2007. The human T-cell leukemia virus type 1 Tax oncoprotein requires the ubiquitin-conjugating enzyme Ubc13 for NF-kappaB activation. *J Virol,* 81**,** 13735-42.

Shen, M. & Horbett, T. A. 2001. The effects of surface chemistry and adsorbed proteins on monocyte/macrophage adhesion to chemically modified polystyrene surfaces. *J Biomed Mater Res,* 57**,** 336-45.

Shendure, J. 2008. The beginning of the end for microarrays? *Nat Methods,* 5**,** 585-7.

Shimomura, O., Johnson, F. H. & Saiga, Y. 1962. Extraction, purification and properties of aequorin, a bioluminescent protein from the luminous hydromedusan, Aequorea. *J Cell Comp Physiol,* 59**,** 223-39.

Shimoyama, M. 1991. Diagnostic criteria and classification of clinical subtypes of adult T-cell leukaemia-lymphoma. A report from the Lymphoma Study Group (1984-87). *Br J Haematol,* 79**,** 428-37.

Shiohama, Y., Naito, T., Matsuzaki, T., Tanaka, R., Tomoyose, T., et al. 2016. Absolute quantification of HTLV-1 basic leucine zipper factor (HBZ) protein and its plasma antibody in HTLV-1 infected individuals with different clinical status. *Retrovirology,* 13**,** 29.

Shirinian, M., Kfoury, Y., Dassouki, Z., El-Hajj, H. & Bazarbachi, A. 2013. Tax-1 and Tax-2 similarities and differences: focus on post-translational modifications and NF-κB activation. *Front Microbiol,* 4**,** 231.

Shuh, M. & Derse, D. 2000. Ternary complex factors and cofactors are essential for human T-cell leukemia virus type 1 tax transactivation of the serum response element. *J Virol,* 74**,** 11394-7.

Siebenlist, U., Franzoso, G. & Brown, K. 1994. Structure, regulation and function of NF-kappa B. *Annu Rev Cell Biol,* 10**,** 405-55.

Silic-Benussi, M., Cannizzaro, E., Venerando, A., Cavallari, I., Petronilli, V., et al. 2009. Modulation of mitochondrial K(+) permeability and reactive oxygen species production by the p13 protein of human T-cell leukemia virus type 1. *Biochim Biophys Acta,* 1787**,** 947-54.

Slattery, J. P., Franchini, G. & Gessain, A. 1999. Genomic evolution, patterns of global dissemination, and interspecies transmission of human and simian T-cell leukemia/lymphotropic viruses. *Genome Res,* 9**,** 525-40.

Smith, A., Carrasco, Y. R., Stanley, P., Kieffer, N., Batista, F. D., et al. 2005. A talin-dependent LFA-1 focal zone is formed by rapidly migrating T lymphocytes. *J Cell Biol,* 170**,** 141-51.

Song, J., Clagett-Dame, M., Peterson, R. E., Hahn, M. E., Westler, W. M., et al. 2002. A ligand for the aryl hydrocarbon receptor isolated from lung. *Proc Natl Acad Sci U S A,* 99**,** 14694-9.

Sprick, M. R. & Walczak, H. 2004. The interplay between the Bcl-2 family and death receptor-mediated apoptosis. *Biochim Biophys Acta,* 1644**,** 125-32.

Strasser, A., Jost, P. J. & Nagata, S. 2009. The many roles of FAS receptor signaling in the immune system. *Immunity,* 30**,** 180-92.

Subach, F. V., Subach, O. M., Gundorov, I. S., Morozova, K. S., Piatkevich, K. D., et al. 2009. Monomeric fluorescent timers that change color from blue to red report on cellular trafficking. *Nat Chem Biol,* 5**,** 118-26.

Sugasawa, K., Ng, J. M., Masutani, C., Iwai, S., van der Spek, P. J., et al. 1998. Xeroderma pigmentosum group C protein complex is the initiator of global genome nucleotide excision repair. *Mol Cell,* 2**,** 223-32.

Sugata, K., Yasunaga, J., Kinosada, H., Mitobe, Y., Furuta, R., et al. 2016. HTLV-1 Viral Factor HBZ Induces CCR4 to Promote T-cell Migration and Proliferation. *Cancer Res,* 76**,** 5068-79.

Sun, X. & Kaufman, P. D. 2018. Ki-67: more than a proliferation marker. *Chromosoma,* 127**,** 175-186.

Takahashi, M., Higuchi, M., Makokha, G. N., Matsuki, H., Yoshita, M., et al. 2013. HTLV-1 Tax oncoprotein stimulates ROS production and apoptosis in T cells by interacting with USP10. *Blood,* 122**,** 715-25.

Takahashi, T., Higuchi, M., Fukushi, M., Oie, M., Ito, M., et al. 2002. Homotypic cell-cell adhesion induced by human T cell leukemia virus type 1 tax protein in T cell lines. *Virology,* 302**,** 132-43.

Takeda, S., Maeda, M., Morikawa, S., Taniguchi, Y., Yasunaga, J., et al. 2004. Genetic and epigenetic inactivation of tax gene in adult T-cell leukemia cells. *Int J Cancer,* 109**,** 559-67.

Tamiya, S., Matsuoka, M., Etoh, K., Watanabe, T., Kamihira, S., et al. 1996. Two types of defective human T-lymphotropic virus type I provirus in adult T-cell leukemia. *Blood,* 88**,** 3065-73.

Tanaka, Y., Fukudome, K., Hayashi, M., Takagi, S. & Yoshie, O. 1995. Induction of ICAM-1 and LFA-3 by Tax1 of human T-cell leukemia virus type 1 and mechanism of down-regulation of ICAM-1 or LFA-1 in adult-T-cell-leukemia cell lines. *Int J Cancer,* 60**,** 554-61.

Taniguchi, Y., Nosaka, K., Yasunaga, J., Maeda, M., Mueller, N., et al. 2005. Silencing of human T-cell leukemia virus type I gene transcription by epigenetic mechanisms. *Retrovirology,* 2**,** 64.

Tattermusch, S., Skinner, J. A., Chaussabel, D., Banchereau, J., Berry, M. P., et al. 2012. Systems biology approaches reveal a specific interferon-inducible signature in HTLV-1 associated myelopathy. *PLoS Pathog,* 8**,** e1002480.

Terskikh, A., Fradkov, A., Ermakova, G., Zaraisky, A., Tan, P., et al. 2000. "Fluorescent timer": protein that changes color with time. *Science,* 290**,** 1585-8.

Thorstensson, R., Albert, J. & Andersson, S. 2002. Strategies for diagnosis of HTLV-I and -II. *Transfusion,* 42**,** 780-91.

Tie, F., Adya, N., Greene, W. C. & Giam, C. Z. 1996. Interaction of the human T-lymphotropic virus type 1 Tax dimer with CREB and the viral 21-base-pair repeat. *J Virol,* 70**,** 8368-74.

Tinevez, J.-Y. & Herbert, S. 2020. The NEMO Dots Assembly: Single-Particle Tracking and Analysis. *In:* Miura, K. & Sladoje, N. (eds.) *Bioimage Data Analysis Workflows.* Cham: Springer International Publishing.

Tinevez, J. Y., Perry, N., Schindelin, J., Hoopes, G. M., Reynolds, G. D., et al. 2017. TrackMate: An open and extensible platform for single-particle tracking. *Methods,* 115**,** 80-90.

Tosswill, J. H., Taylor, G. P., Tedder, R. S. & Mortimer, P. P. 2000. HTLV-I/II associated disease in England and Wales, 1993-7: retrospective review of serology requests. *Bmj,* 320**,** 611-2.

Toulza, F., Heaps, A., Tanaka, Y., Taylor, G. P. & Bangham, C. R. 2008. High frequency of CD4+FoxP3+ cells in HTLV-1 infection: inverse correlation with HTLV-1-specific CTL response. *Blood,* 111**,** 5047-53.

Toulza, F., Nosaka, K., Tanaka, Y., Schioppa, T., Balkwill, F., et al. 2010. Human T-lymphotropic virus type 1-induced CC chemokine ligand 22 maintains a high frequency of functional FoxP3+ regulatory T cells. *J Immunol,* 185**,** 183-9.

Trevino, V., Falciani, F. & Barrera-Saldaña, H. A. 2007. DNA microarrays: a powerful genomic tool for biomedical and clinical research. *Mol Med,* 13**,** 527-41.

Tsai, A. G., Cabrales, P., Hangai-Hoger, N. & Intaglietta, M. 2004. Oxygen distribution and respiration by the microcirculation. *Antioxid Redox Signal,* 6**,** 1011-8.

Uchiyama, T., Yodoi, J., Sagawa, K., Takatsuki, K. & Uchino, H. 1977. Adult T-cell leukemia: clinical and hematologic features of 16 cases. *Blood,* 50**,** 481-92.

Unge, T., Solomin, L., Mellini, M., Derse, D., Felber, B. K., et al. 1991. The Rex regulatory protein of human T-cell lymphotropic virus type I binds specifically to its target site within the viral RNA. *Proc Natl Acad Sci U S A,* 88**,** 7145-9.

Usui, T., Yanagihara, K., Tsukasaki, K., Murata, K., Hasegawa, H., et al. 2008. Characteristic expression of HTLV-1 basic zipper factor (HBZ) transcripts in HTLV-1 provirus-positive cells. *Retrovirology,* 5**,** 34.

Valentin-Vega, Y. A., Okano, H. & Lozano, G. 2008. The intestinal epithelium compensates for p53-mediated cell death and guarantees organismal survival. *Cell Death Differ,* 15**,** 1772-81.

van Engeland, M., Nieland, L. J., Ramaekers, F. C., Schutte, B. & Reutelingsperger, C. P. 1998. Annexin V-affinity assay: a review on an apoptosis detection system based on phosphatidylserine exposure. *Cytometry,* 31**,** 1-9.

Van Prooyen, N., Gold, H., Andresen, V., Schwartz, O., Jones, K., et al. 2010. Human T-cell leukemia virus type 1 p8 protein increases cellular conduits and virus transmission. *Proc Natl Acad Sci U S A,* 107**,** 20738-43.

Vandermeulen, C., O'Grady, T., Wayet, J., Galvan, B., Maseko, S., et al. 2021. The HTLV-1 viral oncoproteins Tax and HBZ reprogram the cellular mRNA splicing landscape. *PLoS Pathog,* 17**,** e1009919.

Varrin-Doyer, M., Nicolle, A., Marignier, R., Cavagna, S., Benetollo, C., et al. 2012. Human T lymphotropic virus type 1 increases T lymphocyte migration by recruiting the cytoskeleton organizer CRMP2. *J Immunol,* 188**,** 1222-33.

Veldhoen, M., Hirota, K., Christensen, J., O'Garra, A. & Stockinger, B. 2009. Natural agonists for aryl hydrocarbon receptor in culture medium are essential for optimal differentiation of Th17 T cells. *J Exp Med,* 206**,** 43-9.

Verdonck, K., González, E., Schrooten, W., Vanham, G. & Gotuzzo, E. 2008. HTLV-1 infection is associated with a history of active tuberculosis among family members of HTLV-1-infected patients in Peru. *Epidemiol Infect,* 136**,** 1076-83.

Verkhusha, V. V. & Lukyanov, K. A. 2004. The molecular properties and applications of Anthozoa fluorescent proteins and chromoproteins. *Nat Biotechnol,* 22**,** 289-96.

Vermes, I., Haanen, C., Steffens-Nakken, H. & Reutelingsperger, C. 1995. A novel assay for apoptosis. Flow cytometric detection of phosphatidylserine expression on early apoptotic cells using fluorescein labelled Annexin V. *J Immunol Methods,* 184**,** 39-51.

Vine, A. M., Heaps, A. G., Kaftantzi, L., Mosley, A., Asquith, B., et al. 2004. The role of CTLs in persistent viral infection: cytolytic gene expression in CD8+ lymphocytes distinguishes between individuals with a high or low proviral load of human T cell lymphotropic virus type 1. *J Immunol,* 173**,** 5121-9.

Wang, L., Brown, J. L., Cao, R., Zhang, Y., Kassis, J. A., et al. 2004. Hierarchical recruitment of polycomb group silencing complexes. *Mol Cell,* 14**,** 637-46.

Wang, L., Yang, J. K., Kabaleeswaran, V., Rice, A. J., Cruz, A. C., et al. 2010. The Fas-FADD death domain complex structure reveals the basis of DISC assembly and disease mutations. *Nat Struct Mol Biol,* 17**,** 1324-9.

Wang, X., Miyake, H., Okamoto, M., Saito, M., Fujisawa, J., et al. 2002. Inhibition of the tax-dependent human T-lymphotropic virus type I replication in persistently infected cells by the fluoroquinolone derivative k-37. *Mol Pharmacol,* 61**,** 1359-65.

Ward, I. M. & Chen, J. 2001. Histone H2AX is phosphorylated in an ATR-dependent manner in response to replicational stress. *J Biol Chem,* 276**,** 47759-62.

Wattel, E., Vartanian, J. P., Pannetier, C. & Wain-Hobson, S. 1995. Clonal expansion of human T-cell leukemia virus type I-infected cells in asymptomatic and symptomatic carriers without malignancy. *J Virol,* 69**,** 2863-8.

Weber, T. S., Jaehnert, I., Schichor, C., Or-Guil, M. & Carneiro, J. 2014. Quantifying the length and variance of the eukaryotic cell cycle phases by a stochastic model and dual nucleoside pulse labelling. *PLoS Comput Biol,* 10**,** e1003616.

Weinberger, L. S., Burnett, J. C., Toettcher, J. E., Arkin, A. P. & Schaffer, D. V. 2005. Stochastic gene expression in a lentiviral positive-feedback loop: HIV-1 Tat fluctuations drive phenotypic diversity. *Cell,* 122**,** 169-82.

Weintraub, S. J., Chow, K. N., Luo, R. X., Zhang, S. H., He, S., et al. 1995. Mechanism of active transcriptional repression by the retinoblastoma protein. *Nature,* 375**,** 812-5.

Williams, S. A., Chen, L. F., Kwon, H., Fenard, D., Bisgrove, D., et al. 2004. Prostratin antagonizes HIV latency by activating NF-kappaB. *J Biol Chem,* 279**,** 42008-17.

Winter, H. Y. & Marriott, S. J. 2007. Human T-cell leukemia virus type 1 Tax enhances serum response factor DNA binding and alters site selection. *J Virol,* 81**,** 6089-98.

Wood, R. D. 1997. Nucleotide excision repair in mammalian cells. *J Biol Chem,* 272**,** 23465-8.

Wu, X. & Sun, S. C. 2007. Retroviral oncoprotein Tax deregulates NF-kappaB by activating Tak1 and mediating the physical association of Tak1-IKK. *EMBO Rep,* 8**,** 510-5.

Xiao, G., Cvijic, M. E., Fong, A., Harhaj, E. W., Uhlik, M. T., et al. 2001. Retroviral oncoprotein Tax induces processing of NF-kappaB2/p100 in T cells: evidence for the involvement of IKKalpha. *Embo j,* 20**,** 6805-15.

Xie, L., Yamamoto, B., Haoudi, A., Semmes, O. J. & Green, P. L. 2006. PDZ binding motif of HTLV-1 Tax promotes virus-mediated T-cell proliferation in vitro and persistence in vivo. *Blood,* 107**,** 1980-8.

Yamano, Y. & Sato, T. 2012. Clinical pathophysiology of human T-lymphotropic virus-type 1-associated myelopathy/tropical spastic paraparesis. *Front Microbiol,* 3**,** 389.

Yang, L., Kotomura, N., Ho, Y. K., Zhi, H., Bixler, S., et al. 2011. Complex cell cycle abnormalities caused by human T-lymphotropic virus type 1 Tax. *J Virol,* 85**,** 3001-9.

Yasunaga, J., Lin, F. C., Lu, X. & Jeang, K. T. 2011. Ubiquitin-specific peptidase 20 targets TRAF6 and human T cell leukemia virus type 1 tax to negatively regulate NF-kappaB signaling. *J Virol,* 85**,** 6212-9.

Yokoyama, K., Ishikawa, N., Igarashi, S., Kawano, N., Masuda, N., et al. 2009. Potent and orally bioavailable CCR4 antagonists: Synthesis and structure-activity relationship study of 2-aminoquinazolines. *Bioorg Med Chem,* 17**,** 64-73.

Yoshida, M., Satou, Y., Yasunaga, J., Fujisawa, J. & Matsuoka, M. 2008. Transcriptional control of spliced and unspliced human T-cell leukemia virus type 1 bZIP factor (HBZ) gene. *J Virol,* 82**,** 9359-68.

Yoshie, O., Fujisawa, R., Nakayama, T., Harasawa, H., Tago, H., et al. 2002. Frequent expression of CCR4 in adult T-cell leukemia and human T-cell leukemia virus type 1-transformed T cells. *Blood,* 99**,** 1505-11.

Yoshita, M., Higuchi, M., Takahashi, M., Oie, M., Tanaka, Y., et al. 2012. Activation of mTOR by human T-cell leukemia virus type 1 Tax is important for the transformation of mouse T cells to interleukin-2-independent growth. *Cancer Sci,* 103**,** 369-74.

Yu, Y., Arora, A., Min, W., Roifman, C. M. & Grunebaum, E. 2009. EdU incorporation is an alternative non-radioactive assay to [(3)H]thymidine uptake for in vitro measurement of mice T-cell proliferations. *J Immunol Methods,* 350**,** 29-35.

Yuen, C. K., Chan, C. P., Fung, S. Y., Wang, P. H., Wong, W. M., et al. 2016. Suppression of Type I Interferon Production by Human T-Cell Leukemia Virus Type 1 Oncoprotein Tax through Inhibition of IRF3 Phosphorylation. *J Virol,* 90**,** 3902-3912.

Zargari, R., Mahdifar, M., Mohammadi, A., Vahidi, Z., Hassanshahi, G., et al. 2020. The Role of Chemokines in the Pathogenesis of HTLV-1. *Front Microbiol,* 11**,** 421.

Zhang, L., Liu, M., Merling, R. & Giam, C. Z. 2006. Versatile reporter systems show that transactivation by human T-cell leukemia virus type 1 Tax occurs independently of chromatin remodeling factor BRG1. *J Virol,* 80**,** 7459-68.

Zhang, W., Nisbet, J. W., Bartoe, J. T., Ding, W. & Lairmore, M. D. 2000. Human T-lymphotropic virus type 1 p30(II) functions as a transcription factor and differentially modulates CREB-responsive promoters. *J Virol,* 74**,** 11270-7.

Zhao, L. J. & Giam, C. Z. 1992. Human T-cell lymphotropic virus type I (HTLV-I) transcriptional activator, Tax, enhances CREB binding to HTLV-I 21-base-pair repeats by protein-protein interaction. *Proc Natl Acad Sci U S A,* 89**,** 7070-4.

Zhao, M., De Crignis, E., Rokx, C., Verbon, A., van Gelder, T., et al. 2019. T cell toxicity of HIV latency reversing agents. *Pharmacol Res,* 139**,** 524-534.

Zhao, T., Yasunaga, J., Satou, Y., Nakao, M., Takahashi, M., et al. 2009. Human T-cell leukemia virus type 1 bZIP factor selectively suppresses the classical pathway of NF-kappaB. *Blood,* 113**,** 2755-64.

Zhao, W., Feng, H., Sun, W., Liu, K., Lu, J. J., et al. 2017. Tert-butyl hydroperoxide (t-BHP) induced apoptosis and necroptosis in endothelial cells: Roles of NOX4 and mitochondrion. *Redox Biol,* 11**,** 524-534.

Zhi, H., Yang, L., Kuo, Y. L., Ho, Y. K., Shih, H. M., et al. 2011. NF-κB hyper-activation by HTLV-1 tax induces cellular senescence, but can be alleviated by the viral anti-sense protein HBZ. *PLoS Pathog,* 7**,** e1002025.

Zhou, Y. H., Sun, L., Chen, J., Sun, W. W., Ma, L., et al. 2019. Tryptophan Metabolism Activates Aryl Hydrocarbon Receptor-Mediated Pathway To Promote HIV-1 Infection and Reactivation. *mBio,* 10.

Zimmer, M. 2002. Green fluorescent protein (GFP): applications, structure, and related photophysical behavior. *Chem Rev,* 102**,** 759-81.

Zou, H., Li, Y., Liu, X. & Wang, X. 1999. An APAF-1.cytochrome c multimeric complex is a functional apoptosome that activates procaspase-9. *J Biol Chem,* 274**,** 11549-56.